Universidade de Lisboa

Faculdade de Medicina

From sensory cues to complex behaviour: towards an understanding of the neuronal computations underlying sensorimotor transformations in *Caenorhabditis elegans*

Daniel Mateus Correia

Orientador I Professor Doutor Manuel Zimmer

Coorientador I Professora Doutora Sandra Vaz

Dissertação especialmente elaborada para obtenção do grau de Mestre em Neurociências

2020

Universidade de Lisboa

Faculdade de Medicina

From sensory cues to complex behaviour: towards an understanding of the neuronal computations underlying sensorimotor transformations in *Caenorhabditis elegans*

Daniel Mateus Correia

Orientador I Professor Doutor Manuel Zimmer

Coorientador I Professora Doutora Sandra Vaz

Dissertação especialmente elaborada para obtenção do grau de Mestre em Neurociências

Research Institute of Molecular Pathology & University of Vienna

2020

A impressão desta dissertação foi aprovada pelo Conselho Científico da Faculdade de Medicina de Lisboa em reunião de 21 de Abril de 2020

The work presented in this master thesis was conducted at the Research Institute of Molecular Pathology (IMP) and at the University of Vienna, under the supervision of Prof. Doctor Manuel Zimmer, from the IMP & University of Vienna, and co-supervised by Doctor Sandra Vaz, from Faculdade de Medicina, Universidade de Lisboa.

ACKNOWLEDGMENTS / AGRADECIMENTOS

I don’t think it is possible to show how much work and personal growth is behind a project as big as a master thesis, but, to the following people, I want you to know that you strongly contributed to my growth both as a professional and as a person for the past year and a half. A huge thank you to everyone for that.

To my supervisor, Manuel. For the opportunity you gave me to have my first real research experience in science in such an awesome lab. The liberty you allowed me to manage my work taught me more professionally than I could have learnt in any other place. Thank you for your guidance and for allowing me to be surrounded by such a creative and mentally stimulating environment.

To Harris. For being such a great mentor. Your capacity to advise a student without making him/her feel a string of judgment is truly remarkable. Thank you for your availability, your constant motivation through all the failures and your constant kindness. I learned more from you than I could ever express. You are a brilliant scientist and I wish you all the success in the world.

To all current and former members of the Zimmer Lab I had the pleasure to meet and work with: Ana, Anton, Charlie, Enrico, Julia, Kerem, Luka, Lukas, Mara, Marc, Matthew, Niklas, Oriana, Philipp, Rich & Ulises. Thank you for being so supportive and open-armed. I learned a lot from each one of you, not only scientifically, but as a person.

À Andreia. Pela amiga enorme que és. Por nunca desistires de ninguém, e de mim, em particular. És uma pessoa absolutamente fantástica, com um ‘coração’ a condizer. Com orgulho afirmo, com certeza, que estarás comigo nos longos anos que advirão. Obrigado por toda a partilha e confiança.

À Sara. A tua amizade foi fundamental no último ano e meio. Obrigado pelo apoio constante e pela paciência para os meus dramas de primeiro mundo infinitos. O teu feitio é (felizmente, ou não) imutável, mas sou muito grato que a tua presença, disponibilidade e confiança em mim tenham sido, também. Obrigado por teres chegado a mim e me conheceres melhor que eu mesmo.

À minha família. Por serem um porto de abrigo firme. Pelo constante suporte e motivação para conduzir esta etapa na minha vida. Obrigado por me apoiarem em passar 16 meses do outro lado da Europa a realizar este projeto. Espero deixar-vos orgulhosos.

A big thank you to everyone who took the time to critically read and comment on the thesis: Manuel Zimmer, Harris Kaplan, Sandra Vaz, Brandon Pin & Sara Nunes.

SUMÁRIO

Sobrevivência em ambientes em rápida mudança requer mecanismos aprimorados que permitam aos organismos responder rapidamente a pistas sensoriais, captadas do meio envolvente, e a adaptarem o seu comportamento de forma adequada. O processamento, por parte do sistema nervoso dos organismos, dos mecanismos subjacentes à integração sensório-motora (a transformação de sinais sensoriais em *outputs* motores) é um dos processos mais fundamentais e, no entanto, mal compreendidos, em neurociências. Neste estudo, visou-se investigar de que forma o nemátodo *Caenorhabditis elegans* (*C. elegans*) efetua a transformação sensório-motora num dos seus principais circuitos neuronais de processamento de informação, fundamental na criação de comportamentos provocados pela perceção de odores.

O conectoma de *C. elegans* foi minuciosamente estudado e mapeado, o que levou a que este nemátodo seja considerado um modelo biológico valioso para o estudo de circuitos neuronais e das suas funções. *C. elegans* é um organismo facilmente manipulável geneticamente. Transgenes que codificam indicadores de cálcio, como é exemplo GCaMP (*genetically encoded calcium indicator*), podem ser facilmente expressos em neurónios de interesse. GCaMP é uma variante de GFP (*Green Fluorescent Protein*) que sofre mudanças conformacionais mediante ligação a iões Ca^{2+} que fluem para o meio intracelular durante um evento de despolarização. Esta mudança conformacional provoca a emissão de fluorescência verde quando o organismo é iluminado com luz azul num *setup* de microscopia. A transparência de *C. elegans* torna indicadores de cálcio muito adequados para medição de atividade neuronal neste organismo.

Com o advento de técnicas de microscopia para medição de atividade neuronal em *C. elegans*, foram desenvolvidos dispositivos microfluídicos que permitem manter o organismo imobilizado e sob condições ambientais controladas. A possibilidade de manter o ambiente exterior do organismo sob condições controladas permite o registo da atividade de neurónios específicos, ou mesmo de todo o sistema nervoso, em resolução *single-cell*, durante ambientes sensoriais constantes ou variáveis, permitindo a atribuição de padrões de atividade neuronal ao efeito de *inputs* sensoriais.

De forma a quimiotaxar em direção a ambientes atrativos, *C. elegans* executa *biased random walks*, que consiste num aumento da duração de períodos de movimento dianteiro e uma diminuição na frequência de manobras de reorientação. Executa também *klinotaxis*, o comportamento de oscilação da zona anterior do corpo em direções preferenciais, durante períodos de movimento dianteiro. Os princípios subjacentes às transformações sensório-motoras que influenciam o comportamento do

organismo, de forma a causar um aumento ou diminuição da frequência de períodos de reversão, são ainda largamente desconhecidos. O interneurónio AIY é particularmente interessante para estudar estas questões, uma vez que este interneurónio recebe sinapses diretas de múltiplos neurónios sensoriais, e estabelece conexões recíprocas com vários neurónios, tendo estes funções na modulação da estratégia de locomoção. AIY foi previamente considerado como sendo fundamental e suficiente para a modulação de circuitos neuronais que, probabilisticamente, influenciam as principais estratégias comportamentais de *C. elegans*. Assim, estudar os mecanismos que estão na base da transformação sensório-motora que ocorre em AIY é da maior importância. Desta forma, será possível compreender os mecanismos empregados pelo sistema nervoso deste nemátodo, que codificam a execução de comportamentos fundamentais para a sua sobrevivência e fitness evolutivo: a habilidade de quimiotaxar em direção a ambientes sensoriais vantajosos.

Em organismos que se movem livremente, o registo da atividade neuronal de células singulares com a gravação simultânea do comportamento do animal, permitiu estabelecer uma relação entre atividade neuronal e a execução de diferentes estratégias de locomoção, em múltiplos neurónios. Foi ainda observado, em estudos anteriores, que neurónios coativos em organismos imobilizados, estão também ativos durante o mesmo estado comportamental em animais que se movem livremente. Assim, a atividade de neurónios ativos em animais imobilizados pode ser diretamente relacionada com uma estratégia de locomoção. Embora o animal não esteja capaz de efetivar o comportamento codificado, um sinal de comando motor é gerado no sistema nervoso do animal. Desta forma, é possível compreender como é que o sistema nervoso do *C. elegans* combina estados comportamentais com *inputs* sensoriais, em animais imobilizados.

Neurónios sensoriais em *C. elegans* possuem terminações nervosas expostas ao meio ambiente envolvente e podem reconhecem uma grande variedade de estímulos sensoriais. Neurónios motores enervam células musculares e são os neurónios ultimamente responsáveis pela geração de comportamentos. Interneurónios são considerados neurónios que carecem de terminações nervosas sensoriais ou junções neuromusculares, por isso estabelecendo a comunicação entre neurónios sensoriais e motores ao formarem uma extensa rede de interações entre os últimos e outros interneurónios.

Neste estudo, foram usadas técnicas de biologia molecular para expressar o indicador de cálcio GCaMP em neurónios de interesse: no interneurónio AIY; num dos seus principais parceiros pré-sinápticos – o neurónio sensorial AWC; e no interneurónio RIM. AWC é um neurónio sensorial envolvido na deteção de múltiplos odores, incluindo odor bacteriano. RIM é um interneurónio pré-

motor cujos períodos de elevada atividade estão relacionados com a codificação de manobras de reversão. Foi utilizada microscopia confocal de disco giratório para registar a atividade dos neurónios acima mencionados, através das variações intracelulares de cálcio das células, tanto em animais imobilizados, como em animais livres.

Observou-se que a atividade de AIY é aqui reportada como sendo dominada por um sinal codificante de estados de comando motor (locomoção dianteira/manobras de reversão), na ausência de mecanismos de *feedback* propriocetivo ativos. Apesar dos circuitos neuronais existentes no sistema nervoso de *C. elegans*, responsáveis pela sinalização do estado motor instantâneo para AIY, não serem dissecados, aqui é observada uma modulação da atividade do neurónio anterior à mudança de estado de comando motor. Esta observação é interpretada como uma indicação de que AIY regula a ocorrência de manobras de reversão. AIY recebe *input* maioritariamente de neurónios sensoriais, sendo, por isso, conhecido como um interneurónio primário. É, por isso, surpreendente encontrar uma regulação de estados de locomoção do animal numa fase tão precoce de transformação sensório-motora. Estas descobertas vão de encontro a estudos recentes realizados em organismos com sistemas nervosos mais complexos.

De seguida, visou-se compreender como é que o sinal dominante que governa a atividade de AIY é combinado com informação sensorial. Para isso, desenvolveu-se um paradigma de estimulação sensorial usando dispositivos microfluídicos que permitem o fornecimento de odores aos animais. Mediu-se a atividade de AWC e AIY em organismos imobilizados, enquanto se providenciou um estímulo sensorial de odor bacteriano. Devido a limitações técnicas do *setup* experimental usado para estimular o animal, não foi possível recapitular as respostas estereotipadas que o neurónio sensorial AWC apresenta aquando da estimulação sensorial, como reportado em literatura prévia. Adicionalmente, não foram encontradas evidências suficientes para afirmar que a atividade de AIY sofreu influência do estímulo. Assim, não foi possível compreender em plenitude de que forma AIY combina informação de estados motores com informação sensorial. No entanto, encontrou-se evidência para transformação sensório-motora, possivelmente através de outros circuitos neuronais que não o aqui estudado, que influenciou a modulação do comportamento animal.

Estudos anteriores mostraram que AIY exibe atividade ao longo do axónio e suas projeções axonais, não existindo relatos de dinâmica de cálcio no núcleo ou corpo celular. Não é claro quão frequentemente neurónios mostram diferentes padrões de dinâmica de cálcio no soma ou neurites e, especificamente, quão frequentemente esta estratégia é usada por interneurónios como forma de integrar informação sensorial e motora no mesmo espaço celular. Não se encontrou evidência de que

esta estratégia é usada por AIY, sugerindo que este neurónio usa outras abordagens para combinar sinais de diferentes origens.

Finalmente, a atividade de AWC e AIY for registada em animais livres de movimento, na presença de um gradiente bacteriano, uma fonte de alimento para *C. elegans* e, por isso, um forte estímulo sensorial. Atividade neuronal em animais restringidos de movimento e animais com a capacidade de se moverem livremente mostra diferenças. Deste modo, visou-se compreender como é que a atividade de AIY varia na presença de *inputs* sensoriais que só um animal livre de locomoção integra (*inputs* proprioceptivos). A fraca expressão de GCaMP que foi possível obter em AIY neste estudo limitou a resolução espacial e temporal dos dados obtidos, que revelaram ser insuficiente para os objetivos propostos.

De um modo geral, este estudo é relevante para a comunidade por sugerir um interneurónio primário como sendo capaz de modular a ocorrência de estados de comando motor em estadios iniciais de integração sensório-motora. Esta estratégia foi recentemente reportada em sistemas nervosos mais complexos, sugerindo ter relevância funcional para múltiplos organismos do reino animal.

Palavras-Chave: Indicadores de cálcio; Microscopia de alta resolução; Integração sensório-motora; *Caenorhabditis elegans*.

ABSTRACT

Survival in fast changing environments requires fine-tuned mechanisms that allow the organisms to rapidly react to sensory cues and adapt their behaviour to respond accordingly. The brain's computations underlying sensorimotor integration, the transformation of sensory signals into motor outputs, is one of the most fundamental, yet poorly understood, processes in neuroscience. Here, we aim to investigate how the nematode *Caenorhabditis elegans* achieves sensorimotor transformation, by studying one of its most fundamental neuronal circuits for information processing and odour evoked behaviours. By expressing genetically encoded calcium indicators in neurons of interest, we performed *in vivo* calcium imaging in immobilised worms, both in an environment deprived of fluctuating sensory stimulation and while delivering an attractive odour to the animals. We reveal the activity of a primary sensory neuron to be dominated by a signal encoding motor command states of the animal, and suggest that this neuron may take part in modulating motor command state transitions in the worm's brain. Moreover, here, we aimed to study how an attractive cue for the worm affects the coding of behavioural states, and how a single neuron can multiplex both behavioural and sensory information. Finally, we recorded the activity of the same neurons in freely crawling animals as an attempt to understand how sensorimotor transformation varies from immobilised to unrestrained animals. Altogether, this work bears potential relevance to the *C. elegans* community by suggesting a primary sensory neuron as being capable of modulating motor commands states at early stages of sensorimotor transformation. This strategy has recently been reported in higher-order organisms as well, suggesting that it has functional relevance for organisms across the animal kingdom.

Keywords: Calcium indicators; single-cell resolution imaging; sensorimotor transformation; *Caenorhabditis elegans*

Table of Contents

List of Main Figures

List of Supplementary Figures

List of Supplementary Tables

1. INTRODUCTION

1.1. How the brain generates behaviour: an everlasting mystery?

Generation of behaviour adequate to the surroundings of all organisms requires a complex processing of environmental cues, perceived by specialized projections of their nervous systems, and their translation into signals in specialized cells, neurons. This processing of sensory information by the nervous system might eventually culminate in the generation of motor command signals; these are intertwined within the brain and relayed to the muscles of the animals to elicit appropriate behaviour. The translation of sensory information to motor output can be referred to as *sensorimotor transformation* and it is one of the most fundamental, yet poorly understood, mechanisms in behavioural neuroscience.

Sophisticated tasks that require complex brain computations are found across the entire animal kingdom. Examples include chasing a prey, olfactory localization, navigation, communication or feeding (Wehner, 2003; Olberg et al., 2007; Coen & Murthy, 2016). The mechanisms underlying sensorimotor integration here are challenging, especially because the neuronal computations behind them need to be flexible (Huston & Jayaraman, 2011). For instance, depending on whether the animal is engaging in active locomotion or if it is in a quiescent state (i.e. depending on the instantaneous behavioural state of the animal), the way perceived sensory input is translated into a behavioural action differs; or whether the origin of the sensory input arises from the external environment or from the animal's own movements (proprioception), the brain must recognise the source and plan the behavioural outcome accordingly (Huston & Jayaraman, 2011). These examples lead to the notion that, to achieve sensorimotor integration, nervous systems not only incorporate sensory information of the external environment with ongoing brain dynamics, but also require constant incorporation of the animal's own internal states and self-movement perception, to optimise the processing of information. Efforts in various species have made it possible to unravel some of these mechanisms. Examples include the concepts of population coding, the processing of information by the joint activities of a population of neurons (Georgopoulos et al., 1986; Georgopoulos et al., 1988; Onken et al., 2014; Ince et al., 2013; Panzeri et al., 2015; Dasgupta et al., 2017); or corollary discharge signals, efference copy signals of internally generated motor commands (encoding the animal's motor states) that are translated to other neurons, in order to predict the sensory effects of movement (Wolpert, et al., 1995; Miall et al., 1996; Straka et al., 2018). These mechanisms argue against the idea of a feedforward, sequential model of sensorimotor integration. Instead, they are supportive of models of

sensorimotor integration as being extremely dynamic and requiring constant relaying of feedback signals from and to the brain (Tsur et al., 2019).

Here, we chose *Caenorhabditis elegans* (*C. elegans*), a tractable organism with less complex behaviours and nervous system than most other animals, to study the functions and computational processes underlying fundamental principles of sensorimotor integration.

1.2. *C. elegans* as a model organism for fundamental neuroscience research

The nematode *C. elegans* feeds on bacteria and, in its natural habitat, lives in the soil, particularly in rotting vegetation. In laboratory conditions, it grows on agar plates cultured with *E. Coli* as a food source. In its adult form it is about 1mm long and it has a very short generation cycle. It develops from an egg, undergoes 4 larval stages (L1-L4), until it reaches its adult form in only about 3.5 days, depending on the temperature. Most of the individuals in a population are self-fertilizing hermaphrodites, although the frequency of males can be increased by various laboratory methods to enable the setting of genetic crosses. Hermaphrodites are composed of only 959 cells. Early efforts have made it possible to know the developmental lineage and identity of every cell in wild-type *C. elegans* (Sulston & Horvitz, 1977). Moreover, its completely sequenced genome and the panoply of molecular tools available nowadays for genetic manipulation, allow the easy production of transgenes by gonad injection. Despite its apparently simple biology, *C. elegans* shows a wide behavioural repertoire, including navigation, foraging, escape, avoidance, mating, egg-laying and learning. For the reasons mentioned here, and for the wide spectrum of work performed in neuroscience research in *C. elegans* every day, this model organism has been and continues to be an excellent and popular model to study fundamental principles of neurobiology.

1.3. The nervous system of *C. elegans*

By studying smaller nervous systems, one might aim to understand the fundamental biological principles that are the basis of complex behaviours. An invaluable resource to tackle the cellular and molecular complexity behind a nervous system is a comprehensive map of its neuronal connections (connectome). Huge effort has been put into getting a connectome in high-order organisms. A comprehensive map of neuronal connections of the brain allows scientists to manipulate neuronal circuits and, ultimately, understand how they integrate sensory information and encode behaviour at a bigger-scale. The *C. elegans* connectome has been thoroughly studied and mapped by electron

microscopy. ~7000 synapses between the 302 neurons compose the nervous system of a hermaphrodite (Varshney et al., 2011). The 302 neurons communicate between each other synaptically, using neurotransmitters or electrical GAP junctions, or extra-synaptically, using neuropeptides and neuromodulators (Bentley et al., 2016). The effects of extrasynaptic pathways employed by the worm's nervous system have not been included in the current synaptic connectome, and are largely unknown. Thus, an additional entire network of connectivity might explain neuronal interactions that are not explained by the synaptic connectome (Bentley et al., 2016).

Neurons are classically divided into sensory neurons, interneurons or motor neurons. Sensory neurons are exposed to the external environment and most of them can recognize a wide range of sensory cues each (Bargmann, 2006). Motor neurons innervate the muscle cells, and are ultimately responsible for the generation of behaviours, transforming a command state into a quantifiable behaviour. Interneurons are considered neurons that lack sensory endings or neuromuscular junctions, thus establishing communication between superficial sensory layers and motor neurons, by creating an extensive network of interactions among themselves and with motor neurons (Kaplan et al., 2018).

C. elegans' neurons are designated by three letters, for example, AIY, with a fourth letter indicating either a left-sided neuron - AIYL - or a right-sided neuron - AIYR. The nervous system of *C. elegans* is bilaterally symmetrical, with most neuron classes existing in pairs (left and right), with similar morphology, anatomical position and function. However, there are exceptions. For example, the sensory neuron AWC exhibits bilateral functional asymmetry, with one of the pairs (AWC^{ON}) being transiently activated by the addition of specific sensory stimuli, and the contralateral partner (AWC^{OFF}) being inhibited by it. Conversely, AWC^{OFF} responds to the removal of stimuli, while its partner AWC^{ON} is inhibited upon removal of the stimulus. Moreover, one of the pairs might sense specific stimuli that the contralateral partner does not (e.g. 2,3-pentanedione). For other stimuli (e.g. Isoamyl Alcohol or Bacterial Odour), both pairs show an odour-OFF response (Wes & Bargmann, 2001; Chalasani et al., 2007; Ha et al., 2010).

1.4. Neuronal activity imaging in *C. elegans*

Transgenes expressing genetically encoded calcium indicators, such as GCaMP, can be easily expressed in neurons of interest in *C. elegans*. GCaMP is a Ca^{2+} dependent GFP variant, whose conformation changes upon binding to Ca^{2+} ions that flow into the cell during an event of neuronal depolarization. This conformational change elicits the emission of green fluorescence when illuminated with blue light under a microscopy setup (Nakai et al., 2001; Chen et al., 2013). Other

markers, like mCherry and Scarlet, are not sensitive to calcium dynamics, and are thus used as neuronal markers.

The *C. elegans* nervous system does not have sodium channels. As an alternative, it uses voltage-gated potassium and calcium channels to generate graded activity (Goodman et al., 1998; Lindsay et al., 2011; Liu et al., 2018). This characteristic, combined with the transparency of *C. elegans*, makes calcium indicators very well suited to image neuronal activity in this organism.

With the advent of imaging techniques to record neuronal activity in *C. elegans*, microfluidic devices that hold the worm in place, while providing a controlled sensory environment, were developed. This tight control of the sensory input to be perceived by the animal, allows recording of the activity of specific neurons, or even the whole brain, at a single-cell resolution, during a constant or varying environment of atmospheric gases (Zimmer et al., 2009), odours or chemical agents (Chronis et al., 2007; Chalasani et al., 2007), allowing the assignment of patterns of neuronal activity to the effect of sensory cues.

Recordings of immobilised worms in microfluidic devices are often combined with paralytic chemical agents, such as the commonly used tetramisol. Being an agonist of acetylcholine, tetramisol promotes persistent contraction of the muscles as a means to achieve immobilisation of the worm. The effect of this chemical agent on the activity of cholinergic neurons, and ultimately on brain dynamics of the worm, is not fully known. As such, recent efforts have made it possible to achieve immobilisation of the worms without the need of drugs. Since histamine is not naturally synthetized by *C. elegans*, expression of a histamine-gated chloride channel from *Drosophila*, known as *hisCl*, in the worm's body wall muscle cells, with subsequent exogenous administration of histamine, enables persistent relaxation of the muscles as a way to achieve immobilisation. Expressing *hisCl* in specific cells has proven to be not only a powerful tool to achieve immobilisation, but also to achieve inhibition of specific neurons (Pokala et al., 2014).

Imaging of a single or a few neurons' activities in moving animals has also been developed by several groups in the *C. elegans* community. Brain-wide imaging in freely moving worms is the next big step to approach a closer representation of the global dynamics of the brain of *C. elegans* in a more naturalistic setting. The first efforts to image the whole-brain of the moving worm have started to appear in the community (Nguyen et al., 2016; Venkatachalam et al., 2016; Scholz et al., 2018), but implementing this technology poses a lot of challenges, and it is thus still at the beginning of its full potential.

1.5. Whole-Brain activity in *C. elegans* reveals a signature of the worm's major behavioural states

As aforementioned, brain-wide calcium imaging is a powerful technology to study the brain dynamics of the immobilised worm in real time. Using pan-neuronally expressed GCaMP in the nucleus of all neurons in the nervous system of *C. elegans*, it is possible to record the activity of the majority of *C. elegans* neurons simultaneously (Schrödel et al., 2013; Kato et al., 2015). These can be identified due to their stereotypical anatomical positions relative to each other and to the worm's major anatomical structures, as well as by their patterns of activity. Previous work from our lab used principal component analysis (PCA), a dimensionality reduction technique that groups neurons with correlated patterns of activity into principal components (PCs), to show that 3 PCs explain most of the variance in the dataset (Kato et al., 2015). In other words, most of the brain activity of restrained worms can be explained by just three dynamic signals (each of which include the activity of many neurons). If these 3 components are plotted against each other in 3D phase plots, it is possible to visualize a manifold representing recurring patterns of activity, along which the brain activity cycles **(Figure 1A)** (Kato et al., 2015).

Single neuron imaging in freely crawling worms, while simultaneously recording their behaviour, allowed the assignment of many neurons' activities to specific behavioural states. Our group observed that co-active neurons in the immobilised worm were all active during a particular behavioural state in the moving worm. Thus, the activity of neurons in restrained animals can be directly assigned to a specific behavioural state. For example, the activity of the interneuron RIM has been shown to be low during forward movement and high during reversing periods in the freely moving worm. The activity of RIM in the immobilised worm was shown to highly correlate with the activity of several other neurons, those also known to be active during reversing periods in the crawling worm. Hence, if RIM is active in the immobilised worm, one can interpret that as the worm's brain encoding a reversal manoeuvre (motor command signal). Different segments of the manifold represent the different motor command states of the animal: forward crawling, forward slowing, three reversal crawling command states, as well as ventral and dorsal turns (Kato et al., 2015) **(Figure 1B)**. Thus, by imaging the activities of individual neurons, one can have a readout of the behavioural state the worm is encoding at a particular moment. In conclusion, whole-brain calcium imaging at a single-cell resolution in *C. elegans* reveals a global brain signal that follows a stereotyped cyclical sequence of motor commands representing the worm's major action cycle.

This global signal showed to be largely robust to sensory stimulation. However, stimuli such as high/low O_2 levels (Kato et al., 2015; Nichols et al., 2017) or salt gradients (Luo et al., 2014) seem to influence motor command generation probability, thus showing to be integrated with the ongoing dynamics representing motor command states. These work shows that sensorimotor transformations occur and can be studied in immobilised conditions as well. It is suggested that sensory inputs cause, in a probabilistic manner, pre-patterned network activity that, despite being nearly indistinguishable from the ongoing dynamics, modify its dynamics for the sake of decision-making (Gordus et al., 2015, Kato et al., 2015). Effectively, the process of decision making, which ultimately leads to the execution of a certain behaviour, could perhaps be encoded in the continuous neural dynamic before the transition of motor command state (Kato et al., 2015). The existence of this state of decision between alternative motor commands probably depends on the result of the integration of ongoing motor dynamics with multiple sensory inputs, by interneurons.

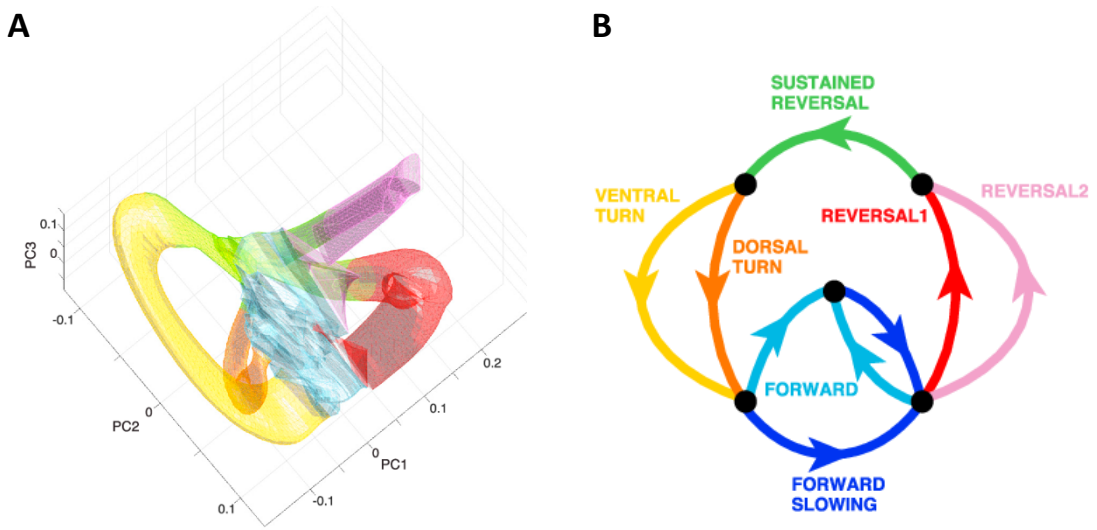

Figure 1: (A) Manifold representing the dynamical, recurring, cyclical pattern of activity of the brain, coloured by the six motor command states (forward crawling, three reversal crawling command states, as well as ventral and dorsal turns). **(B)** Flow diagram indicating the brain's motor command states, represented in the manifold. Figure modified from Kato et al. (2015).

1.6. Pan-neuronal imaging with nuclear-localized Ca^{2+} reporters does not reveal the full scope of neuronal interactions and activities of all neurons in the brain of *C. elegans*

Although whole-brain imaging in the worm has proven to be a powerful technology that enabled the discovery of important fundamental biological principles in the worm, as a global brain state underlying the *C. elegans* command sequence (Kato et al., 2015) and sleep behaviour (Nichols et al., 2017), there are some technical limitations to this technology.

In previous whole-brain data from our lab, recorded in immobilised worms, nuclear Ca^{2+} activity was not found in interneurons such as RIA or AIY (Kato et al., 2015). It was not clear why that is, as this could be due to biological constraints, e.g. these neurons only showing Ca^{2+} activity in its axonal processes, and/or technical constraints, e.g. previously used GCaMP variants not being sensitive enough to pick up potential weak nuclear activity fluctuations of these neurons. Additionally, it is possible that these neurons do not show Ca^{2+} dynamics related to motor states in an immobilised setup, perhaps because they require proprioceptive input. Indeed, the first option seems to be the case for the interneuron RIA. The neurite of the interneuron RIA has been shown to exhibit three compartments with independent calcium dynamics, two showing a positive correlation with the instantaneous head-bend angle of the worm - either dorsal or ventral bending -, and the third receiving sensory input (Hendricks et al., 2012). The sensory-encoding compartment modulates the motor related dynamics in RIA and allows the worm to steer towards attractive sensory cues (Liu et al., 2018). Moreover, it has been shown that the neurite of RIA shows Ca^{2+} dynamics in immobilised worms, indicating that the lack of signals in the nucleus is not due to a requirement for movement (Hendricks et al., 2012). Although the mechanisms underlying sensorimotor integration in AIY are not as well studied as in RIA, previous work showed that AIY exhibits Ca^{2+} activity in its axonal processes as well (Chalasani et al., 2010; Larsch et al., 2013; Li et al., 2014; Liu et al., 2018), while there are no reports of Ca^{2+} dynamics in its nucleus or soma. This led us to ask whether this mechanism of compartmentalisation of sensory and motor signals also occurs in AIY. A detailed measurement of Ca^{2+} dynamics along the dendro-axonic process of AIY has never been performed and the location from where Ca^{2+} signals were measured in previous studies is not completely clear, leading to an incomplete knowledge of how AIY integrates both motor and sensory information within its cellular space. Thus, here, we hypothesize that AIY might show compartmentalised activity along its dendritic-axonal processes, as it is the case for the interneuron RIA, as a way to achieve sensorimotor integration within its subcellular space. As an alternative hypothesis, AIY could multiplex these signals by showing activity patterns that are computed from both motor and sensory inputs.

Imaging neuronal activity in non-constrained animals gives a more realistic representation of neuronal activities in a natural environment since, contrary to imaging in immobilised animals, worms are not deprived of proprioceptive feedback signals. However, if imaging of worms immobilised in microfluidic devices appeared initially due to the technical challenges of imaging freely moving worms, today is a powerful tool to distinguish between motor command signals and proprioception. This is possible by comparing individual neurons' activities both in immobilised and unrestrained conditions.

In conclusion, whole-brain imaging does not reveal the full scope of neuronal activity of the worm's brain. Surpassing these limitations might be important to unravel interesting answers regarding how sensorimotor integration is achieved by the nervous system of *C. elegans*.

1.7. Sensorimotor integration in *C. elegans*

Classical models describe the process of sensorimotor integration in *C. elegans* as following a rather intuitive sequential neuronal flow of information: a sensory cue is first perceived by sensory neurons and its passed on to 1st and 2nd layer interneurons (Gray et al., 2005), these responsible for processing the received signals; the signal finally converges to pre-motor interneurons and motor neurons, ultimately activating the muscles and producing the appropriate behavioural response. Pre-motor interneurons receive a large amount of input and represent a bottleneck to the motor periphery in the ventral nerve cord; hence they are commonly thought to function as command neurons between the processing of external stimuli and the generation of behavioural responses (White et al., 1986; Kaplan et al., 2018).

In light of this, it seemed logical to assume that the shallow network of primary sensory interneurons was mainly responsible for receiving sensory input from upstream sensory neurons and, perhaps, transform those signals before outputting them to the next layer. Indeed, several studies with controlled stimuli delivery to immobilised worms have shown that first layer interneurons receive sensory input directly from upstream sensory neurons (Clark et al., 2006; Chalasani et al, 2007; Chronis et al., 2007; Chalasani et al., 2010; Larsch et al., 2015; Oda et al., 2011; Kunitomo, et al., 2013; Guillermin et al., 2017). However, work in the past decade has been challenging such an intuitive view of sequential neuronal flow of information. Surprisingly, calcium imaging studies in freely moving worms revealed that the activity of all four 1st layer interneurons (AIA, AIB, AIY, AIZ) is also linked to the worm's instantaneous behaviour (Piggott et al., 2011; Flavell et al., 2013; Li et al., 2014; Luo et al., 2014; Kato et al., 2015; Laurent et al., 2015). Whether all these interneurons show the same modulation to behavioural states in immobilised worms still remains to be studied. If that happens to

be the case, then the behavioural state representation found in these neurons could not be solely due to an integration of proprioceptive input (from the worm's own movement). Finding such representation in primary sensory neurons is not trivial, as it could support the idea that neurons as upstream as primary interneurons are involved in the modulation of motor states. In this case, somehow, these interneurons would be responsible for performing the computations necessary to integrate sensory input from the external environment into an ongoing brain-wide motor signal, modifying its dynamics and influencing motor command generation probability (Kaplan et al., 2018). Collectively, these studies challenge the common layered feed-forward scheme of information transfer in the worm's brain. Instead, they point to a view where interneuron activity is extremely dynamic, establishing an extensive network of interactions among 1st and 2nd layer interneurons and motor neurons (Kato et al., 2015; Kaplan et al., 2018).

In order to chemotax towards attractive sensory environments, *C. elegans* exhibits biased random walks, an increase in the duration of forward runs and decrease in the frequency of reversals to navigate towards preferred environments (Albrecht&Bargmann, 2011), as well as klinotaxis, the behaviour of head steering to preferred directions during forward movement (Iino&Yoshida, 2009). The fundamental principles behind sensorimotor transformation that influence the worm's behaviour to, for example, cause an increase or decrease in the frequency of reversals, are still largely unknown. The interneuron AIY is a particularly interesting neuron to tackle these questions, for reasons that will be described below.

AIY receives sensory input from several (9) sensory neurons (see **Supplementary Figure S1**), and it is the major postsynaptic partner of the sensory neurons AWC, ASE and AFD. Despite having only five olfactory neurons, *C. elegans* can respond to dozens of odours, both attractive and repellent (de Bono & Maricq, 2005). To achieve that, each olfactory neuron in *C. elegans* can detect several sensory cues. For example, AWC recognizes several volatile odorants, as well as bacterial odours (Chalasani et al., 2007, Ha et al., 2010). In response to the removal of an attractive odorant, AWC^{OFF} depolarizes (odour-OFF response) and stimulates reversal occurrence, thus contributing to a local search behaviour upon food removal and directing chemotaxis towards attractive stimuli (Larsch et al., 2013; Chalasani et al., 2007; Albrecht and Bargmann, 2011; Gray et al., 2005). AWC further inhibits AIY via glutamate-gated chloride channels, while activating AIB via AMPA-type glutamate receptors. Upon AWC inhibition by stimuli, AIY gets activated, thus seeming to invert the sensory polarity of an odour-OFF response from the sensory neuron AWC into an odour-ON response (Chalasani et al., 2007; Chronis et al., 2007). The circuit mediating olfactory attraction via AWC is very well characterized **(Figure 2)**. As such, in this

study, we chose AWC as a readout of the sensory input transferred to AIY while using controlled sensory environments of either isoamyl alcohol or a bacterial odour, in immobilised experiments, or a bacterial food lawn, in freely moving experiments. These are sensory cues to which the worms are attracted and are known to detect by employing the above described olfactory circuit.

Receiving such a wide array of sensory input, AIY has been reported to have a central role in chemotaxis (Kocabas et al., 2012), by recruiting downstream circuits to drive motor programs that lead the worm towards the attractive stimuli. Previous studies have shown increased forward movement upon laser ablation/inhibition of AIY, leading to the idea that AIY controls the duration of forward runs (Tsalik and Hobert, 2003; Wakabayashi et al., 2004; Gray et al, 2005). In more recent studies, it was possible to measure AIY cytoplasmic activity in freely moving animals. Here, AIY activity was shown to correlate negatively with the onset of reversals (Flavell et al., 2013; Li et al., 2014; Luo et al., 2014) and to correlate positively with increased locomotion speed (Li et al., 2014; Luo et al., 2014), as well as direction of locomotion (Kocabas et al., 2012). AIY was reported as inhibiting reversal occurrence in a binary manner (all-or-none fashion) by establishing inhibitory connections with the downstream neuron AIZ, and as promoting increased locomotion speed, in a graded form, by establishing excitatory synapses with the downstream interneuron RIB (Li et al., 2014). However, AIY activity related to motor states of the worm was never measured in immobilised animals, so it is still unclear whether this neuron requires proprioceptive feedback to modulate motor states, or whether AIY engages in the spontaneous dynamical activity that is coordinated with the worm's global brain signal to encode motor command states (Kato et al., 2015). If proprioceptive feedback is not a necessary requisite for AIY to modulate motor states in the worm, how this single neuron integrates both motor state information with sensory signals can be studied in immobilised worms as well. Brain dynamics of constrained worms is known to be very different from those observed in freely moving worms. A striking example of this is the duration of reversal states, known to be significantly longer in immobilised worms. This is hypothesized as being a mechanism for the worm to maintain its attempt at reversing, until the motor command that was encoded has been completed (Kato et al., 2015). As such, how sensorimotor transformation is computed in AIY could differ in immobilised versus freely moving worms.

Furthermore, AIY establishes multiple synaptic connections with the downstream interneuron RIA, which is majorly involved in modulating steering of heading angles (Hendricks et al., 2012). AIY has been shown to relay sensory information to RIA, ultimately influencing the modulation of klinotaxis (Hendricks & Zhang, 2013; Liu et al., 2018). The reasons above put AIY as an extremely important

neuronal hub to modulate short-timescale behaviours (reversal frequency, locomotion speed and head steering) that ultimately allow the worm to exhibit long-timescale behaviours to exploit variable sensory environments.

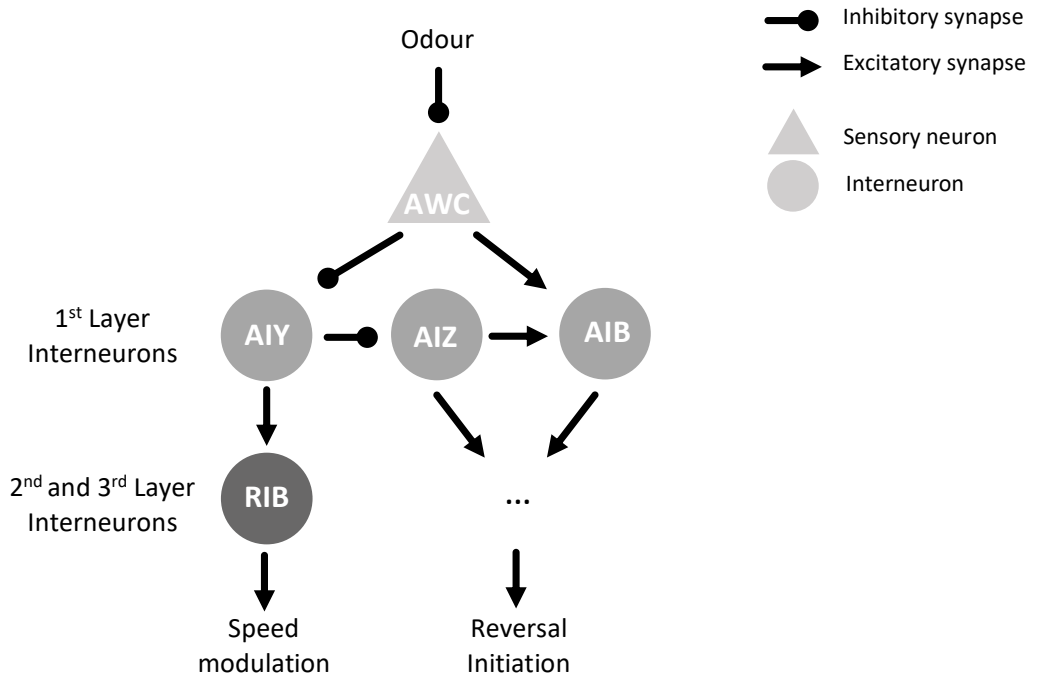

Figure 2: Simplified scheme of anatomical connections between AWC sensory neurons and downstream interneurons. AWC is inhibited by odours. AWC's inhibitory connection to AIY causes AIY to be activated in the presence of odours. Conversely, AWC establishes an excitatory connection to AIB. AIY promotes speed increase through RIB and reversal inhibition through the interneuron AIZ. AIZ and AIB recruit downstream circuits to promote reversal occurrence.

1.8. Aims of the study

Understanding how nervous systems integrate sensory information from the surrounding environment with ongoing brain dynamics, and the computations performed within their brains to ultimately elicit appropriate behaviour, is a long-standing question in behavioural neuroscience, with largely unknown fundamental mechanisms. Here, we perform calcium imaging to record the activity of AWC, a sensory neuron essential for chemotaxis to a wide array of stimuli and to induce local search behaviour, and its major postsynaptic partner, AIY, a fundamental interneuron in *C. elegans* to coordinate behavioural responses, allowing the worm to chemotax towards attractants. Using spinning-disk confocal microscopy, we imaged both immobilised and freely moving worms, aiming to address the following questions/hypotheses:

1. Does AIY activity show motor state modulation in immobilised animals, as in freely moving animals?

2. How does AIY achieve sensorimotor integration? How are motor states combined with sensory signals received from upstream synaptic partners?

   Two distinct hypotheses are proposed as answers to this question:

   2.1. Sensory activity is gated by behavioural state: AIY encodes sensory information, but only when engaged in forward movement.

   2.2. Gain control: the sensory gain or dynamic range of AIY is modulated by behaviour.

3. How is Ca^{2+} activity distributed in the cytoplasm of AIY? Does AIY show compartmentalised activity in its axonal processes?

4. How does sensorimotor transformation in AIY vary between immobilised and freely moving animals?

   As part of the answer to this question, we aim to test the validity of the following hypothesis:

   4.1. Precise motor control: the widespread motor command representation in worms is integrated with proprioceptive feedback to optimize the execution of behaviour.

2. RESULTS

2.1. Strain Characterisation

A transgenic line of worms expressing GCaMP and Scarlet under the promoter *ttx-3*, a promoter known to exhibit specific expression in AIY (Hobert et al., 1997), was created, following standard microinjection protocols for extrachromosomal arrays. Additionally, GCaMP and Scarlet were expressed under the promoter *odr-1*, for specific expression of GCaMP and Scarlet in the sensory neuron AWC, along with mCherry expression under the promoter *flp-17*, to drive expression in the sensory neuron BAG. BAG::mCherry was used as a co-injection marker (for selection of transgenic worms during strain maintenance) and as a bright marker that enabled centering of the worm's head on the microscope objective in freely moving imaging experiments (Faumont et al., 2011).

Extrachromosomal arrays are plasmids, containing the genes of interest, exogenously injected into the animals. Since extrachromosomal arrays are not incorporated into a chromosome, they are not transmitted with a 100% fidelity to the progeny. Thus, screening for transgenic animals when multiple arrays (expressing different genes of interest) are present in a strain might be challenging, as it is the case of the strain used in this study, which is discussed further below. Additional information about injected concentrations of the plasmids (containing the transgenes of interest) and genetic background of the strains used in this study can be found in **Supplementary Table S1**.

Due to inefficiency of the construct for GCaMP expression in AIY (under the promoter *ttx-3*), the achieved expression pattern in the cytoplasm of AIY proved to be weak. Extensive work was performed to overcome the weak pattern of GCaMP expression in AIY, including: dozens of injections with variable ranges of concentrations of the same construct as the one used to obtain the strain used for imaging in this study; a construct with a modified sequence of the *ttx-3* promoter; GCaMP and Scarlet expression driven by the Cre-LoxP system, using combinations of promoters uniquely overlapping in AIY (more information about part of all the generated strains can be consulted in **Supplementary Table S2**). The strain used in this study yielded the strongest GCaMP expression pattern of all created strains, even though it has proved to be sup-optimal for some of the goals of the study, as it will be further discussed.

Chemotaxis assays in the presence of a gradient of food were performed, in order to ensure that the transgenic strain could detect bacterial odours and showed normal chemotaxis behaviour. We performed experiments in the presence of a bacterial lawn of *E. coli* OP50 resuspended at an absorbance of 20 at 600nm (OD20). Control experiments, without bacterial food, were also conducted

(see **Supplementary Figure S4**). The strain showed to be able to detect bacterial odours, as it is shown by the higher chemotaxis index in the experiments in the presence of a lawn of bacterial food, in comparison to control assays (**Figure 3**) (for further details, see *Materials, Experimental Methods and Data Analysis* section).

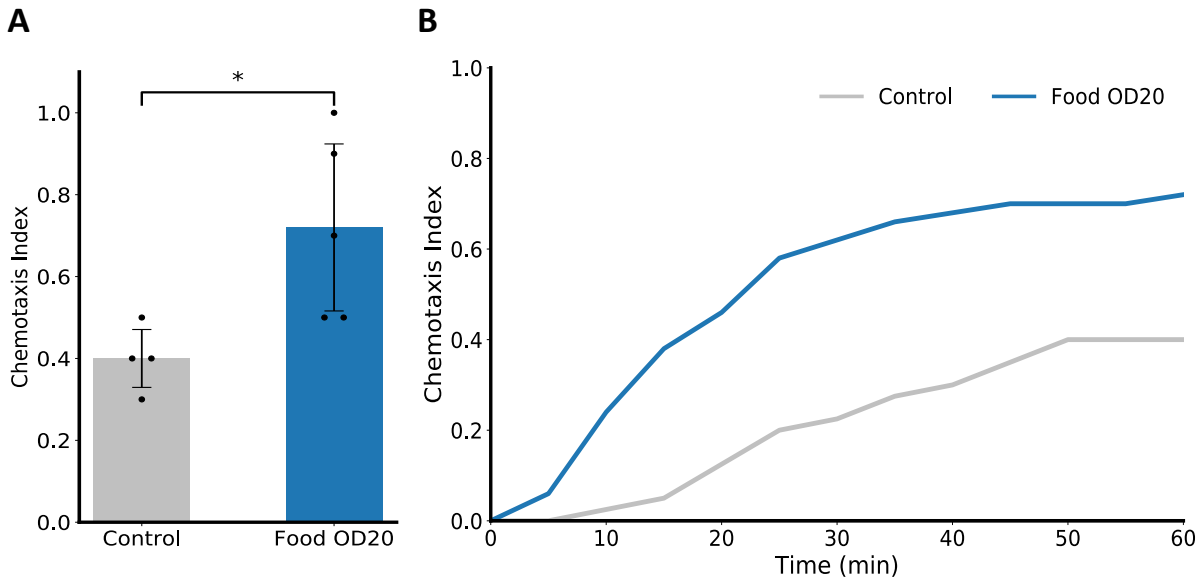

Figure 3: Chemotaxis assays to bacterial food. **(A)** Mean chemotaxis index ± SD for transgenic animals (strain ZIM2097) in the presence of a bacterial gradient (Food OD20) (n=5/50) and in an isotropic environment, without the food gradient (Control) (n = 4/40). N is indicated as follows: *number of assays / number of total animals*. Chemotaxis Index (CI) was calculated according to the following formula: CI = # worms that reached the food lawn / # worms placed in the arena. *p<0.05, Mann-Whitney test. **(B)** Mean chemotaxis index calculated every 5 minutes throughout the total length of the recording (60 minutes).

Later, this strain was crossed with a line expressing GCaMP in the interneuron RIM. RIM was shown to exhibit a binary relationship to the behavioural state of the worm (low during forward states and high during reversing periods), therefore allowing to read out the instantaneous behavioural state of the worm from its activity. This interpretation was confirmed by imaging many neurons, simultaneously, in immobilised worms, and by imaging neurons, one by one, in crawling worms (Kato et al., 2015), as aforementioned.

Additionally, this strain was also crossed with another line of worms expressing *hisCl*, a histamine-gated chloride channel from *Drosophila*, under the promoter *myo-3*. This promoter drives the expression of the protein *myosine-3* in the muscle cells of the body wall muscles. Since AIY is known to be a cholinergic and glutamatergic neuron, by using this approach we aimed to achieve

immobilisation of the worm (by relaxing all of the worm's body wall muscles), while ruling out the possibility of tetramisol, an agonist of acetylcholine typically used for paralysis, interfering with normal AIY function.

2.2. Immobilised Imaging in the Absence of Fluctuating Sensory Input

2.2.1. Neuronal activity of AIY is dominated by motor-state representations, in the absence of fluctuating sensory input

We first started by asking whether AIY shows fluctuations in activity related to motor command states. For this, we recorded immobilised worms in an inverted spinning-disc confocal microscope setup and achieved an acquisition rate of ~2.3 volumes/second (for further details, see *Materials, Experimental Methods and Data Analysis* section). The animals were immobilised by the *myo-3*::HisCl approach previously discussed, and constrained in a microfluidic device that allows the maintenance of a constant gaseous environment of 21% of O_2 (henceforth also called Oxygen Chip) and deprived of fluctuating sensory input **(Figure 4A**).

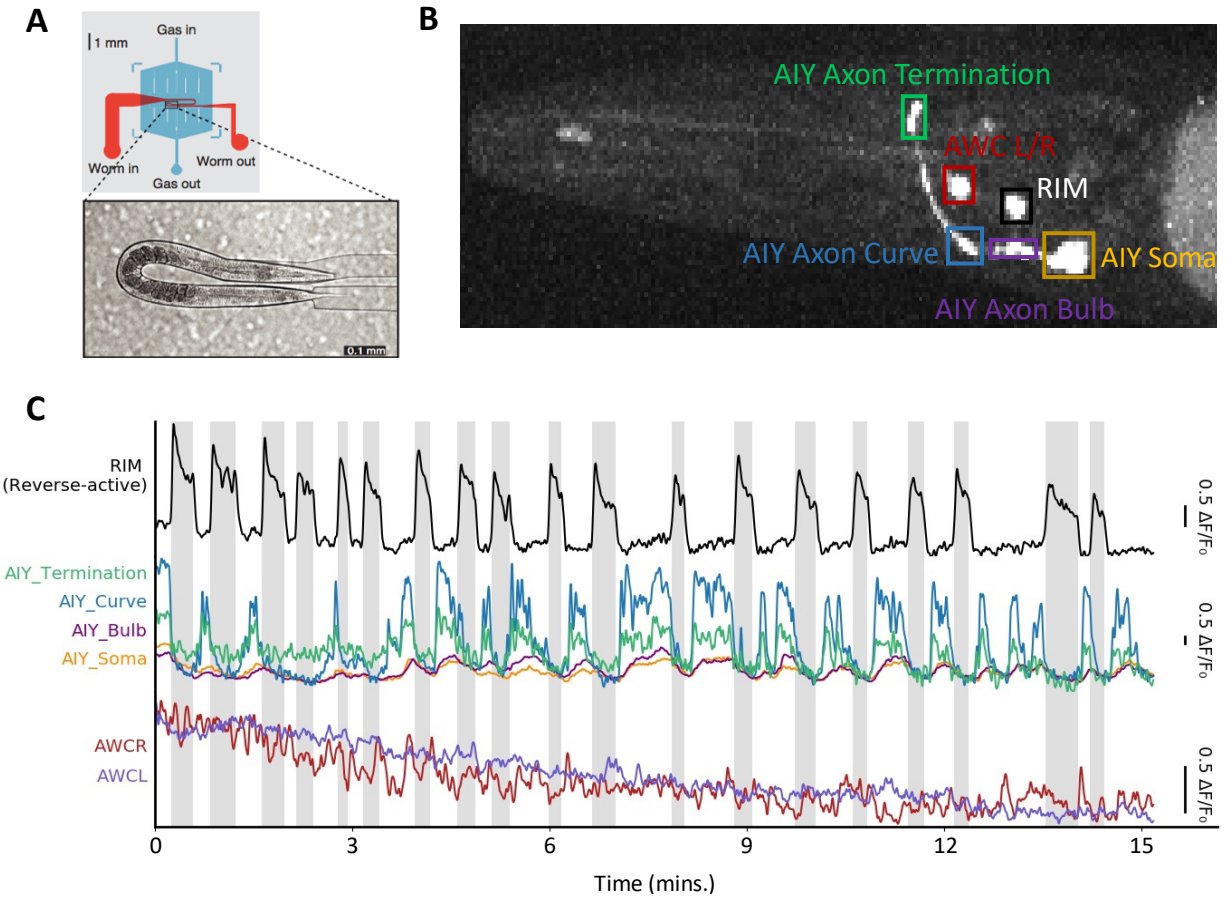

Figure 4: Ca^{2+} imaging in the absence of fluctuating sensory stimulation. **(A)** Technical scheme of microfluidic device used for Ca^{2+} imaging in immobilised worms, in the absence of sensory stimulation (retrieved from Kaplan et al., 2018). **(B)** Maximum Intensity Projection (MIP) from volumetric confocal data of the strain used for imaging of immobilised worms.

(legend continued on next page)

These gaseous conditions are standard for imaging in microfluidic devices, thus the results obtained here are comparable with previous imaging experiments. We recorded the Ca^{2+} activity of AIY and used the activity of the premotor interneuron RIM, a neuron whose activity is known to correlate positively with reversal events, in an all-or-none fashion, to decode the behavioural state being encoded in the worm's brain (**Figure 4C** for example traces of a Ca^{2+} imaging recording).

AIY enters the nerve ring of the worm from the ventral side, runs dorsally within the nerve ring until it meets its contralateral neuron through a GAP junction (see **Supplementary Figure S2**). In this study, AIY Ca^{2+} signals were measured in the cell body, previously reported to show no or very shallow fluctuations of activity (Li et al., 2014; Luo et al., 2014), and in three different regions along the neurite of the neuron: the *axon bulb*, an enlarged region of AIY neurite close to the soma; the *axon curve*, a region where AIY neurite curves and enters the nerve ring from the ventral side, known to be densely rich in synaptic input (see **Supplementary Figure S3**); and the *axon termination*, where AIY neurite meets its contralateral partner **(Figure 4B)**.

All neuronal activity traces from the recordings obtained in this experimental setup, used for subsequent analysis, can be seen in **Supplementary Figure S6**. See **Supplementary Movies S1-S4** for Maximum Intensity Projection of example recordings.

We found a dominant signal governing the activity of AIY to be negatively correlated with the activity of RIM (**Figures 5B** and **5C**). Interestingly, all regions of AIY neurite from where Ca^{2+} signals were measured showed activity tightly coupled to motor command states, including the activity from the cell body of AIY, where we could still reliably observe decreased activity during reversals (**Figure 5A**). This indicates that the soma of AIY does show fluctuations in activity. This fact may have been missed in previous studies due to previous available GCaMP variants not being sensitive enough to Ca^{2+} fluctuations in the cells. Additionally, these findings indicate the link between AIY activity and the internal behavioural state of the worm is not due to re-afferent input (proprioception), as these experiments were performed in constrained worms, deprived of fluctuating proprioceptive inputs. Interestingly, we observed no coupling of the activity of sensory neuron AWC to motor command states (**Figures 5A).**

In the figure are indicated the locations of the soma and the three measured regions along the neurite of AIY (*Axon Bulb*, *Axon Curve*, *Axon Termination*), AWC and RIM for the green (GCaMP) channel. **(C)** Neuronal activity traces of an example animal. Grey shaded regions denote periods of reverse motor-state, inferred from the activity of RIM. Scale bars on the right represent 0.5 $\Delta F/F_0$.

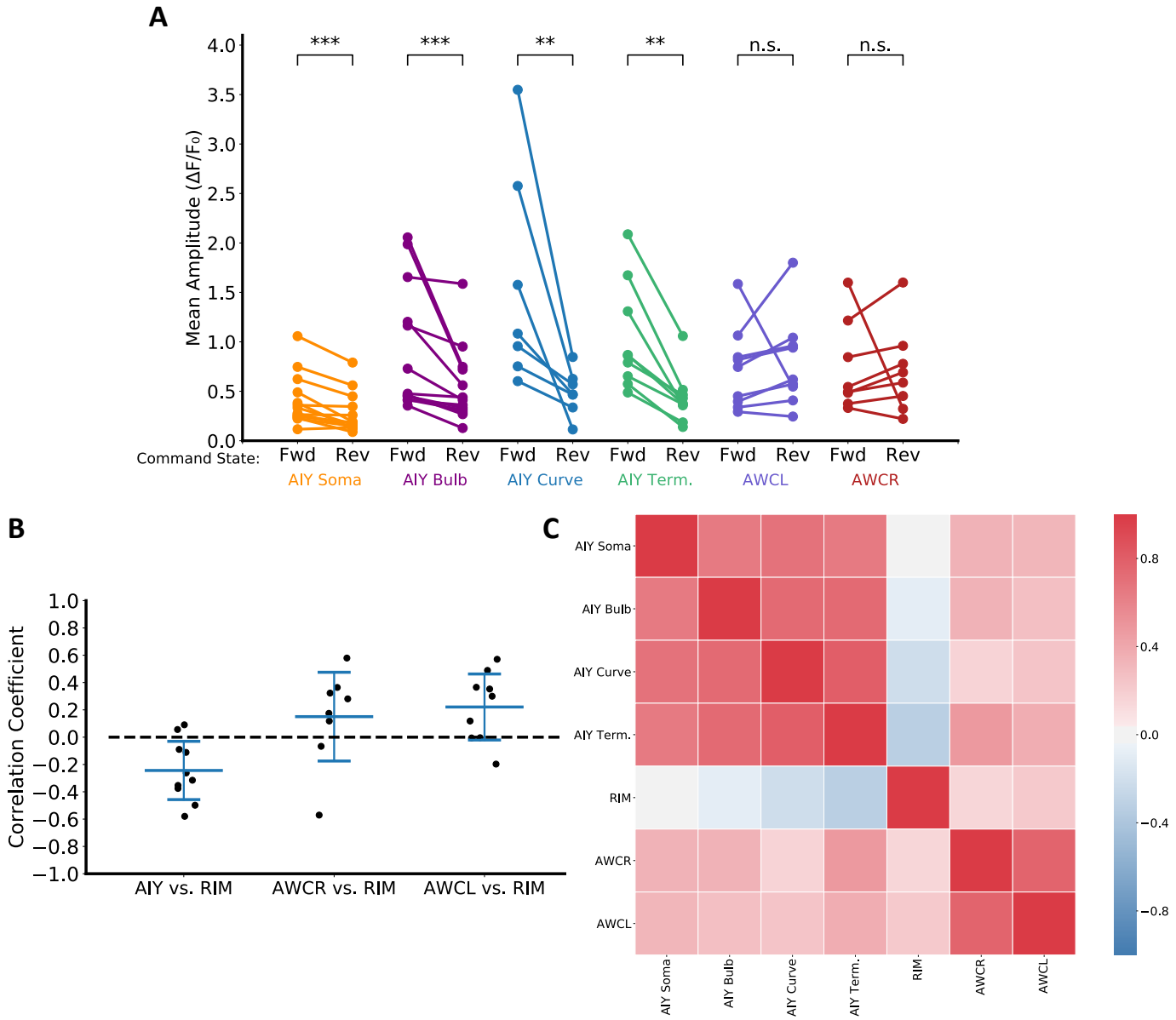

Figure 5: AIY activity is dominated by a motor-state representation encoded by the worm's brain. **(A)** Quantification of the mean $\Delta F/F_0$ during Forward (Fwd) and Reverse (Rev) periods, for all measured AIY regions: AIY Soma (n = 14), AIY Axon Bulb (n = 13), AIY Curve (n = 7) and AIY Termination (n = 9) , and AWC - Left (AWCL) (n = 9) and Right (AWCR) (n = 8) pairs. **p<0.01, ***p<0.001, Wilcoxon matched-pairs signed rank test; n.s., not significant. **(B)** Scatter plot of Pearson correlations between AIY (n=10), AWCL (n=9) or AWCR (n=8) and RIM. Bars indicate the mean correlation ± SD. Correlations tested positive for significance using a Wald Test with t-distribution. **(C)** Heatmap of Pearson correlations between all measured regions in AIY, AWC (Left and Right pairs) and RIM. All correlations tested positive for significance using a Wald Test with t-distribution. For more details, see *Materials, Experimental Methods and Data Analysis* section.

2.2.2. AIY plays a role in modulating the transition of motor command state

We then asked whether AIY plays a role in modulating the behavioural state of the worm. To tackle this question, we started by looking at the activity of AIY at the onset of motor command state transitions (forward to reverse command state and reverse to forward command state) (**Figure 6**). RIM rises precisely align with reversal onset (Kato et al., 2015) (also showed in **Figure 6**, top row; data pooled from the data used in this study). We observed strong changes in the activity of AIY before the transition of motor state, supporting the hypothesis that the drop in activity of AIY occurs before the onset of a reversal manoeuvre and, conversely, an increase in the activity of AIY precedes the end of a reversal (**Figure 6**, middle rows) (see arrow in **Figure 6, 3rd row**, for indication of activity change before the onset of transition of motor command state). We did not observe a modulation of AWC activity at the onset of motor command state transitions (**Figure 6**, bottom row), further confirming that AWC activity does not appear to be coupled to motor command states in restrained animals.

To further study the hypothesis that AIY modulates behavioural states, we performed cross-correlation analysis between vectors of the derivatives of the normalised traces of AIY and RIM (**Figure 7**). Working with vectors of the derivatives of the normalised Ca^{2+} traces gives, in some cases, better measures of relationships between neurons and of their activities to behaviour (Kato et al., 2015). Here, we observed the maximum degree of correlation to occur with a delay of ~ 0.85 seconds when the Ca^{2+} activity traces of RIM were shifted in relation to the traces of AIY. This observation suggests that the Ca^{2+} activity of AIY precedes a reversal manoeuvre before the command state signal reaches downstream interneurons and motor neurons. Hence, AIY likely plays a role in modulating the transition of internal behavioural states of the worm.

Interestingly, the absolute correlation between the activity of AIY and RIM was not drastically high (see **Figures 5B** and **5C**). One factor that can be contributing to lower this correlation is photobleaching of the neuronal traces due to exposure of the animals to high laser intensity powers under the microscopy setup. In these datasets, we did not correct the neuronal activity traces for photobleaching in the post processing analysis (for more details, see *Materials, Methods and Data Analysis section*). Depending on the level of brightness of the neurons, photobleaching can affect them differently, leading to drifting of both neurons' activity traces throughout the period of the recording and, ultimately, contributing to a lower correlation between them. Nonetheless, we found clear evidence for a tight coupling of the activity of AIY to motor command states, quantified in **Figures 5A**, **Figure 6** and **Figure 7**.

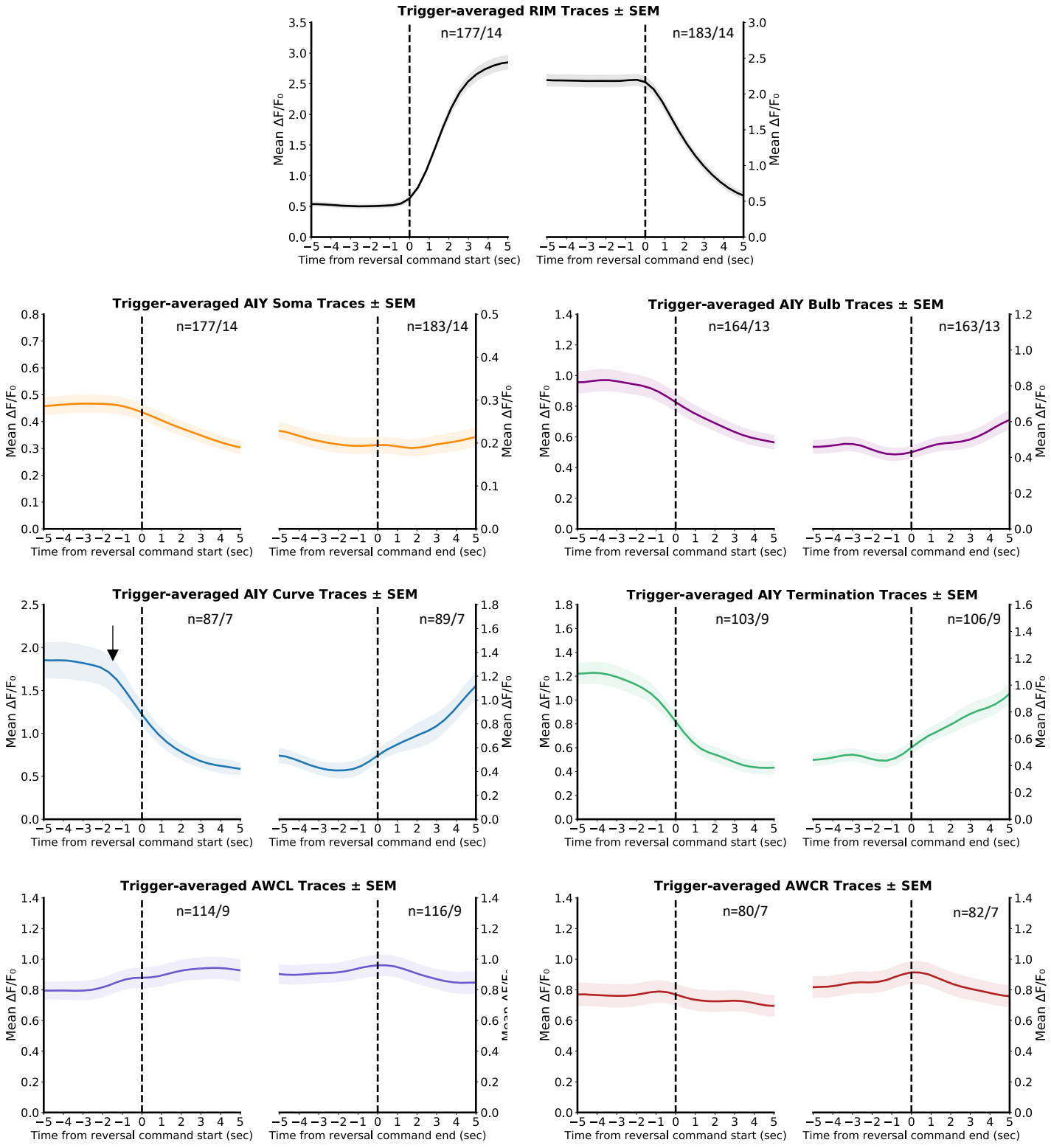

Figure 6: Trigger-averaged $\Delta F/F_0$ ± SEM traces from recordings of RIM (top row), AIY soma, AIY Bulb, AIY Curve, AIY Termination (middle rows) and AWC – Left and Right pairs (bottom row) - activities, aligned to forward-to-reverse (left) and reverse-to-forward (right) command state transitions. The n for each measured region is indicated in the corresponding panel as *number of motor state transitions / number of pooled animals.*

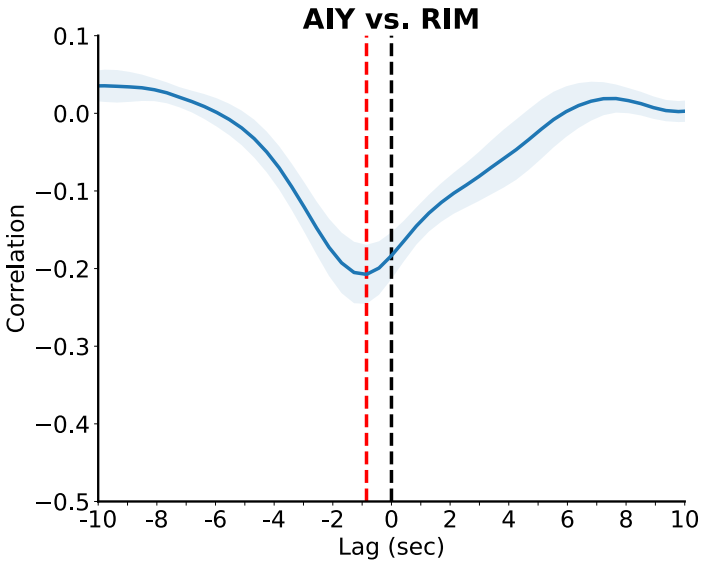

Figure 7: Average cross-correlation ± SEM between the neurite of AIY (reference neuron) and RIM (shifted neuron) Ca^{2+} activities (n=10). Cross-correlations were performed between vectors of the derivatives of the corresponding normalised Ca^{2+} traces. Sharp drop in correlation indicates that AIY correlates negatively with the activity of RIM. Red dashed line indicates lag (displacement, in seconds, of the activity of RIM relative to AIY's) of the highest absolute correlation value. For more details, see *Materials, Experimental Methods and Data Analysis* section.

2.2.3. AIY does not show compartmentalised motor-state related activity along its neurite

As previously addressed, a detailed study of Ca^{2+} dynamics along the neurite of AIY has been lacking, leading to signals being measured in different regions across studies, masking potential compartmentalised activity in the neurite of AIY. Thus, by measuring the signals along the neurite of AIY, we sought to validate the hypothesis that AIY employs a strategy of signal compartmentalisation along its neurite.

From **Figure 5A**, we observed a clear decrease in activity of all AIY structures during reversing periods, meaning that all neuronal regions encode motor command signals. Furthermore, correlations between all AIY structures were high (**Figure 5C** and **8A**), suggesting that the Ca^{2+} dynamics in all regions is similar. To further study this, we performed cross correlation analysis between all measured structures in the neurite of AIY (**Figure 8B**). A significant time-lag was observed when cross-correlation was performed between the Soma or the *Axon Bulb* and any other structure. Although this could be indicative of different patterns of activity, we do not think that is the case, as correlations between all AIY structures were high and differences were not statistically significant (**Figure 5C** and **Figure 8A**). Instead, we hypothesize that these differences could be due to slower Ca^{2+} dynamics observed in the soma and *Axon Bulb* regions, which is both suggested by observing the neuronal traces (see **Supplementary Figure S6**) and by **Figure 9**, where it is possible to observe an increased change in amplitude (from forward to reversing states) in the *Axon Curve* and *Axon Termination* regions, statistically significant from the change in activity observed in the Soma and *Axon Bulb*. Altogether, we did not find evidence for compartmentalised Ca^{2+} dynamics relative to motor command states along the neurite of AIY.

These results likely explain why previous whole-brain studies, measuring pan-neuronal nuclear activity, have not picked up this motor state related activity in AIY: the dominant, motor state encoding signal governing AIY Ca^{2+} activity is more strongly encoded in the neurite, with the cell body showing very shallow fluctuations in activity **(Figure 9)**.

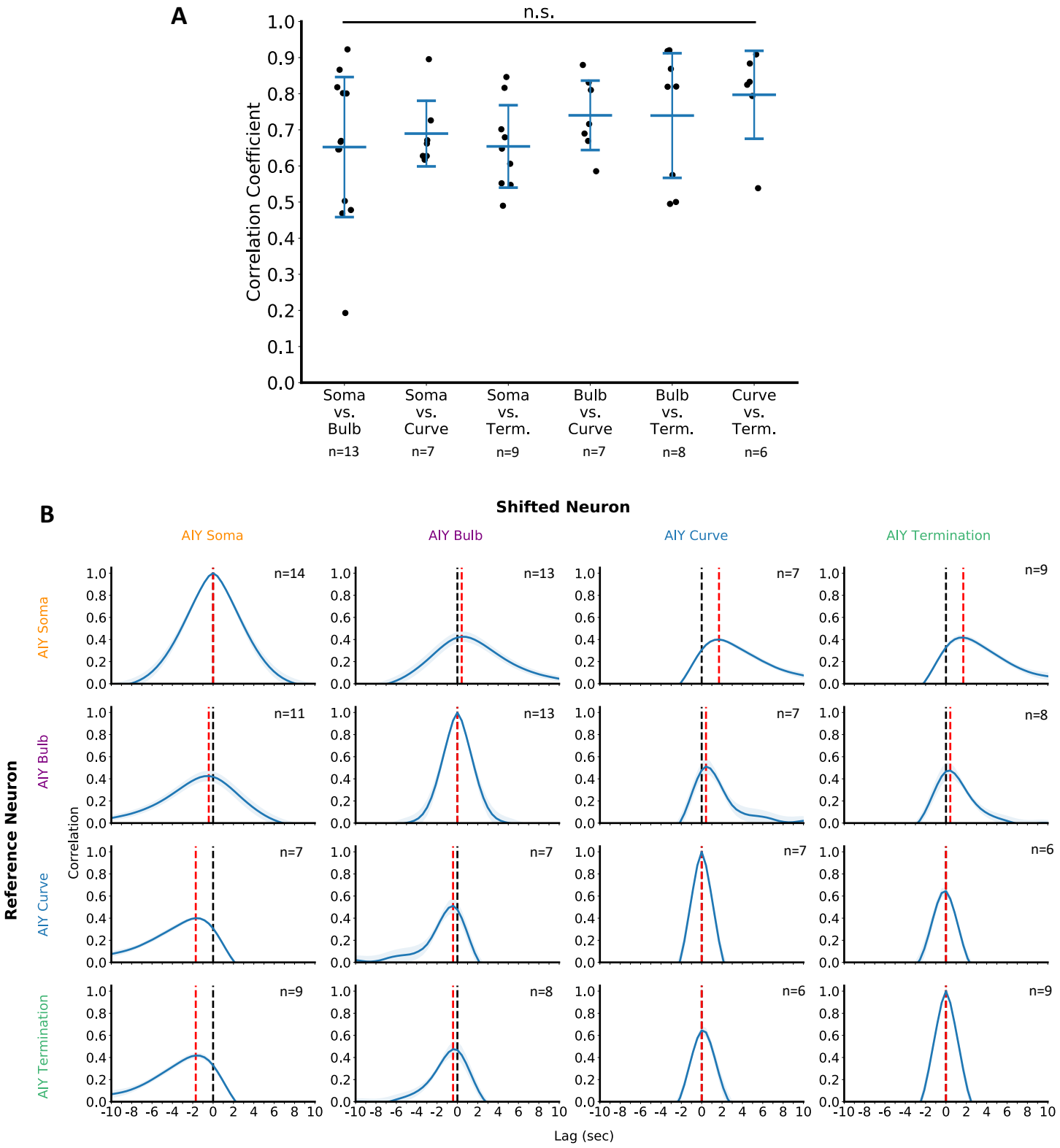

Figure 8: (A) Scatter plot of Pearson correlations between all AIY measured regions. Bars indicate the mean correlation ± SD. *n.s., Mann-Whitney test. All correlations were tested positive for significance using a Wald Test with t-distribution. **(B)** Matrix of average cross-correlations ± SEM between all AIY measured regions.

(legend continued on next page)

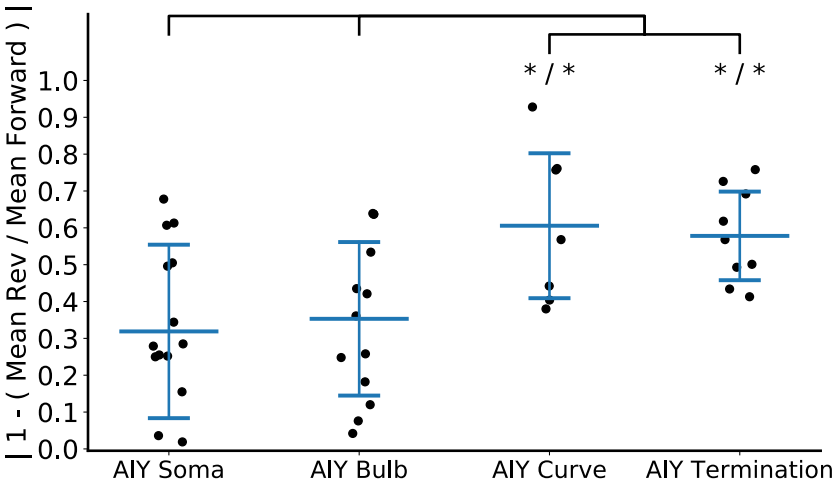

Figure 9: Absolute value of the ratio between the average $\Delta F/F_0$ value during reversal command periods and forward command periods, subtracted to the unit, for all AIY measured regions – AIY Soma (n=14), AIY Bulb (n=13), AIY Curve (n=7) and AIY Termination (n=9). Each data point represents a different animal. Bars indicate the mean value ± SD. *p<0.05, Mann-Whitney test.

Cross-correlations were performed between vectors of the derivatives of the corresponding normalised Ca^{2+} traces. Red dashed lines indicate lag (displacement, in seconds, of the shifted neuron relative to the reference neuron) of the highest absolute correlation value. N is indicated in the corresponding panel.

2.2.4. AIY does not appear to be modulated by AWC in an immobilised setup

Given the tight coupling between AWC and AIY predicted by the connectome of *C. elegans*, we sought to determine if the spontaneous activity that we and others consistently observe in AWC (in an environment deprived of fluctuating sensory stimulation) would affect the activity of the downstream neuron AIY. We observed some variability in AWC activity traces across datasets. In some, AWC activity appears to be quite stable, with some shallow local changes; in others, we observed peaky, variable traces, with strong fluctuations in activity (see **Supplementary Figure S6**). This variability in AWC responses is consistent with whole-brain data acquired in our lab (Kato et al., 2015). Additionally, gradually decreasing AWC traces are observed in most of the datasets. In these experiments, we did not starve the worms previously. It is hypothesized that this gradual AWC activity decrease is a prolonged response to the removal from food, that is sustained for several minutes. Nonetheless, we sought to determine whether the faster spontaneous AWC activity fluctuations correlated with AIY changes in activity.

Correlations between AWCL or AWCR and AIY were low (**Figure 5C** and **Supplementary Figure S5**). We performed cross correlation analysis between vectors of the derivatives of AWC traces and of AIY traces (**Figure 10**). Here, we did not find any significant correlation at a lag of 0, as we did not find any significant lag between the correlation of both, suggesting that in these conditions AIY is not entrained with the activity of its upstream sensory neurons AWC. This finding is both surprising and interesting if we think that AIY is the major postsynaptic neuron of AWC, receiving multiple synaptic connections from it. This result indicates that these synapses might not be effective under the conditions the worm is exposed to during imaging or, if so, not in a straightforward manner.

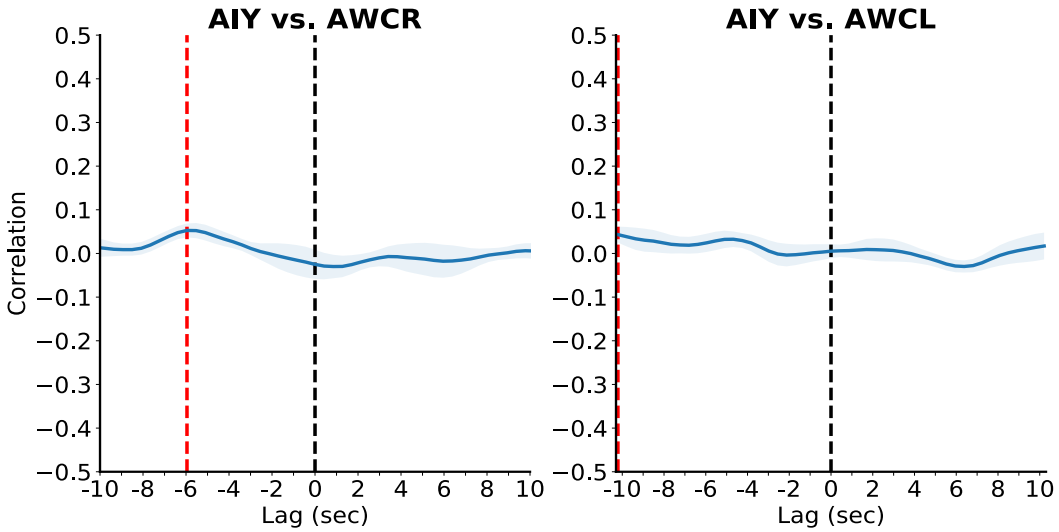

Figure 10: Average cross-correlations ± SEM between AIY neurite (reference neuron) and AWCL (n=6) or AWCR (n=6) (shifted neurons) Ca^{2+} activities. Cross-correlations were performed between vectors of the derivatives of the corresponding normalised Ca^{2+} traces. Red dashed lines indicate lag (displacement, in seconds, of AWC relative to AIY) at which both neurons show the highest absolute correlation value. For more details, see *Materials, Experimental Methods and Data Analysis section*.

2.3. Immobilised Imaging with Sensory Stimulation

2.3.1. AIY activity is coupled to motor-states in the olfactory chip

To study the influence of a sensory input on AWC and, ultimately, AIY activity, we performed imaging of AIY during stimulation of the worm with a sensory stimulus. We started by stimulating the worm with isoamyl alcohol, a chemical compound very well known to be attractive to the worm. Due to the technical challenges that were found (described below), we moved on to stimulating the worm with a bacterial odour. We hypothesized that a bacterial odour would be a stronger stimulus to the worm, thus perhaps allowing us to surpass the difficulties that were found (data for stimulation with isoamyl alcohol is not shown here).

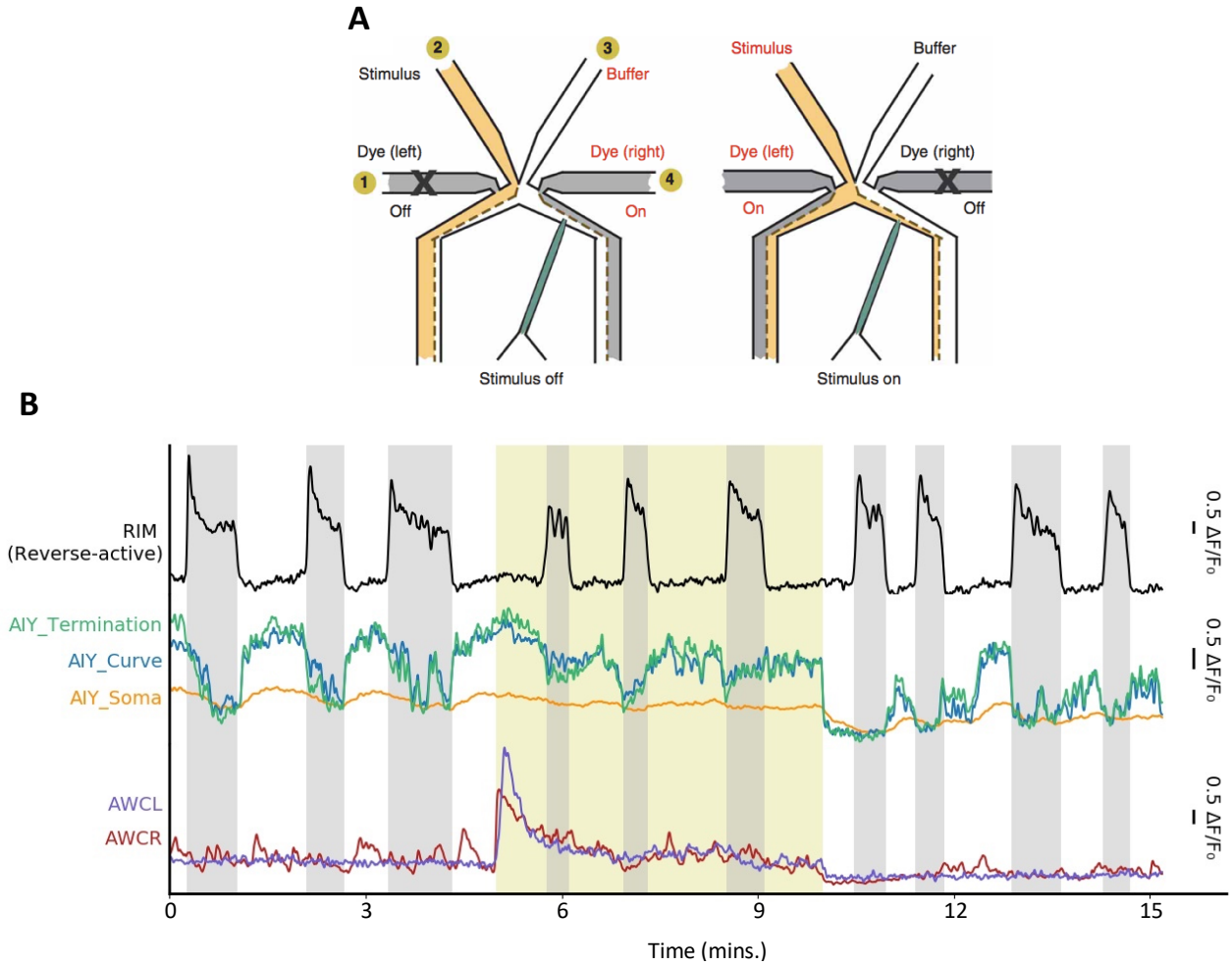

Figure 11: Ca^{2+} imaging with sensory stimulation. **(A)** Technical scheme of microfluidic device used for Ca^{2+} imaging in immobilised worms with sensory stimulation (Olfactory Chip) (retrieved from Chronis et al., 2007). Here, it is possible to appreciate the fluid streams running in an ON and OFF odour stimulation condition. For further description of its functioning, see *Materials, Experimental Methods and Data Analysis section*.

(legend continued on next page)

We started by recapitulating the motor command state dependency of AIY activity, previously found in the Oxygen Chip, in these new recording conditions. We used a microfluidic device that allows delivery of an odour stimulus to the worm's nose by using fluid streams under laminar flow (henceforth also referred to as Olfactory Chip). A representation of the experimental setup for worm stimulation can be visualized in **Figure 11A**. (for further details, see *Materials, Experimental Methods and Data Analysis* section). The olfactory chip does not allow the controlling of the gaseous environment of the worm, as the Oxygen Chip did. Moreover, the olfactory and oxygen chips have very distinct geometries, and in the olfactory chip the worm experiences a constant flow going past its nose, so we sought to rule out the hypothesis of these new conditions having an effect on the worm that could prevent normal AIY activity. This was not the case, as we were able to recapitulate the motor-state dependency of AIY activity in this microfluidic device, when using a stimulation paradigm of NGM buffers (the same buffer used in previous experiments): NGM vs. NGM condition (stimulation of the worm with NGM in the "OFF" condition, and stimulation of the worm with NGM in the "ON" condition, upon buffer switch) (see **Supplementary Figures S7** and **S8**).

Besides NGM vs. NGM (Control), two other conditions were tested: NGM+LB vs. NGM+LB (Control) and NGM+LB vs. Bacterial Odour. Growth of E. Coli OP50 in NGM medium was limited, so we added an excess of LB medium to NGM, in order to favour bacterial growth until the desired optical density (OD).

All neuronal activity traces from the recordings obtained in this experimental setup, used for subsequent analysis, can be seen in **Supplementary Figure S9** and **S10**. See **Supplementary Movies S5-S6** for Maximum Intensity Projection of example recordings.

(B) Activity traces of example neurons. Grey shaded regions denote periods of reverse motor command state, inferred from the activity of RIM. Yellow shaded region denotes period of sensory stimulation with the bacterial odour. Scale bars on the right represent 0.5 $\Delta F/F_0$.

2.3.2. AWC activity does not follow the expected response to the stimulus

We next asked whether the stimulation with a bacterial odour resembled the responses previously reported for the sensory neurons AWC. Chalasani et al. (2007) and Gordus et al. (2015) showed that both AWC neurons respond similarly to bacterial odour, by showing an odour-OFF response to this stimulus, i.e. AWC is inhibited during delivery of this sensory stimulus to the worm. Conversely, AWC responds to bacterial odour removal with a sharp rise in Ca^{2+} activity, followed by a return to baseline levels.

Unexpectedly, in these conditions, we found responses from the sensory neuron AWC at the onset of the buffer switch (both at time = 5 minutes and time = 10 minutes), both in control experiments and assays with the stimulus (see example of pressure response at the transition of buffer in **Figure 11B** and in **Supplementary Figures S8, S9 and S10**). The response of AWC to the odour has been reported as being very stereotyped (Chalasani et al., 2007; Gordus et al., 2015). Hence, we hypothesize that these responses are not responses of AWC to the stimulus, but rather a mechanosensory response from this neuron to the pressure change created at the moment of buffer switch. Effectively, *C. elegans* has been shown to exhibit multiple mechanoreceptor neurons in the nose, for example ASH or FLP (Schafer, 2014). Mechanoreceptor neurons in wild *C. elegans* are essential to detect collisions with particles from the environment or other animals, to detect bacterial food sources, as well as to detect its own movement. AWC could, potentially, take part in similar functions, as an addition to detecting odours. As an attempt to overcome this issue, two other experimental setups were tested:

- First, we aimed for a precise flow rate of buffers into the microfluidic device, by using a syringe pump (Harvard Apparatus PHD 2000) that allowed to control the rate at which each of the buffers were injected into the microfluidic device;

- We hypothesized that the 3-way valve regulating the direction of the stimulating buffer was inputting pressure into the system at the onset of buffer switching, creating pressure on the worm's nose, leading to the observed pressure responses in the sensory neurons AWC. Hence, in the second experimental setup tested, we removed the need for the valve. We used an experimental setup (MAESFLOW^{TM}-TM) where we could computationally control the flow-rate at which the two side streams (controlling the direction of the stimulus) (1 and 4, in **Figure 11A**) were injected into the microfluidic chamber.

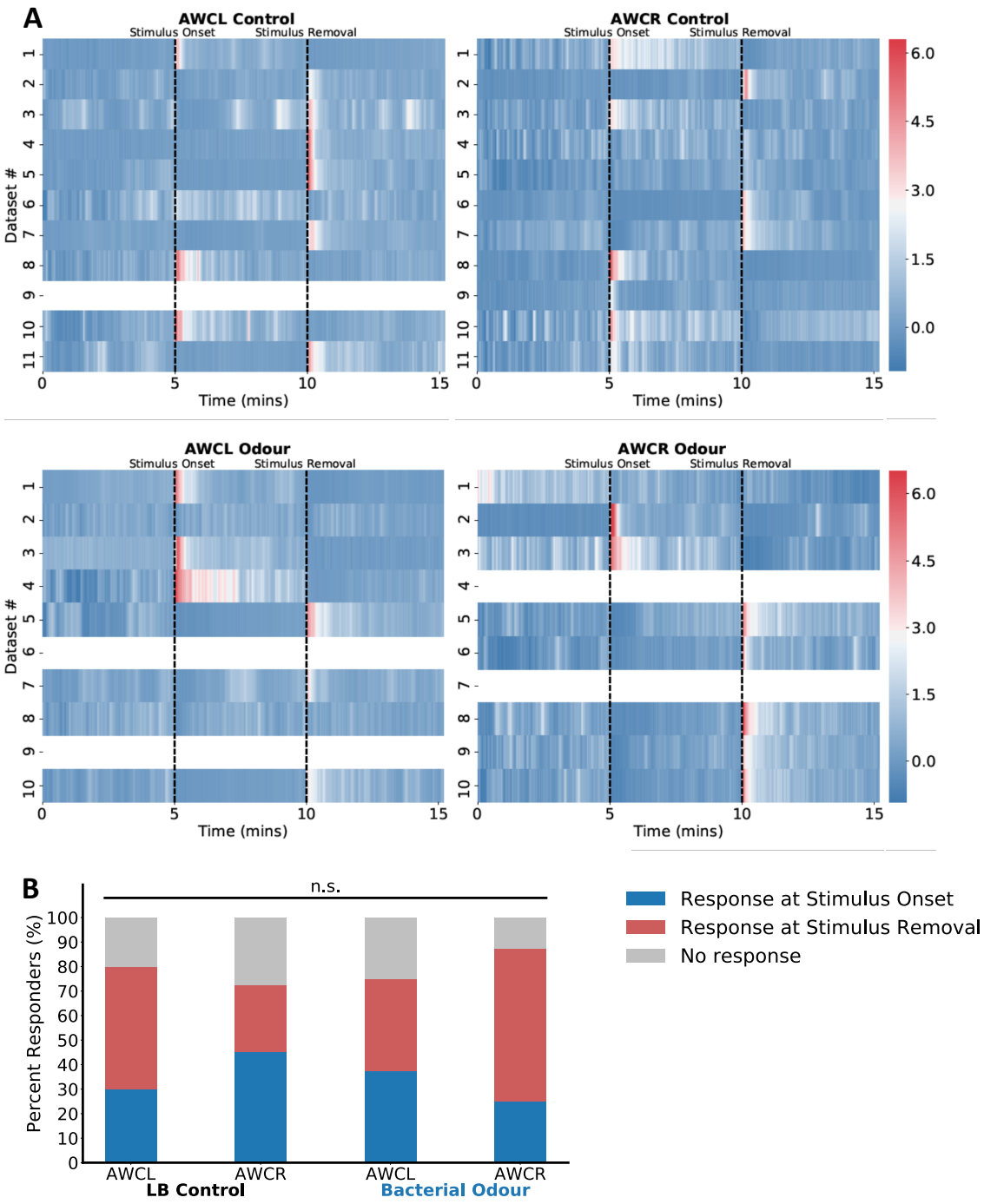

Figure 12: AWC activity in response to the olfactory stimulus. **(A)** Heatmaps of the $\Delta F/F_0$ activities of AWC (left and right pairs) over the entire length of the recordings (~15 minutes) for control experiments (top) and experiments with stimulation with a bacterial odour (bottom). Each row represents a distinct assay. Black dashed lines denote moment of the onset and removal of the stimulus. **(B)** Cumulative histogram showing percentage of responses from AWCL and AWCR to the onset and removal of the stimulus, both for control assays and assays with olfactory stimulation.

We were not able to eliminate the observed mechanosensory responses from AWC with these alternative experimental setups, as we still observed high peaks of activity synchronized with the buffer switching, both in control experiments and experiments with stimulation with the bacterial odour (data not shown). We also encountered similar challenges when stimulating the worm with an odour of isoamyl alcohol (data not shown). These responses were not always synchronized with the removal of the stimulation buffer, differed from AWCR to AWCL within recordings, and its amplitude and timing (at the stimulation onset or removal) varied across recordings. The inconsistency of these responses might be explained by mixed responses to the odour and pressure responses, and by the fact that the pressure responses might depend on the experimental setup, in an uncontrollable manner.

Despite the mechanosensory responses from AWC, shown in **Figure 12A** through heatmaps and quantified in **Figure 12B**, we proceeded to using the original experimental setup and studied whether we still observed AIY activity to be modulated by the sensory stimulus.

2.3.3. Effect of the sensory stimulus on the activity of AIY

We first started by asking whether we saw a modulation of the activity of AIY synchronised to odour onset and/or odour removal. **Figure 13** (left column) shows no evidence for an increase of AIY activity aligned to the onset of odour presentation. We observed a decrease in activity not precisely aligned to removal of the stimulus in assays where we delivered the bacterial odour to the worms, not seen in control experiments (**Figure 13**, right column). It is unclear if this is a response to the removal of the stimulus or if, on the other hand, it is a response of AIY to the decreased reversal frequency seen during the stimulation period, as it will be discussed below.

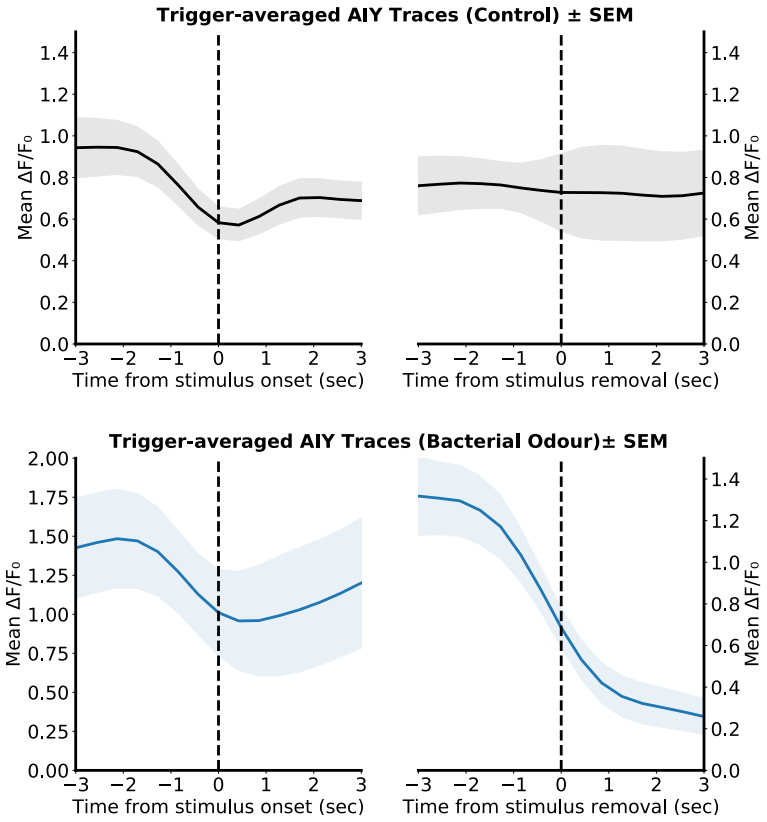

Figure 13: AIY response to the onset and removal of sensory stimulation: trigger-averaged $\Delta F/F_0$ ± SEM traces from AIY, aligned to stimulus-OFF to stimulus-ON (left) and stimulus-ON to stimulus-OFF (right) transitions, both for control experiments (n=11) (top) and experiments with olfactory stimulation (n=10) (bottom). For more details, see *Materials, Experimental Methods and Data Analysis section.*

We then asked whether AIY activity was higher during the period of the sensory stimulus. To investigate that, we started by averaging the $\Delta F/F_0$ throughout the entire period of stimulus delivery. We observed an increased activity of AIY during periods of stimulation with the bacterial odour, in comparison to control experiments (**Figure 14A**). Interestingly, we also observed a reduction of time spent in reversal command state during periods of stimulation with the bacterial odour (**Figure 14B)**, suggesting that the odour was perceived by the worm and had an effect on the modulation of its motor commands (as read out by RIM activity). An increase in time spent in forward command states while perceiving attractive odorants is expected, based on previous literature. This can be interpreted as a strategy of the worm to prolong runs when navigating towards attractive cues; conversely, when moving away from attractants the worm increases the frequency of reversals as an attempt to reorient itself in order to find attractive stimuli again (Albrecht & Bargmann, 2011; Gordus et al., 2015).

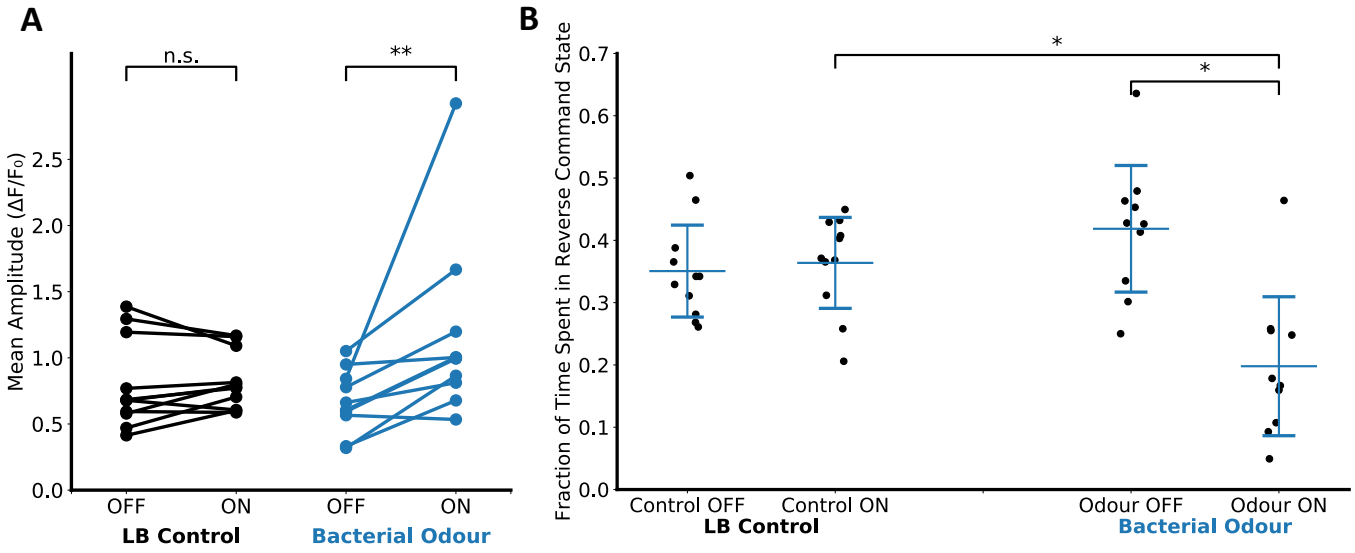

Figure 14: Ca^{2+} activity of AIY during sensory stimulation. **(A)** Quantification of the mean $\Delta F/F_0$ of AIY during ON and OFF periods of sensory stimulation, both for control assays (n=11) and assays with olfactory stimulation (n = 10). **p<0.01, Wilcoxon matched-pairs signed rank test; n.s., not significant. For more details, see *Materials, Experimental Methods and Data Analysis* section. **(B)** Fraction of time spent in reverse command state over the periods of sensory stimulation - Control-ON or Odour-ON - and periods OFF sensory stimulation - Control-OFF or Odour-OFF -, divided by entire length of the recordings (~15 minutes). Each data point represents a different animal. Bars indicate the mean value ± SD. *p<0.05, Mann-Whitney test.

Previously, we have shown that AIY activity during reversal command periods is decreased. Thus, we hypothesized that the higher mean $\Delta F/F_0$ during the period of stimulation, calculated in **Figure 14A**, could simply be due to a decrease in the amount of time spent in reversal command states. Thus, we

disentangled the influence of the stimulus on AIY activity during forward and reverse command periods, separately, by comparing the mean activity of AIY 10 seconds into the transition of motor state (i.e. 10 seconds after the transition from forward to reverse command state and the 10 seconds after the transition from reverse to forward command state), separately during stimulus-on and stimulus-off periods. **Figure 15** shows an increased activity of AIY during both forward and reverse command states that occur during stimulation periods, which is not seen in control experiments. This observation was surprising for a few reasons, debated next.

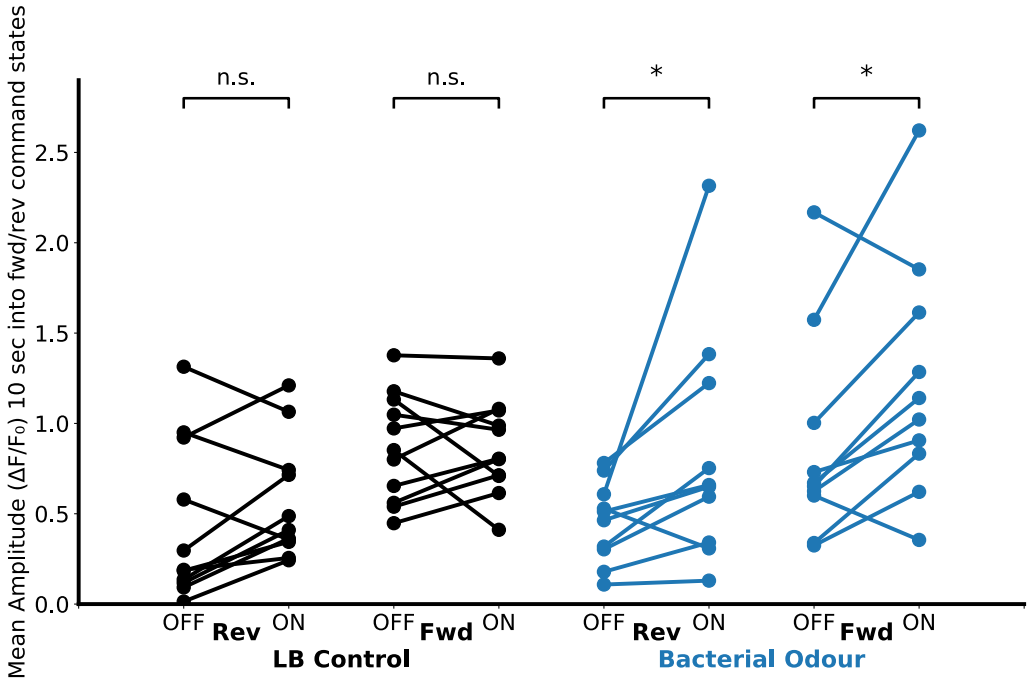

Figure 15: Mean $\Delta F/F_0$ of AIY during periods of reverse and forward command states, occurring over periods ON and OFF stimulus, both for control assays (n=11) and assays with bacterial odour stimulation (n=10). *p<0.05, Wilcoxon matched-pairs signed rank test; n.s., not significant. For more details, see *Materials, Experimental Methods and Data Analysis* section.

First, as aforementioned, AWC did not show a response to the presence of the stimulus as expected by previous literature (Chalasani et al., 2007; Gordus et al., 2015). Thus, we have no evidence that AIY is receiving the sensory input from one of its major presynaptic partners (AWC). We cannot, however, rule out the possibility of other neuronal circuits being involved in relaying sensory information to AIY, thus having mild modulation on its activity.

Second, if, indeed, the bacterial odour had an effect on the activity of AIY, we would expect to see an increased average activity of AIY aligned to the onset of stimulation and, conversely, a decreased

average activity aligned to the removal of the odour. We have shown that the odour had, indeed, an effect on the modulation of the internal motor states of the animal (**Figure 14B**). Thus, the observed decrease in the average activity of AIY a few seconds prior to the offset of stimulation (**Figure 13**, right column), could simply be due to the end of a period of sustained forward states that was induced by the presence of the stimulus.

In conclusion, we did not find enough evidence to confidently say that we observed a modulation of the activity of AIY by the bacterial odour. Consequently, it was not possible to prove that AIY had a role in biasing the system to stay longer in forward commands states.

2.4. Freely Moving Imaging

We next sought to understand how AIY activity varies in freely crawling worms, while the worms chemotax to an attractive sensory cue: bacterial food. To achieve this, we have performed Ca^{2+} imaging in freely crawling worms while simultaneously recording their behaviour with an infrared (IR) camera (**Figure 16A**, right panel). We obtained fluorescent data from both green (**Figure 16C**, left panel) and red channels (**Figure 16A**, middle panel), allowing us to obtain fluorescent data from GCaMP expressing neurons (AIY and AWC) and Scarlet or mCherry expressing neurons (AIY, AWC and BAG), respectively. Red markers like Scarlet or mCherry are not sensitive to Ca^{2+} dynamics. Hence, a readout of its intensity can be used to correct Ca^{2+} activity for movement artefacts, created as a result of natural movement of the worm.

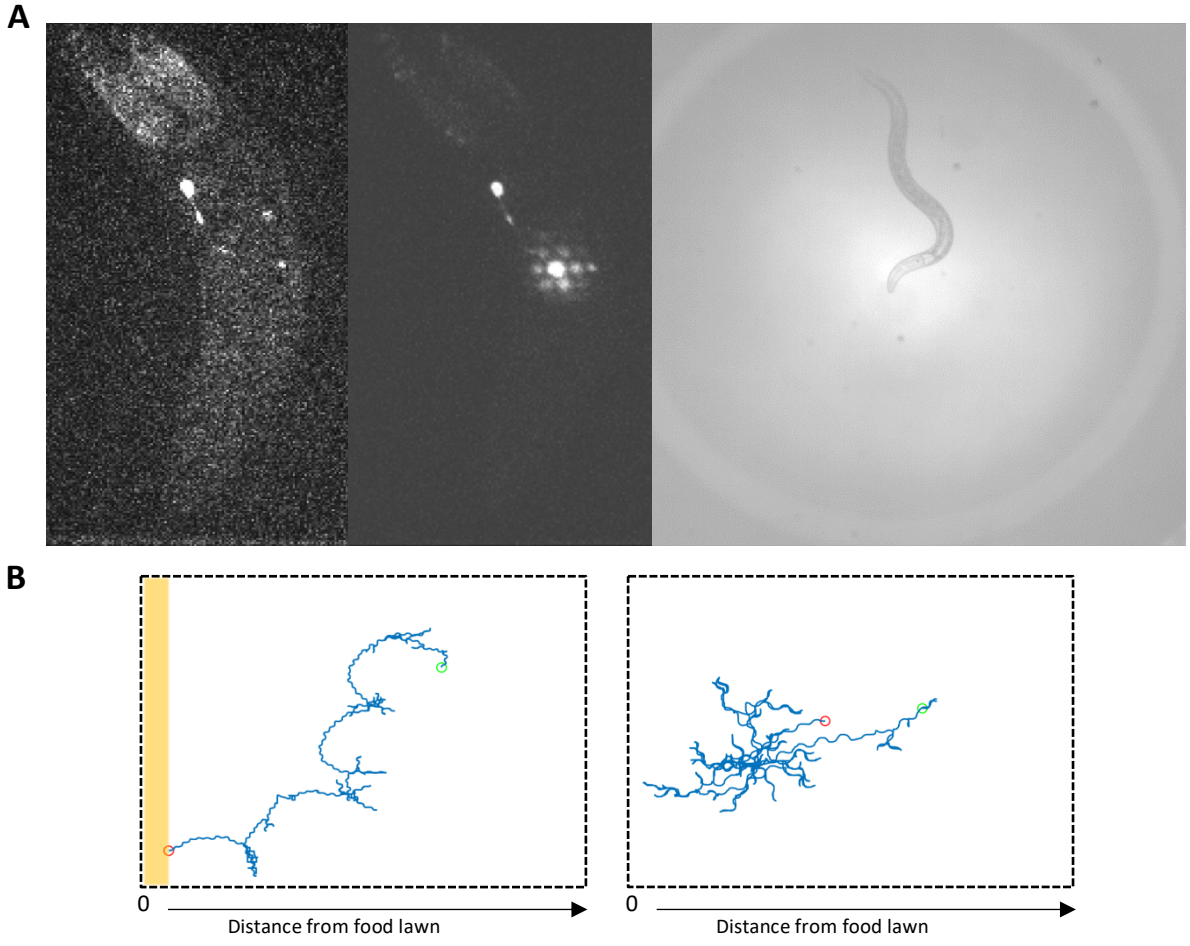

Figure 16: Experimental setup of Ca^{2+} imaging in freely crawling worms. **(A)** Example fluorescent data: green channel (CGaMP) on the left and red channel (Scarlet) in the middle. Example image of the recorded behaviour of the worm shown on the right. **(B)** Tracks (not to scale) of two worms from two distinct experiments with a food lawn (left, orange stripe) and without a lawn of food (right, control experiment). Green circle denotes initial position of the worm; red circle denotes final position of the worm, after ~10 minutes of imaging.

As a way to keep track of the worm in the field of view during freely moving experiments, we expressed a red marker in neuron BAG. Part of the red emission is directed to a quadrant PMT. The system detects skew on the four quadrants to determine in which direction the worm's head is moving and update the stage position accordingly. Expressing BAG::mCherry was necessary to keep track of the worm as this requires bright red expression, stronger than the one achieved with the red fluorophores in AWC and AIY. A programmed motorized stage followed the movement of the worm and logged its position overtime, allowing to obtain tracks of the worm over the length of the recording (**Figure 16B**). Unexpectedly, we observed an imaging artefact, likely created by scatter of light, due to the strong expression of the red marker in BAG (see **Figure 16A**, middle panel). This artefact prevented a reliable readout of the intensity of the neuronal markers in most of the neurite of AIY, precluding to obtain Ca^{2+} activity traces from the *Axon Curve* and *Axon Termination* regions.

The inherent weak GCaMP expression in AIY of this strain limited the frame rate and resolution of the acquired data. We recorded the worms at an acquisition rate of ~2.3Hz (exposure time of 20 milliseconds, in 21 z-planes). Due to the high laser intensity power (4% for the green channel), used as an attempt to increase the intensity of the signal, major photobleaching was observed. Exposing *C. elegans* to high light powers for long periods of time can damage them and cause their locomotion to become sluggish. To surpass these difficulties, we were forced to limit the length of the recordings down to 10 minutes, which is insufficient for the worms to chemotax to food (see **Figure 3** for quantification of time required for chemotaxis under similar experimental conditions in behavioural assays; chemotaxis quantification of the data acquired in the spinning disk confocal microscope is not shown here) and to get a deep understanding of the relationship between neuronal activity and the animal's long timescale behaviours.

A total of 10 control experiments and 11 experiments with a bacterial lawn of food was obtained (see **Supplementary Movies S7-S8**). However, all the difficulties described above prevented us from getting reliable Ca^{2+} activity traces from the activity of AIY (data not shown). Therefore, we could not analyse this data further.

3. DISCUSSION

3.1. A revised notion of the coding activity of AIY in the immobilised worm

Here, we imaged the activity of AIY with and without the presence of sensory stimuli to determine how AIY dynamics interact with ongoing motor commands and incoming sensory inputs. We report AIY to be differently active depending on the internal instantaneous motor state encoded by the worm. Moreover, we report AIY activity to be dominated by the worm's internal motor states.

Previous work from other labs have reported AIY activity to respond positively to the presence of several stimuli, in immobilised animals (Chalasani et al., 2007). However, this body of literature did not dissect the relation of AIY activity to behavioural states. Chalasani et al. (2007) reports AIY activity to increase upon odour presentation. They describe AIY activity in response to the stimuli as follows: "AIY responses [to the odour] were brief, poorly synchronized to odour onset, and appeared sporadically throughout the period of odour presentation". By observing the data presented in this thesis, the pattern of activity described in Chalasani et al. (2007) seems consistent with being correlated to the worm's behavioural states. Moreover, in the present study, we have shown that upon presentation of an attractive sensory stimulus - bacterial odour -, the worm tends to reverse less (**Figure 14B**) and, as a cause and/or consequence, AIY activity is increased (**Figure 14A**). We speculate that previous studies measuring the influence of sensory input in AIY activity, in immobilised worms, might have mistaken the increased activity of AIY during stimuli presentation simply due to a sustained forward command state, for a direct response from the neuron to the delivered sensory stimulus. Having recorded for short periods pre-stimulus, previous studies might have not analysed ongoing neuronal activity. Future work imaging AIY activity in immobilised animals experiencing sensory stimulation should account for the influence of behavioural states in AIY activity, and carefully disentangle the influence of each in the coding activity of AIY.

3.2. Extra-synaptic pathways explain neuronal interactions not predicted in connectome of *C. elegans*

Although immobilisation of the worms was originally a necessary step to record neuronal activity at a single-cell resolution in the worm, today it constitutes an insightful tool to distinguish motor command signals from proprioceptive feedback. Besides the slower neuronal dynamics observed in immobilised worms (in comparison to freely moving animals), imaging worms in these conditions can be an

advantage to find neuronal connections not predicted by the *C. elegans* connectome. Indeed, imaging AIY activity in the immobilised preparation allowed us not only to observe a different activation of AIY that was dependent on the worm's instantaneous behavioural state, but also to observe a modulation of the activity of AIY before the transition of motor state.

AIY is traditionally known as being a first-layer interneuron. In fact, AIY seems to receive synaptic input from 9 sensory neurons and only 1 interneuron, besides having a GAP junction with RIM, highly unlikely to be inhibitory (see **Supplementary Figure S1**). It is thus unlikely that any of these synaptic connections, predicted in the *C. elegans* connectome, are responsible for the signalling of motor commands to AIY. Thus, our results hint to the existence of extrasynaptic pathways responsible for controlling state dependent activity in AIY. This result is simultaneously interesting and surprising as it indicates that extrasynaptic pathways can, additionally to the connections predicted by the synaptic connectome, create extensive networks in the nervous system of *C. elegans* to dominate the activity of neurons that, ultimately, modulate the behaviour of the worm. As these interactions in the nervous systems of *C. elegans* are largely unknown and play a big role in command state modulation, more effort should be put into studying them.

Future studies should focus on performing a candidate genetic screen to identify the neuromodulator(s) / neurotransmitter(s) that control state dependent activity in AIY. Once found candidates responsible for this signalling of internal motor states to AIY, this neuron should be imaged in the background of mutants for the biosynthesis of those neuromodulator(s)/neurotransmitter(s). In a positive result, one would expect to see the negative correlation between AIY activity and reversing periods to decrease in magnitude, indicating that the targeted neuromodulator(s) / neurotransmitter(s) were responsible for the signalling of state dependent activity to AIY.

3.3. A full understanding of the coding activity of AIY in the immobilised preparation is incomplete

Li et al. (2014) showed that the activity of AIY in freely moving animals is correlated to the instantaneous forward speed of the worm in a rather gradual manner, with higher AIY activity correlating with higher speeds, and vice-versa. Kato et. al (2015) showed that the worm's speed can be inferred from the whole-brain activity, from neurons like RIB or AVB. Whether speed modulation by AIY is also seen in immobilised worms, without the input of the animal's own behaviour, is unclear. One could cross the imaging strain used in this study with a strain expressing GCaMP in RIB, an

interneuron known to modulate forward movement speed in the freely crawling worm, and showing fluctuations during periods of forward state in the immobilised worm, interpreted as speed command changes (Kato et al., 2015). Imaging AIY in this strain would allow us to have a readout of the worm's encoded behavioural state and the worm's brain encoded speed. Consequently, one could understand whether speed modulation by AIY is also seen in the absence of proprioceptive feedback, and potentially disentangle how that modulation is achieved in immobilised worms, and how it differs from a freely moving setting.

Moreover, to achieve a full scope of neuronal activity correlations to AIY activity, whole brain imaging should be performed in a strain expressing a pan-neuronal nuclear Ca^{2+} sensor, subsequently crossed with a strain with a Ca^{2+} reporter expressed in the axonal-dendritic processes of AIY. To avoid overlap of the neurite of AIY with the nucleus of other targeted neurons that might overlap with the neurite of AIY, the Ca^{2+} indicator RCaMP could be used as an alternative label to GCaMP (Dana et al., 2016). Development of a strain like this would guarantee precise measurement of Ca^{2+} dynamics in axonal processes of neurons in a whole-brain setup.

Here, we have stimulated immobilised worms with an attractive stimulus, bacterial odour. Due to the experimental limitations previously presented, we were not able to have a reliable readout of the sensory effect on the activity of AIY. We found responses from the sensory neuron AWC to the stimulus onset and offset that were not consistent across recordings, individuals or even in the left and right neuronal pairs of the same worm. We hypothesize that the observed peaks in activity are mechanosensory responses of the neuron to the pressure inputted in the animal by the change in the fluid streams inside the microfluidic device at the onset/offset of sensory stimulation (for more details, see *Materials, Methods and Data Analysis* section). To surpass this, one could design a microfluidic device that minimises these pressures created upon change in the stream of fluids inside the chip. Alternatively, one could image another of AIY's major sensory inputs. Even if ASE, one of AIY's major synaptic partners responsible for chemosensation of salts and multiple chemical agents (Bargmann et al., 1991), showed to respond to the pressure changes as AWC did, one could study AFD, another of AIY's major synaptic partners involved in thermosensation. In this case, a difference device could be used to delivery temperature inputs to the worm and study the influence of temperature during ongoing activity of AIY.

Although we did not detect a reliable response from the sensory neuron AWC to the bacterial odour, or a convincing positive response from its major postsynaptic partner AIY, we did observe an influence of the odour in the frequency of reversals. This observation gives us confidence that the worm was,

indeed, sensing the stimulus and relaying the odour information to downstream neurons. However, the circuit responsible for influencing the worm's behaviour is unclear, as the bacterial odour could be sensed by other groups of odour chemosensory neurons, other than AWC (Fujiwara et al., 2002; Ben Arous et al., 2009). The fact that we did not observe a reliable modulation of the stimulus on the behavioural modulation in AIY could also be aggravated by the fact that the sensory effects on motor commands are less efficient compared to moving animals, given the prolonged duration of motor commands. Thus, sensorimotor transformation in *C. elegans* should, ultimately, be assessed in freely crawling animals, where they are not deprived of proprioceptive mechanisms.

3.4. Strategies of signal codification

It is unclear how typical it is for single neurons to show different patterns of Ca^{2+} dynamics in their somas and neurites in *C. elegans* and, specifically, how frequent this is the case in interneurons as a means to achieve sensorimotor integration within its subcellular space. Here, we set as a goal to test whether AIY shows compartmentalised activity along its neurite. Compartmentalised motor-state related activity along axonal processes was not found in AIY (see **Figure 8**). Rather, we suggest that the different magnitudes of Ca^{2+} changes of the different regions of the neurite (see **Figure 9**) can be explained by local synaptic input and local GCaMP concentration. By observing the map of synaptic connectivity of AIY (see **Supplementary Figure S3**), it is clear that most sensory neurons synapse with AIY in the *Axon Curve* region, and almost no synapses are found near the soma. This might also explain why the *Axon Curve* region shows the most dramatic changes in Ca^{2+} activity: signals from other neurons might be densely received in this region and might fade further down the process, thus explaining the weaker signals observed in the *Axon Bulb* and *Soma*. A way of confirming this hypothesis could be to use electron microscopy data to determine whether neurons that show larger amplitude Ca^{2+} changes in the nucleus are those that have synapses closer to the cell body. If that is proven to be true, one could predict in which neurons Ca^{2+} activity should be measured in the cytoplasm. Effectively, electron microscopy studies showed that several neurons have spatially segregated synaptic domains along their neurites (White et al., 1986). Thus, analysing these data could help predict which neurons show compartmentalised Ca^{2+} dynamics.

Furthermore, the different magnitudes of change in Ca^{2+} activity in the different regions of the neurite of AIY might also be a function of local GCaMP concentration: bigger structures, like the soma, aggregate higher quantities of GCaMP; conversely, the thinner dendro-axonic domains aggregate

smaller quantities of GCaMP. Assuming an equal distribution of Ca^{2+} channels along the cellular membrane of neurons, structures with lower densities of GCaMP will show a faster saturation of GCaMP molecules in its activated state which, ultimately, is translated in signals with increased amplitude and faster dynamics. Conversely, in structures that accumulate increased quantities of GCaMP, enough calcium ions need to enter the cell to produce a similar response (in magnitude) which, ultimately, is translated in neuronal traces that peak with delay (in comparison to the previous), as observed in **Figure 8**. In conclusion, both synaptic density and local GCaMP concentration could contribute to the different magnitudes and dynamics of Ca^{2+} activity observed along the neurite and soma of AIY.

Although we did not find compartmentalised motor-state related activity along the neurite of AIY, since we could not get a reliable sensory representation in AIY, we cannot exclude the hypothesis that compartmentalised sensory-induced activity might be found along the neurite of AIY. Future work measuring both motor and sensory representations along the neurite of AIY should be performed. Moreover, previous studies have measured sensory activity in the same regions as we measured motor activity here (the *Axon Curve* region, although not completely clear across studies) (Chalasani et al., 2007; Larsch et al., 2013; Li et al., 2014; Ji et al., 2020), making it unlikely that AIY employs a strategy of signal compartmentalisation to encode both signals. Moreover, the fact that we found a behavioural state signal pervading AIY activity, makes us hypothesize that AIY multiplexes motor state signals and sensory information. In this scenario, AIY integrates sensory input on top of its instantaneous coding for behaviour.

3.5. The freely moving preparation

In this study, we aimed at imaging the cell body and neurite of the interneuron AIY, as well as the sensory neuron AWC. Recording the activity of the neurite of a neuron in a freely moving animals poses technical challenges. First, it is crucial to achieve high resolution data, to reliably pick up the activity of the single cell and its axonal processes. Second, it is important to ensure a fast z-scanning speed in a confocal microscope, in order to capture activity that might be happening in the neurons at short timescales. Additionally, it is necessary to keep track of the moving animal by keeping it in the field of view, while it moves in the x and y axis, as well as in the z axis.

Getting high resolution and high frame rate data in this experimental setup is challenging and requires optimization of microscopy and experimental settings to achieve the best trade-off between them. Hence, under these working conditions, it is crucial to work with a strain of transgenic animals with

strong GCaMP expression in the neuron(s) of interest. Better signals allow the user to reduce the exposure time of the recording cameras for each frame and to maximize the imaging settings that permit the acquisition of high-resolution data, while allowing a fast z-scanning of the sample, assuring data with high frame rate.

From data presented in past studies, it is known that neuronal dynamics highly changes from immobilised to freely moving animals. A prominent example are the prolonged reversing periods observed in immobilised worms (Kato et al., 2015). These same authors also observed less variation in the amplitude of reverse-active neurons, in comparison to freely moving animals, and Kaplan et al. (2019) describes slower frequency oscillations of motor neurons. Additionally, freely moving animals show additional amplitude variations and integrate proprioceptive signals, which are lacking in an immobilised setup. Thus, brain dynamics in freely moving animals is thought to be much faster and more complex in comparison to the dynamics observed in immobilised animals. The weak GCaMP expression in AIY in the imaged strain was the major limitation to get high frame rate and high resolution data in this experimental setup, which has proven to yield data that is insufficient for the measurement of the activity of the Axon Curve / Termination regions of AIY neurite in freely moving worms. A clear modulation of AIY activity by internal motor states was not observed in this setup in the Soma or Axon Bulb (data not shown), very likely to be due to the slow frame acquisition rate and noisy data that was possible to acquire. As such, it is imperative that a strain with stronger GCaMP expression in the neurite of AIY is obtained before moving on to acquiring data in a similar experimental setup.

3.6. Recent findings on the role of AIY to the computations underlying sensorimotor transformation in the worm's nervous system

Recent work from Ji et al. (2019) (preprint posted in bioRxiv in December of 2019, waiting for review at the time of writing of this thesis) tackles similar topics to the ones studied in our work. They report a behavioural state modulation of AIY, both in moving worms, as well as in immobilised animals. The results reported in this thesis, regarding the coupling of AIY to behavioural states, are corroborated by the data presented by their work. The authors further study the neuronal circuits responsible for the relaying of both thermosensory and behavioural inputs to AIY. By optogenetically and genetically manipulating key neurons of the proposed circuit, they suggest that RIM sends a corollary discharge signal to AIY: upon its ablation, the motor state representation in AIY is largely impaired and the worm's ability to sustain forward movement during thermotaxis is reduced. The exact pathways by

which the feedback signal reaches AIY are not dissected. However, the *C. elegans* wiring diagram predicts a single electrical synapse between AIY and RIM, highly improbable to be inhibitory. In our data, we observe that the behavioural modulation of AIY seems to start before the onset/offset of reversals (these inferred from RIM activity) (**Figure 7**). This pre-reversal-onset activity was not reported by Ji et al. (2019). Thus, we suggest that additional extra-synaptic pathway(s), other than the feedback loop from RIM to AIY, might be responsible for the relaying of motor command signals to AIY. This observation might have been missed by Ji et al. (2019) given their slow frame acquisition rate of ~1 volume/second.

Upon RIM ablation, thermosensory input from AIY is capable of reaching downstream premotor interneurons (downstream of RIM) and the ability of the animal to sustain forward periods is impaired, suggesting that both neurons establish a positive feedback loop that allow the animal to sustain behavioural states (Ji et al., 2019). The authors suggest that the coupling of AIY to thermosensory input happens only during periods of forward crawling, supporting our initial hypothesis that sensory activity is gated by behavioural state. Through this mechanism, AIY is capable of gating the transmission of sensory information to downstream layers, allowing the worm to sustain motor states that carry it up a temperature gradient. In the present study, we have studied the impact of the olfactory circuit on AIY activity. Since we were not able to obtain a reliable sensory representation in AIY, whether these mechanisms remain to be true in the olfactory circuit remains unclear.

In another very recent study from Ji et al. (2020) (preprint posted in bioRxiv in February of 2020, waiting for review at the time of writing of this thesis), the authors set as a goal to investigate the circuits that control the selection of dwelling and roaming states in *C. elegans*, the two alternative long-lasting behavioural states employed by the worm to either exploit or explore food sources, respectively. By recording Ca^{2+} activity of a selected group of neurons for long periods of time (~40 minutes) in freely crawling worms, they were able to show that the activity of a few neurons had different activity in roaming and dwelling states. Among these neurons is AIY, whose activity (of the neurite) was found to be higher during periods of roaming. This is particularly interesting as it puts AIY as a neuron whose activity is modulated both by short timescale behaviours - reversals and locomotion speed - and long-lasting behaviours. This idea had been already suggested by Flavell et al. (2013), but this is the first time AIY activity is recorded for long enough to be associated with exploration behaviour. Roaming periods are characterized by long forward runs and increased speed of locomotion. Thus, increased activity of AIY during roaming does not necessarily link AIY activity with modulation of this long-lasting behaviour of food exploration, but highlights the role of AIY, a primary sensory neuron, in the modulation of short timescale behaviours that, ultimately, allow the worm to

find attractive sensory cues. However, the authors identified AIA, another primary sensory neuron, as having a major influence in the modulation of roaming and dwelling. This discovery puts AIA as a major hub of the *C. elegans* nervous system to control one of the most fundamental behaviours employed by the worm to ensure its survival: food exploration. Modulation of both short and long timescale behaviours by environmental cues can thus start to be modulated at very early stages of sensory processing.

Their work raises the question of whether exploitation behaviours are encoded by brain-wide activity, as it was seen for motor-states (Kato et al., 2015). This question could be answered by imaging brain-wide activity in freely crawling worms in the presence of a controlled sensory environment. The first efforts to image the whole brain of the moving worm have started to appear in the community (Nguyen et al., 2016; Venkatachalam et al., 2016; Scholz et al., 2018). This technology promises to be the next big step to get near a closer representation of the global dynamics of the brain in a more naturalistic environment, hopefully allowing us to decipher the neuronal computations underlying sensorimotor transformation in the brain of *C. elegans*.

3.7. Sensorimotor transformation: from the worm to higher-order organisms

In this study, we report the activity of AIY to be dominated by a motor command signal. Although we did not perform whole-brain imaging, the results here presented put AIY as part of the global, pervasive brain signal that represents the worm's major motor actions. AIY is a primary sensory neuron, commonly believed to exert functions primarily in sensory processing. It is thus surprising and, perhaps, counterintuitive, to find the activity of neurons whose major synaptic input comes from sensory neurons, to exhibit such a tight coupling to the animal's ongoing behaviour.

A brain-wide signal related to the animal's ongoing behaviour is not exclusive to the worm. Indeed, recent studies have reported the brain of the flies (Aimon et al., 2019) and mice (Stringer et al., 2019; Musall et al., 2019; Salkoff et al., 2019) to be dominated by motor representations that are maintained independently of sensory input, task or recording conditions that the animals face. Moreover, in mice, these signals were shown to be shared by a large proportion of the animal's brain - cortical (including primary sensory) and subcortical areas (Niell et al., 2010; Stringer et al., 2019; Musall et al., 2019; Salkoff et al., 2019). For instance, Stringer et al. (2019) showed that in the mouse primary sensory cortex (V1 area), motor information is as well represented as sensory information, and that the representation of sensory stimuli and behavioural states were encoded by the same neurons. One can

then wonder and speculate what the function and origin of such an early representation of behaviour in *C.elegans* and higher-order organisms' neuronal networks might be.

Recent work across species has shown that the behavioural state of the animal highly affects sensory processing (Artiushin and Sehgal, 2017; Nichols et al., 2017). Niell et al. (2010) and Fu et al. (2014) proved that behaviour-related signals in the V1 area of mice control the gain of sensory responses. Saleem et al. (2018) further proved that visual responses in the V1 area depend on the animal's encoding of its position. In flies, dopaminergic neurons were shown to encode information about both the animal's external context and internal states to output different patterns of activity that allow for behavioural flexibility (Cohn et al., 2015; Berry et al., 2015). Here, we hypothesized that the processing of sensory input in AIY could depend on the instantaneous behavioural state of the worm. Due to the technical difficulties aforementioned, we could not verify the veracity of this presumption. However, Ji et al. (2019) recently showed that the thermosensory response in AIY is restricted to episodes of forward crawling. Thus, the processing of sensory input is known to depend on the behavioural state of the organisms.

Behaviour is represented by brain-wide networks that include primary sensory neurons (Kato et al., 2015). Such an early modulation of motor states in the nervous system could be important to allow sensory input to be fed into these networks and influence behaviour modulation at different points. Whether these primary sensory neurons are involved in the generation of the motor commands, or if they simply receive copies of motor commands from downstream neurons, is unclear. As aforementioned Ji et al. (2019) reported that a command copy is sent from RIM to AIY to maintain the motor command and, consequently, the behavioural action that allows the worm to chemotax towards attractive stimuli. However, here, we observed the activity of AIY to change before the onset of reversals. This fact might hint for the notion that primary sensory neurons, as AIY, can actually be involved in the generation of motor commands, to ultimately influence behaviour. In zebrafish, the tectum (a visual processing area) was shown to exhibit activity that preceded the execution of tail movements, even in the absence of any visual input (Romano et al., 2015; Pietri et al., 2017). This suggests that neurons of the visual processing area of zebrafish drive the behaviour of the animal. Moreover, in mice, there is evidence that the somatosensory cortex is directly involved in driving whisker movements (Matyas et al., 2010) and locomotion (Karadimas et al., 2019). Thus, work across species suggests that representations of behaviour in the nervous systems, as early as sensory areas, can generate or contribute to downstream networks that generate motor commands, ultimately driving behaviour.

Another hypothesis to explain the existence of such early representation of behaviours in the nervous systems is to predict the effects of self-generated (re-afference input) behaviours. Having internal command signals in such early areas for sensory processing might be useful to account and extract the contributions of the animal's own actions when detecting input from the external environment. For example, in order to reduce desensitization to external sounds, the cricket has been shown to send a corollary discharge signal to the auditory system to inhibit the auditory system's response to the animal's own singing (Poulet & Hedwig, 2002). This way, the nervous system evolved to ensure that singing, a behaviour essential to successful mating of the organism, does not compromise its own survival. Both flies (Fujiwara et al., 2016) and mice (Schneider et al., 2018) relay walking signals to sensory areas for the same purposes.

3.8. Conclusions and Prospects

In this thesis, we aimed to understand how AIY, a primary sensory neuron previously known to process sensory information and modulate behavioural states of the worm, computes both internal motor state signals and sensory input, to ultimately influence the animal's actions. Here, we showed that AIY activity in immobilised animals is dominated by an internal representation of behaviour. The pervasive pattern of activity governed by internal motor state signals that we found while imaging restrained worms, lacking re-afferent input, makes us confident that previous studies reporting sensory-related signals in AIY (Chalasani et al., 2007) might have overlooked the influence of motor commands in this neuron's activity. Further, this motor command signal is encoded in the neurite of AIY, and no evidence for compartmentalised Ca^{2+} dynamics along its dendro-axonic processes was found. Even though we aimed at seeing how the sensory response of the worm to olfactory stimuli was processed in AIY, during different behavioural states (forward crawling versus reversing periods), we were not able to have an accurate/reliable readout of the stimulus on AIY activity. Understanding the influence of sensory stimuli on ongoing dynamics of AIY, in immobilised animals, would be interesting, as it would provide insights about how this neuron integrates and multiplexes both internal motor states and sensory information at slower temporal dynamics. Thus, future efforts should focus on trying to surpass the limitations faced here to deliver an odour to the worm in our experimental setup.

This work bears potential relevance to the *C. elegans* community by presenting a primary sensory neuron as being capable of modulating motor commands at early stages of sensorimotor transformation. This strategy is seen in higher-order organisms as well, suggesting that integrating

sensory information with internal representations of behaviour at an early phase of signal processing, likely has functional relevance for organisms across the animal kingdom.

Finally, we aimed to record the activity of AIY in unrestrained animals, while having the readout of one of its major pre-synaptic partners involved in local search behaviour: AWC. Unfortunately, we could not overcome weak expression of GCaMP in AIY. The GCaMP expression in our strain has proven not to be sufficient to get reliable data to extract the coding activity from the neurite of AIY. Exhaustive work should be performed to create new strains with a stronger pattern of expression of GCaMP in AIY before moving on to imaging freely crawling worms in the experimental and technical conditions here used.

4. MATERIALS, EXPERIMENTAL METHODS AND DATA ANALYSIS

4.1. Experimental model and subject details

All experiments were performed in *lite-1 (ce314)* animals, resistant to the blue light delivered during calcium imaging (Liu et al., 2010). Young adult hermaphrodites (0 eggs to 1 row of eggs) were used in all experiments. Worms were maintained using standard methods (Brenner, 1974) and grown on Nematode Growth Medium (NGM) 6cm agar plates seeded with *Escherichia coli* OP50 as a bacterial food source. Animals were maintained at 20°C. A list of all transgenic strains created and used in this study is provided in **Supplementary Table 1**.

4.2. Experimental Procedures

4.2.1. Chemotaxis Assays

For food chemotaxis assays, custom made NGM agar (4.5cm x 4cm) arenas were prepared, placed on 15cm covered Petri Dishes and let dry overnight. 4 hours prior to the beginning of the assays, *E. coli* OP50 grown overnight in LB medium at 37ºC were resuspended at an absorbance of 20 at 600nm (OD20) and pipetted onto the arena, in order to form a vertical homogeneous lawn of bacterial food. The arena was then incubated at room temperature to let the bacterial food diffuse into the agar and create a food gradient. Control assays, lacking the bacterial lawn, were also performed (Controls). 10 transgenic worms (young adults, 1 row of eggs) were transferred from their original growing plate to an intermediate 15cm food-free NGM agar plate and let crawl away from the picking point, to remove food remnants attached to their bodies. The individuals were then placed on the centre of the arena, ~3cm away from the food source. The arena was next covered with a 45mm x 50mm #1.5 coverglass, so that the worm was between the coverglass and the arena. 20mM Copper Chloride ($CuCl_2$), a known repellent for the worms, was quickly pipetted along the borders of the arena (~20uL per border), to prevent the worms from escaping. The Petri dishes containing the NGM agar arena were immediately transferred to the recording station. Movies were recorded at 10 frames per second (fps), using either Genie TS-M2500 or BM-500GE cameras and Streampix software. Worms were recorded for 60 minutes.

4.2.2. Ca^{2+} imaging in immobilised animals

4.2.2.1. Imaging in the Oxygen Microfluidic Chamber (absence of fluctuating sensory input)

Experiments were performed with custom-made microfluidic two-layer polydimethylsiloxane (PDMS) devices as previously described by Schrödel et al. (2013), Kato et al. (2015) and Kaplan et al. (2019) (**Figure 4A**). The worm channel of the microfluidic device was connected to a syringe filled with NGM buffer + Histamine 20mM (Zimmer et al., 2009; Pokala et al., 2014; Hums et al., 2016).

Transgenic young adults (1 row of eggs) were picked onto a 6cm NGM agar + Histamine 20mM plate (+His; histamine dihydrochloride, Sigma-Aldrich) or an equal volume of water (-His), seeded with OP50. 3 to 4 worms were incubated at a time in either a +His plate or a -His (control) plate for 30-45 min. Worms that completely paralyzed after the incubation period in the +His plate were transferred to an intermediate 15cm food-free NGM agar plate and immersed in a drop of NGM + Histamine 20mM buffer to remove attached bacteria. Animals were then sucked into Tygon tubing by manually applying a brief vacuum with the syringe, which was subsequently connected to the worm inlet of the microfluidic device. Animals were finally loaded into the worm channel and arranged in the curved channel by applying slight pressure in the syringe. All components were connected using Tygon tubing (0.02 in ID, 0.06 in OD; Norton) or polyethyelene tubing (0.066 in ID, 0.095 in OD; Intramedic), using 23G Luerstub adapters (Intramedic). Standard gaseous conditions of 21% O_2 mixed with nitrogen were used. The gases were mixed by means of a gas mixer attached to mass flow controllers (Vögtling Instruments) regulated by LabView software, and delivered at a constant flow rate of 50ml/min to the gas inlet.

The microfluidic device was then placed in the microscope stage and 5 minutes were given to the worms to acclimate to the environment before starting the recording. The volume spanning the animals' head ganglia was recorded with the camera binning set to 2 (128x128 pixels), in 14 1-1.4 μm z-planes, each illuminated for 30ms to record GCaMP fluorescence, resulting in acquisition rates of ~2.3 volumes/sec (~32 fps). Each worm was recorded for 15 minutes.

4.2.2.2. Imaging in the Olfactory Microfluidic Chamber (delivery of sensory input)

Experiments were performed in custom-made microfluidic PDMS devices, as previously described by Chronis et al. (2007) and Chalasani et al. (2007). These chips trap the worms and allow their simultaneous stimulation, while being imaged, as depicted in **Figure 11A**. The flow of two side streams (1 and 4, in F**igure 11A**) was used to control the direction of the stream of two fluids under laminar

flow (2 and 3, in **Figure 11A**) – an NGM + dye buffer and the stimulus -, allowing the stimulus buffer to be directed to or away from the worm's nose. The stream running from either channel 1 or channel 4 was controlled by means of device (Valve Bank II) that allows a connected three-way valve to direct the buffer mixed with a fluorescent dye (fluorescein, 12nM) to enter the chip either from inlet 4, in which case the stimulus buffer is directed away from the worm's nose (OFF condition), or from inlet 1, in which case the stimulus buffer is directed towards the worm's nose (ON condition). The stimulus buffer enters the chip from inlet 2. From inlet 3, a buffer mixed with 7nM of a fluorescein enters the chip. The fluorescent dye mixed in two of the fluids allow the visualization of all three streams of fluids inside the chip, in order make sure no mixtures between them occur, which would result in no stimulation or premature stimulation of the worm. The flow in all microfluidic channels was kept running by means of a negative pressure created by a vacuum pump connected by Tygon tubing to the outlet channel of the chip.

The inlets of all microfluidic channels were connected, via tubing, to 30mL syringes placed at about 50cm above the level of the chip. All components were connected using Tygon tubing (0.02 in inner diameter (ID), 0.06 in outer diameter (OD); Norton) or polyethyelene tubing (0.066 in ID, 0.095 in OD; Intramedic) using 23G Luerstub adapters (Intramedic).

After pre-incubation on a 20nm histamine plate, transgenic young adults (1 row of eggs) were picked onto a foodless 15cm NGM agar and immersed in a drop of NGM medium. Individual worms were sucked into Tygon tubing filled with an NGM buffer + Histamine 20mM, by applying a brief manual negative pressure in a connected 3mL syringe. The end of the tube was subsequently connected to the worm inlet of the microfluidic chip and animals were loaded into the worm channel by applying a slight positive pressure in the syringe. The microfluidic device was then placed in the microscopes' stage and 5 minutes were given to the worms to acclimate to the environment before starting the recording.

The stimulation buffer of bacterial odour (*E. Coli* OP50) was prepared by incubating bacteria overnight in an NGM + LB medium at 26ºC, until it reached an absorbance of 0.5 at 600nm. The supernatant of the medium was then filtered in a 2μm pore diameter filter, not allowing bacteria to go through, but preserving odour molecules in the buffer. The same procedure was performed for a control of NGM buffer with the same volume of LB medium added (NGM + LB). The volume spanning the animals' head ganglia was recorded with the camera binning set to 2 (128x128 pixels), in 14 1.4 μm z-planes, each illuminated for 30ms to record GCaMP fluorescence, resulting in acquisition rates of ~2.3 volumes/second (~32 fps). 5 minutes were given to the worms to acclimate to the environment before

starting the recording. Each worm was recorded for 15 minutes, including a first 5-minute-long period OFF stimulus, followed by a 5-minute period ON stimulus, followed by a final 5-minute period OFF stimulus.

4.2.3. Simultaneous calcium imaging of neuronal activity and behaviour in freely moving animals

Transgenic young adults (1 row of eggs) were picked onto a foodless 15cm NGM agar plate, allowed to crawl away from the picking point and then picked to an agar arena, similar to the one used in the food chemotaxis assays. The arena, containing the worm, was then covered with a with a 45mm x 50mm #1.5 coverglass, so that the worm was between the coverglass and the agar. Under these conditions, worms move slower but with qualitatively normal body shapes and behaviour. For assays with a gradient of food, the same procedure to seed the arena as the one used in chemotaxis assays to food was followed, with the exception that the worms were placed closer to the food lawn, at a distance of about 1-1.5cm. The coverglass was then placed in the microscope stage.

2x binned images (128x128 pixels) were acquired across 21 z-planes with a step of 1.5μm between them, each illuminated for 20ms to record GCaMP and Scarlet fluorescence, resulting in acquisition rates of about 2.3 volumes/sec. Behaviour of the worm was recorded simultaneously using a Basler acA1300-200μm camera, with a 2x telecentric objective with in line near infrared (820 nm) illumination, and a similar frame rate as the fluorescent data, allowing to capture a behavioural frame for each corresponding fluorescence frame. A PhotoTrack (Applied Physics Instruments) unit was used to keep the worm in the field of view as it moved (Faumont et al., 2011). A programmed motorized microscope stage P-736 PInano Z Microscope Scanner was used to obtain the tracks of the worms, by logging the position of the stage that follows the worm as it moves. The stage and all cameras were synchronized by trigger signals. Each worm was imaged for approximately 10 minutes.

For all imaging experiments above described, fluorescent data were acquired with an inverted spinning disk confocal microscope (Zeiss Axio Observer Z1 combined with a spinning disk unit Yokogawa CSU-S1 spinning disk - 5000rpm), using a 40x water-immersion LD LCI Plan - Apochromat objective. A dual camera (EMCCD - Evolve 512) system was used to record both GCaMP and Scarlet/mCherry fluorescence. A blue (488nm) and an orange (561nm) lasers were used to excite GCaMP and Scarlet/mCherry, respectively. Green and Red channels were separated by a Dichroic

mirror FF580-FDICO1 splitting at 580nm: green emission filter 515/30 and red emission filter 617/73. VisiView software (Visitron Systems GmbH) was used to acquire the data.

4.3. Data Analysis

4.3.1. Chemotaxis Assays

Worms that chemotax and reached the food lawn were manually counted by examining the infrared movies. For control assays, an equal area as the one occupied by the food lawn in the movie frame was considered. Worms that, in the control assays, reached this area, left it and came back within the period of the recording, were counted once. Worms that left the arena by escaping through its borders were considered for the calculus of the Chemotaxis Index (CI). The CI was calculated as follows: # worms reaching food lawn / # total worms placed in the arena.

4.3.2. Ca^{2+} imaging in immobilised animals

When no discrimination of the AIY neurite region being measured is mentioned, the traces corresponding to either the *Axon Curve* or the *Axon Termination* (by that order of preference/availability) were used, as these regions showed the highest mean changes in amplitude (with no significant difference between both) between periods of Forward and Reverse command states, and because previous studies have measured sensory signals in AIY here (Chalasani et al., 2007; Larsch et al., 2013; Li et al., 2014; Ji et al., 2020).

4.3.2.1. Neuronal time series extraction from volumetric data

Neuronal activity traces were obtained using MetaMorph software (Molecular Devices). For the experiments performed in the oxygen chip, the z-plane where each desired nucleus, cell body or neurite region looked the brightest was manually chosen, and a stack of the selected z-planes over the entire length of the recording was created. Due to the weak GCaMP expression of the imaging line being used, for the experiments performed in the olfactory chip, a movie of the Maximum Intensity Projection was created, and signals were taken from it. A region of interest (ROI) containing the nucleus, cell body or neurite region of interest was selected, and its position tracked in each frame. An adjacent ROI was used to subtract background from the tracked area. The average intensity of the

pixels within the selected ROIs was logged into text files, as well as the corresponding frame number and the timestamp of acquisition.

$\Delta F/F_0$ was calculated as the percent change in fluorescence relative to the 10^{th} lowest percentile (F_0) from the entire recording, according to the following formula: $(F - F_0) / F_0$. All $\Delta F/F_0$ traces were smoothed over a window of 3 frames. Due to the higher laser intensity powers used in the imaging in the olfactory chip, these datasets were corrected for bleaching.

4.3.2.2. Motor command state identification

RIM activity was used as a readout of the behaviour state commands being encoded by the immobilised worm. Since reversal initiation and termination occur in an all-or-none fashion, RISE, HIGH, FALL and LOW phases were assigned to RIM activity traces based on the time derivative value of each time point: time derivative values greater than a small positive threshold defined the HIGH state and time derivative values smaller than a small negative threshold allowed to define the LOW phase. RISE and FALL phases were assigned based on behavioural state sequence and a threshold (as described further in Kato et al., 2015). High intensity RIM Ca^{2+} signals (RISE or HIGH phases) were defined as reversal command periods, whereas low intensity RIM Ca^{2+} signals (FALL or LOW phases) were defined as forward command periods.

4.3.2.3. Mean activity differences

The mean $\Delta F/F_0$ for each neuron or neurite region was calculated in all forward and reverse command periods (for **Figure 5**) or Odour-ON and Odour-OFF periods (for **Figure 14**), separately.

To disentangle the stimulus effect on AIY activity during Forward and Reverse Periods (**Figure 15**), the mean $\Delta F/F_0$ of AIY during the 10 seconds following the onset of a Forward or Reverse motor state were used. This was done to prevent biasing of higher AIY activity during Odour-ON stimulus solely due to the observed decrease in reversal frequency.

4.3.2.4. Pearson Correlation analysis

Wald Tests with t-distribution were used to obtain the significance of the correlation within each dataset (correlation between two traces of a single individual). p-values for individual correlations

within each analysis (e.g. AIY vs. RIM) were averaged and a final p-value was obtained. All correlations tested positive for significance ($p<0.05$).

4.3.2.5. Cross-correlation analysis

All cross-correlations analyses were performed between vectors of the derivatives of the Ca^{2+} activity traces of the neurons/neuronal regions being tested. Cross correlation reports the correlation of "target" neuron at different time delays, relative to a "reference" neuron.

4.4. Quantifications and Statistical Analysis

All data were analysed using either Python 3.7 or MATLAB (Mathworks) scripts. Custom code written by the author and specific for the aims of this study is available from the author without restriction. Statistical tests were performed using Graphpad Prism 7 software. These tests, along with the N and what N represents, are indicated in the legends of the respective figures.

5. SUPPLEMENTARY MATERIAL

5.1. Supplementary Figures

Supplementary Figure S1

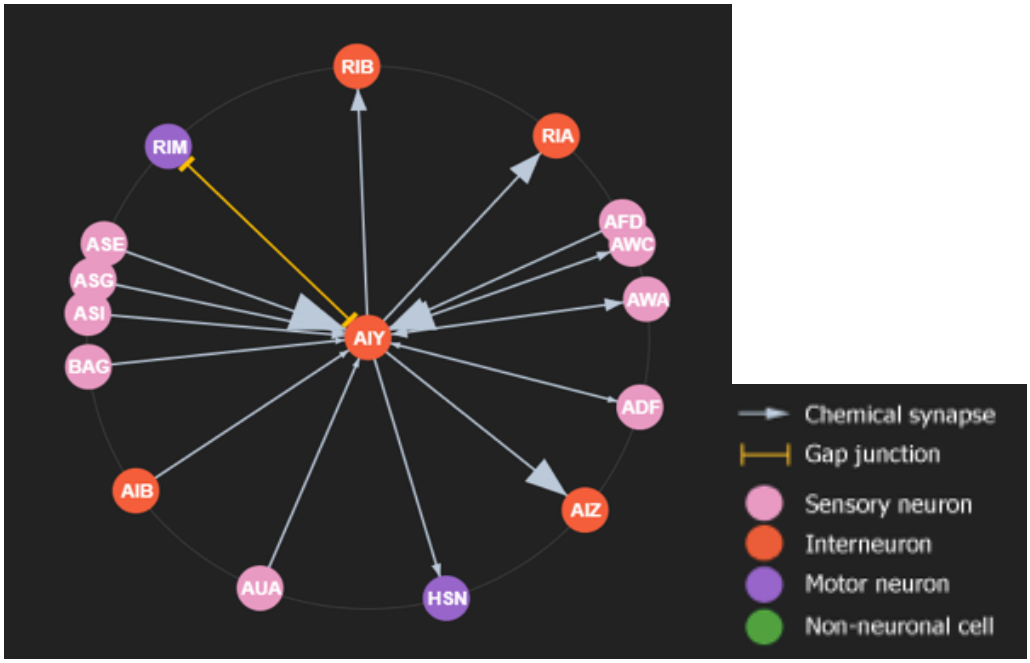

Supplementary Figure S1: AIY neuronal network. Figure retrieved and adapted from WORM WEB (available at wormweb.org/neuralnet#c=AIY&m=1).

Supplementary Figure S2

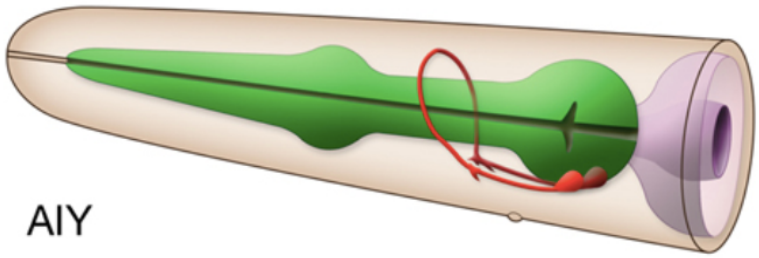

Supplementary Figure S2: AIY soma and axon location and trajectory. Figure retrieved from WORMATLAS (available at wormatlas.org/neurons/individual%20Neurons/AIYframeset.html).

Supplementary Figure S3

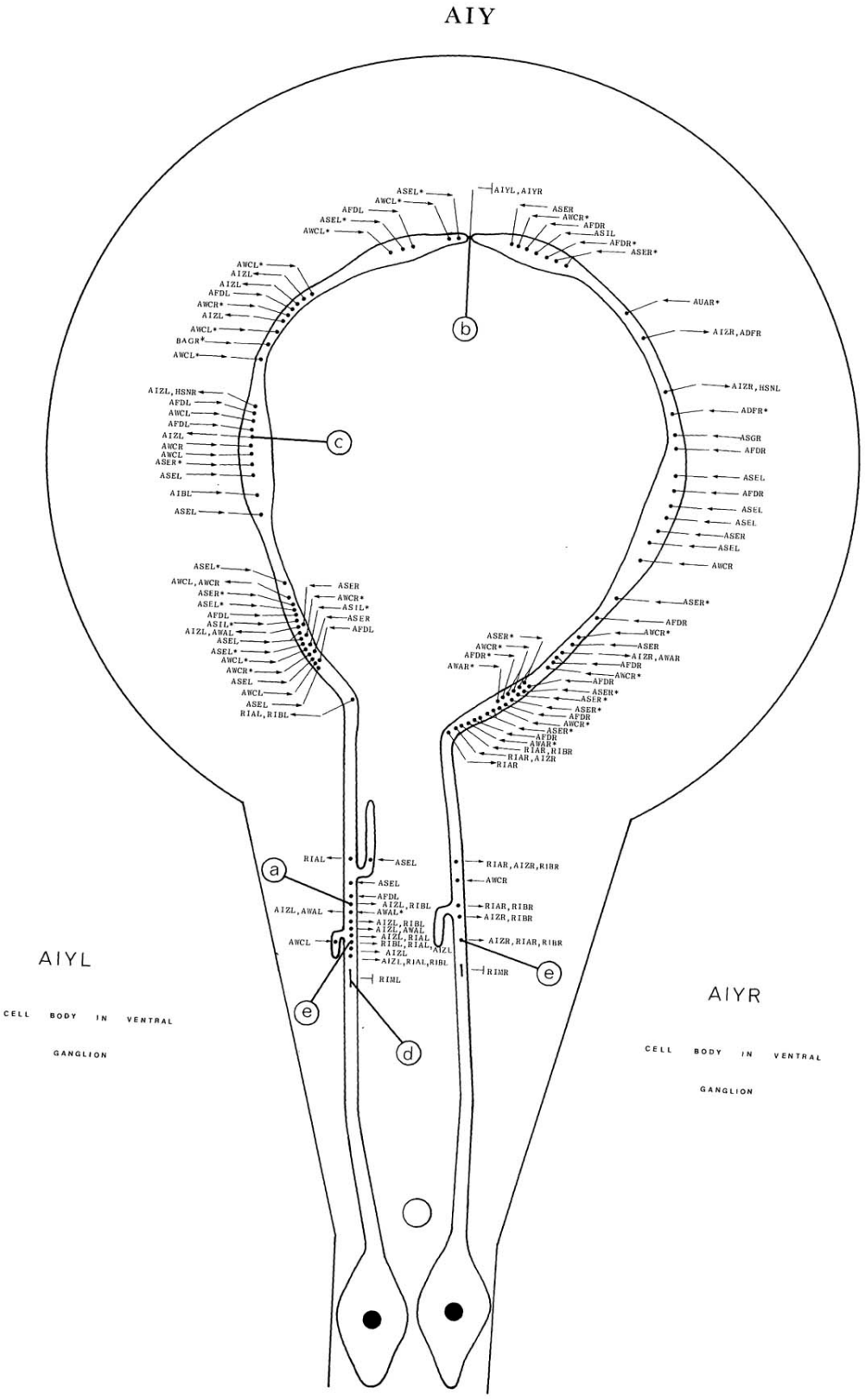

Supplementary Figure S3: Scheme of synaptic connectivity of AIY along its neurite. Retrieved from WORMATLAS (available at wormatlas.org/MoW_built0.92/cells/aiy.html).

Supplementary Figure S4

Supplementary Figure S4: Image from a typical recording, displaying the experimental setup of assays of chemotaxis to food. Blue cross denotes initial position of the population of worms; yellow bar represents location of the food lawn (OP50 at an OD20), to which the worms chemotax (no food lawn in control assays).

Supplementary Figure S5

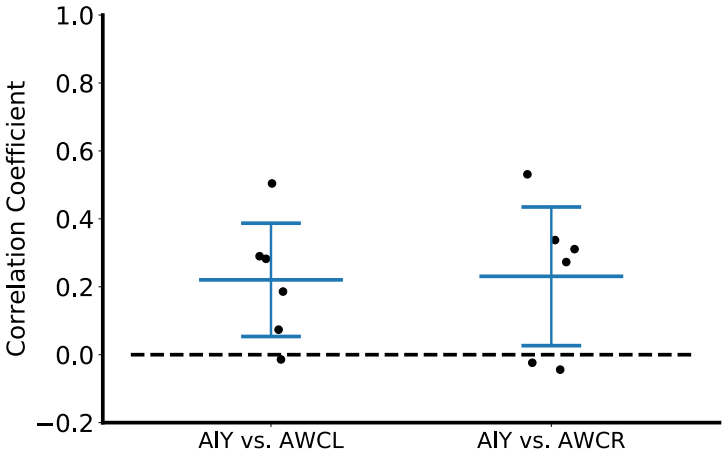

Supplementary Figure S5: Scatter plot of Pearson correlations between AWCL or AWCR and AIY. Bars indicate the mean correlation ± SD. Correlations tested positive for significance using a Wald Test with t-distribution

Supplementary Figure S6

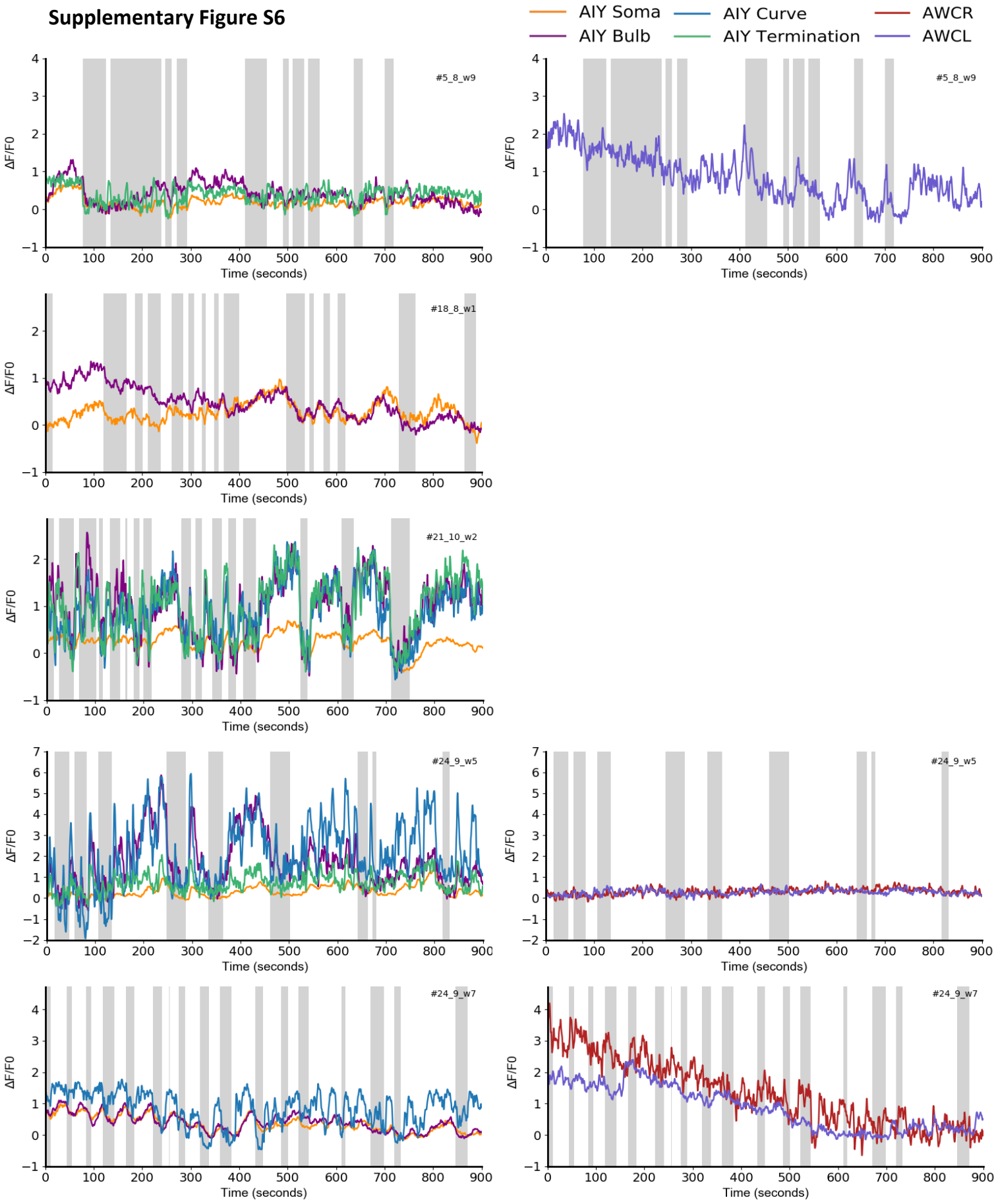

Supplementary Figure S6 (cont.)

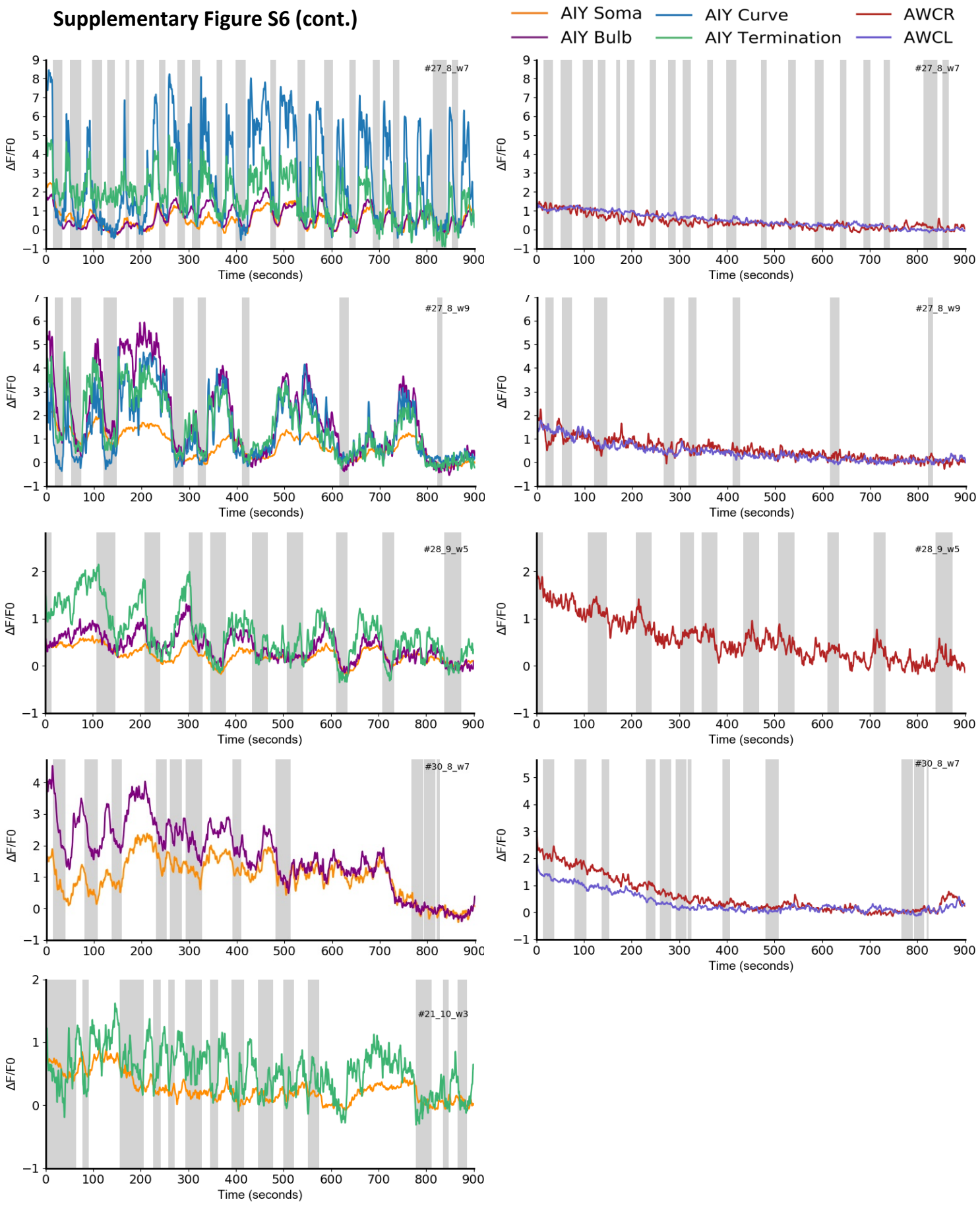

Supplementary Figure S6 (cont.)

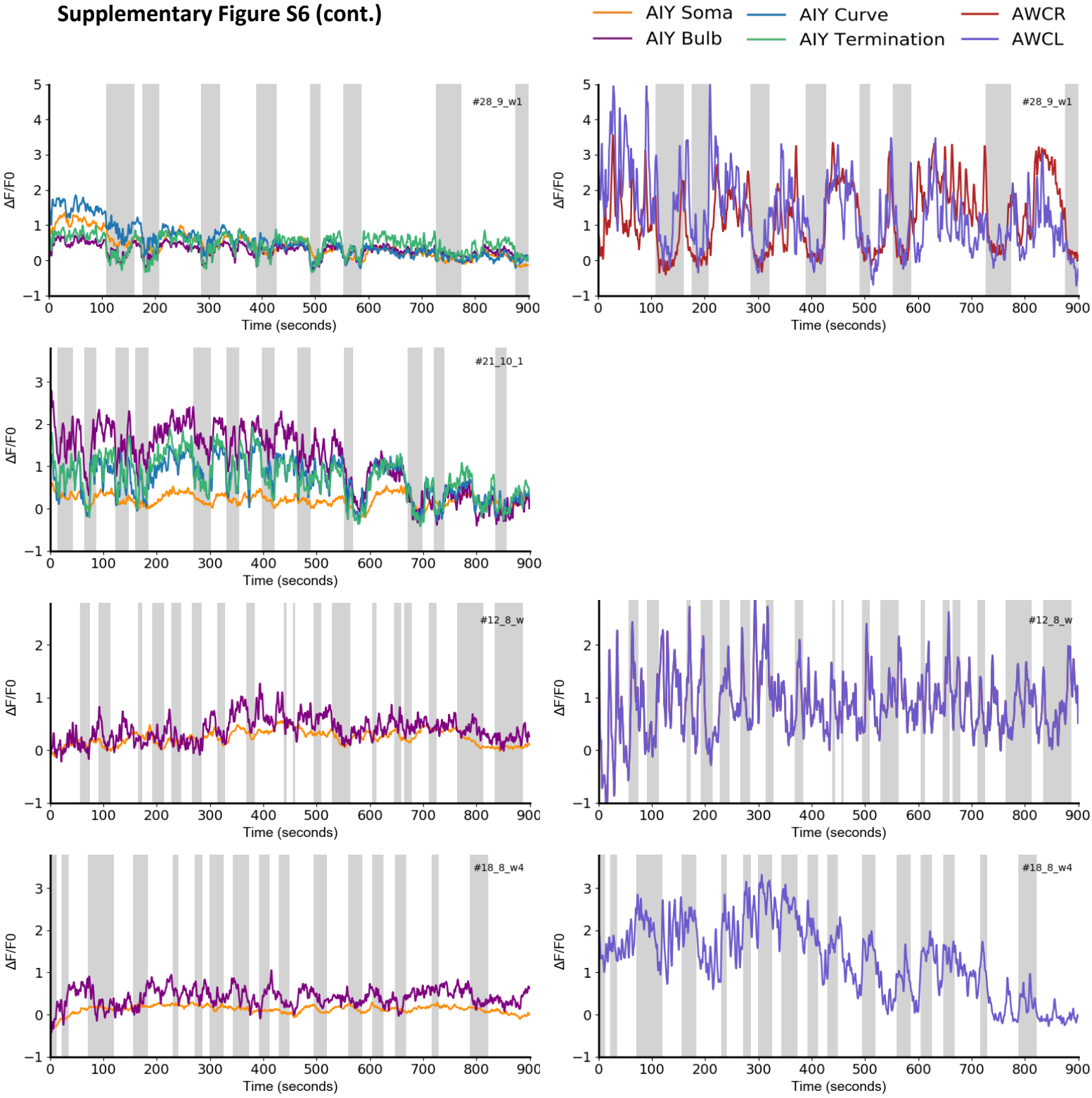

Supplementary Figures S6: All $\Delta F/F_0$ traces of recordings in the Oxygen Microfluidic Chamber used for subsequent analysis. Traces for AIY soma and neurite regions are plotted on the left and AWC (Left and Right pairs), for the same worm, are plotted on the right. Worms were recorded for a total of 15 minutes. Grey shaded bars denoted reversing periods (inferred from RIM activity).

Supplementary Figure S7

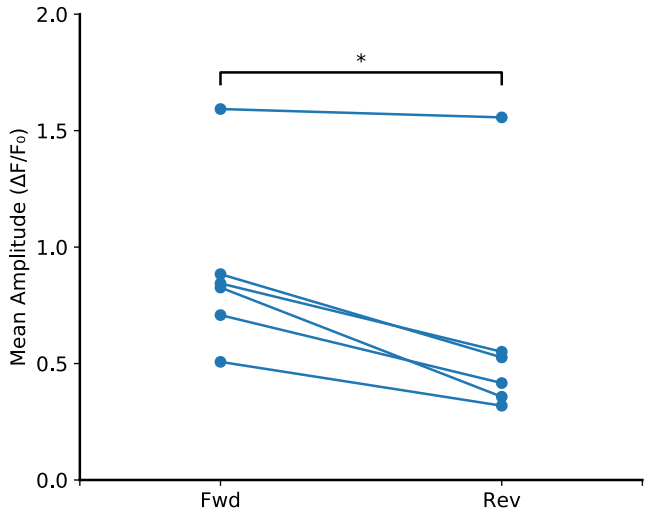

Supplementary Figure S7: Quantification of the mean $\Delta F/F_0$ during Forward (Fwd) and Reverse (Rev) periods, for AIY (no distinction between measured region) in the olfactory chip. Worms were stimulated with a control buffer of NGM (Control NGM vs. NGM condition). *p<0.05, Wilcoxon matched-pairs signed rank test.

Supplementary Figure S8

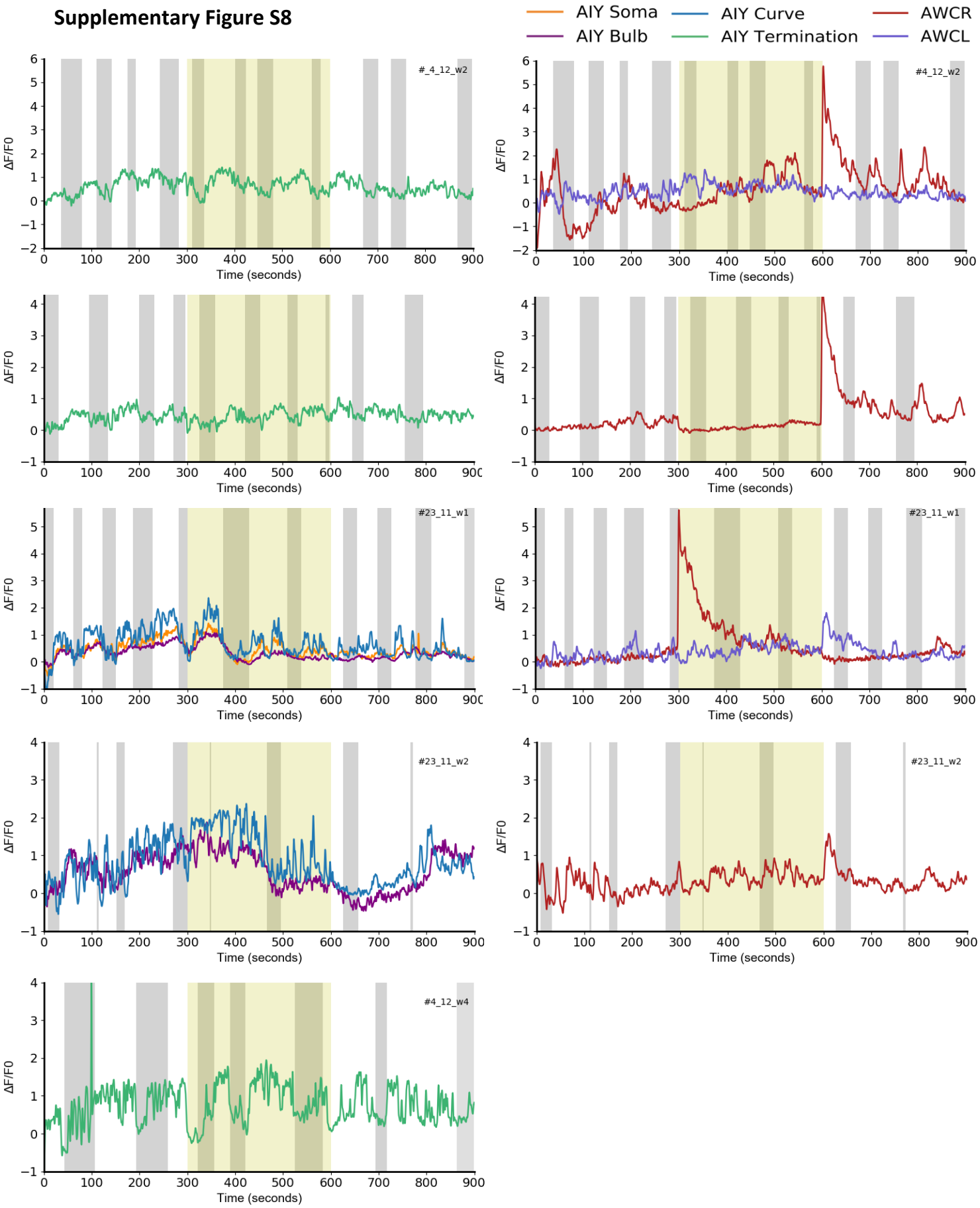

Supplementary Figure S8 (cont.)

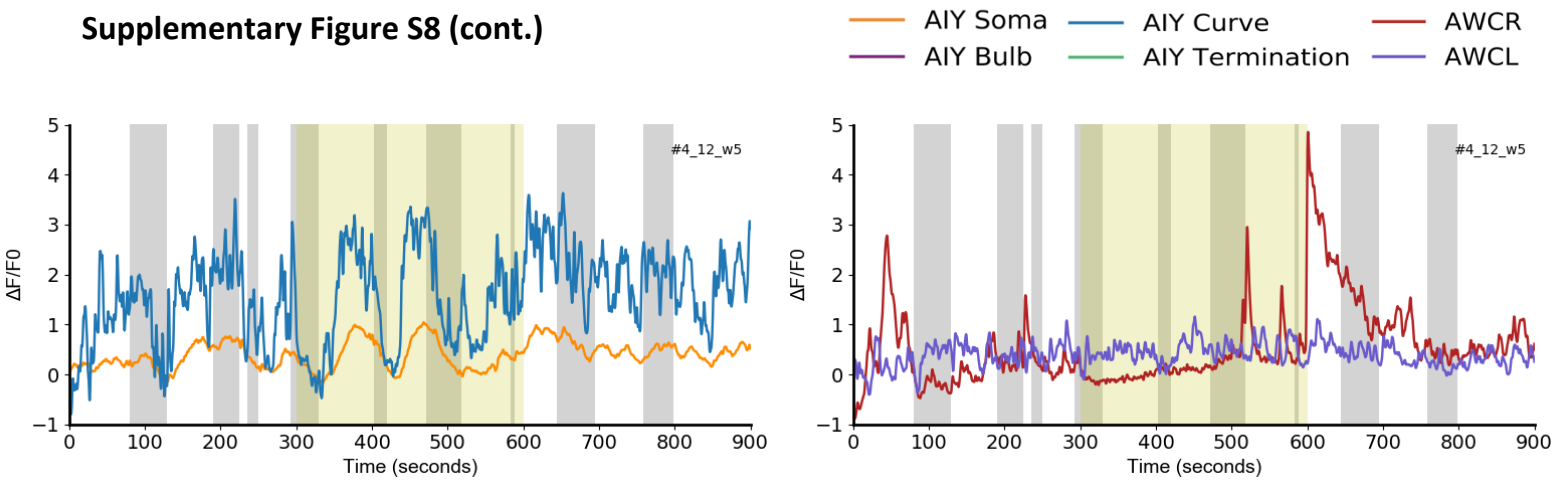

Supplementary Figure S8: All $\Delta F/F_0$ traces of the condition Control NGM vs. NGM in the Olfactory Microfluidic Chamber, used for subsequent analysis. Traces for AIY soma and neurite regions are plotted on the left and AWC (Left and Right pairs), for the same worm, are plotted on the right. Worms were recorded for a total of 15 minutes. Grey shaded bars denoted reversing periods (inferred from RIM activity) and yellow shaded period denotes period of stimulation (5 minutes).

Supplementary Figure S9

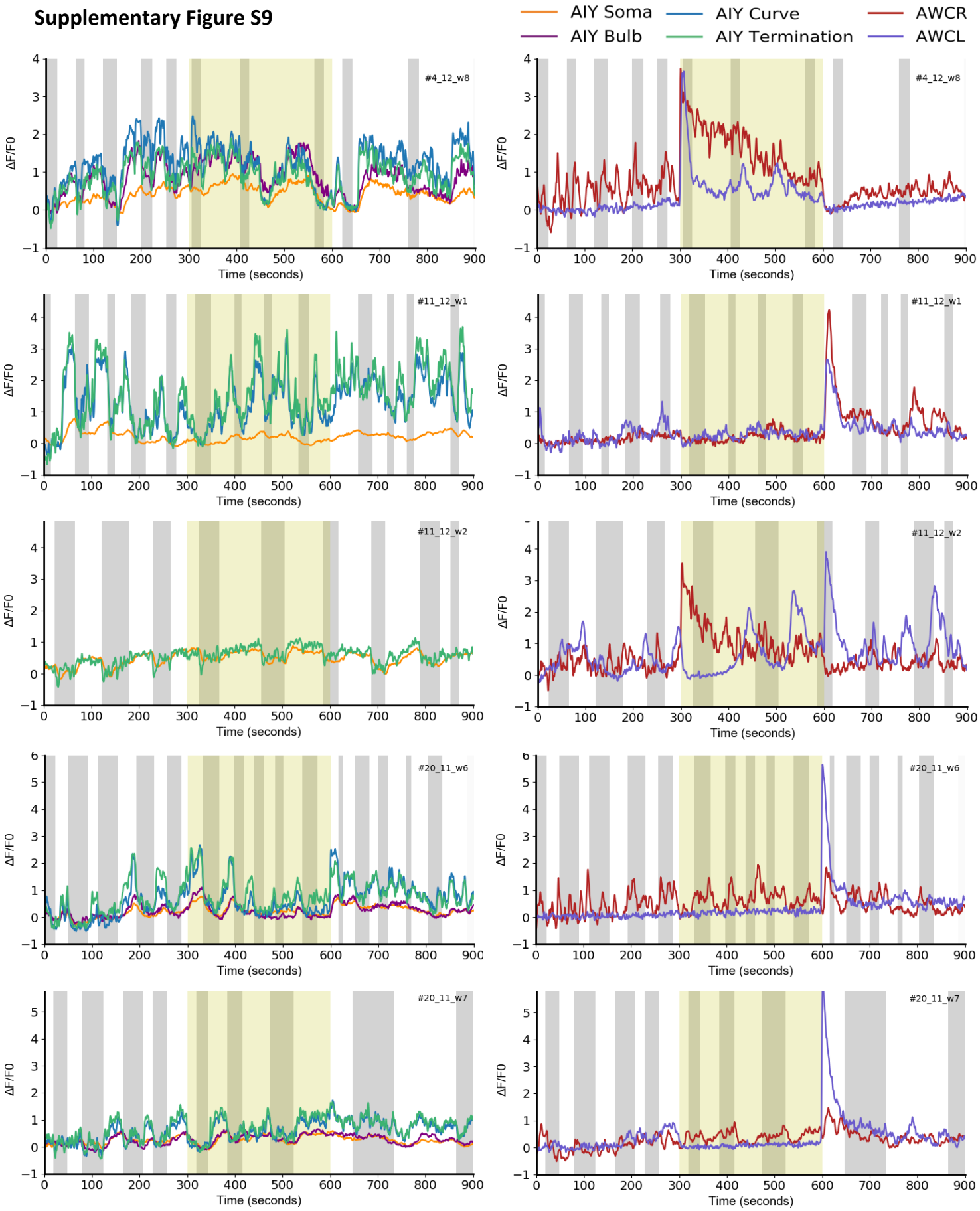

Supplementary Figure S9 (cont.)

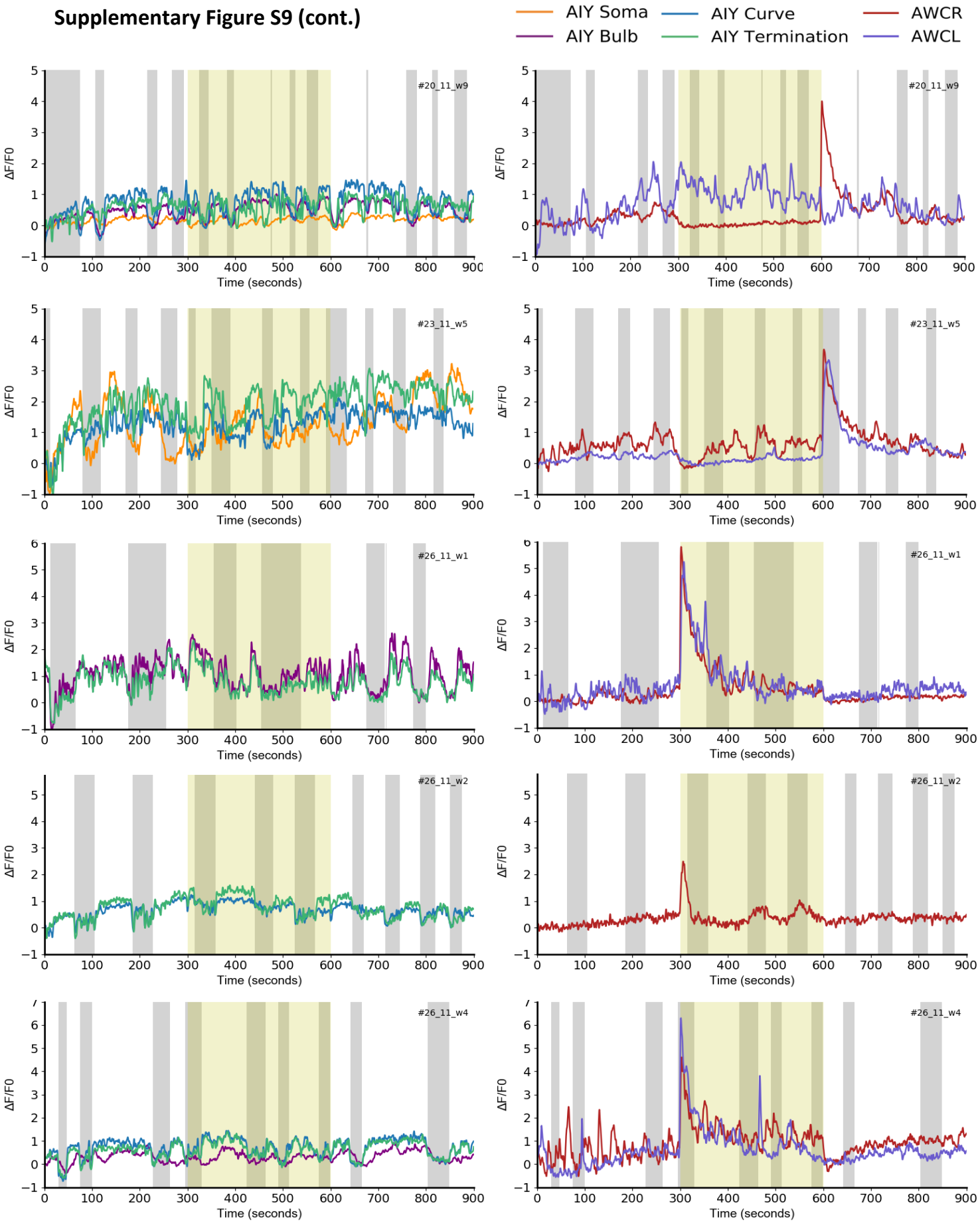

Supplementary Figure S9 (cont.)

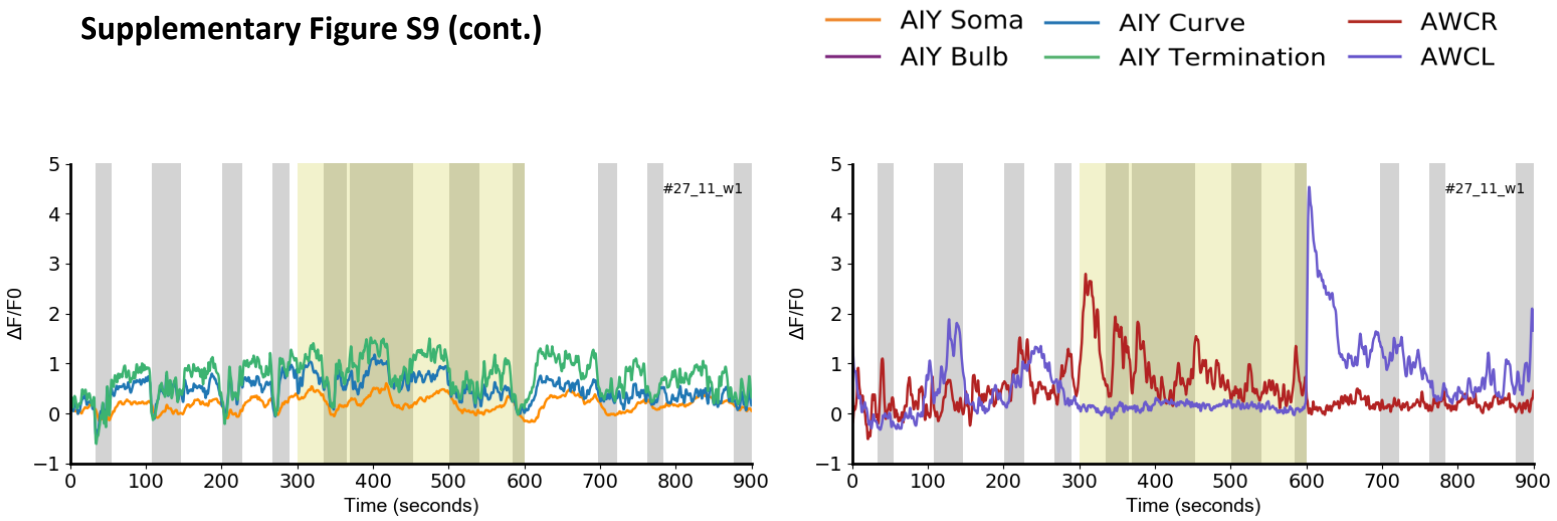

Supplementary Figure S9: All $\Delta F/F_0$ traces of the condition Control NGM + LB vs. NGM + LB in the Olfactory Microfluidic Chamber, used for subsequent analysis. Traces for AIY soma and neurite regions are plotted on the left and AWC (Left and Right pairs), for the same worm, are plotted on the right. Worms were recorded for a total of 15 minutes. Grey shaded bars denoted reversing periods (inferred from RIM activity) and yellow shaded period denotes period of stimulation (5 minutes).

Supplementary Figure S10

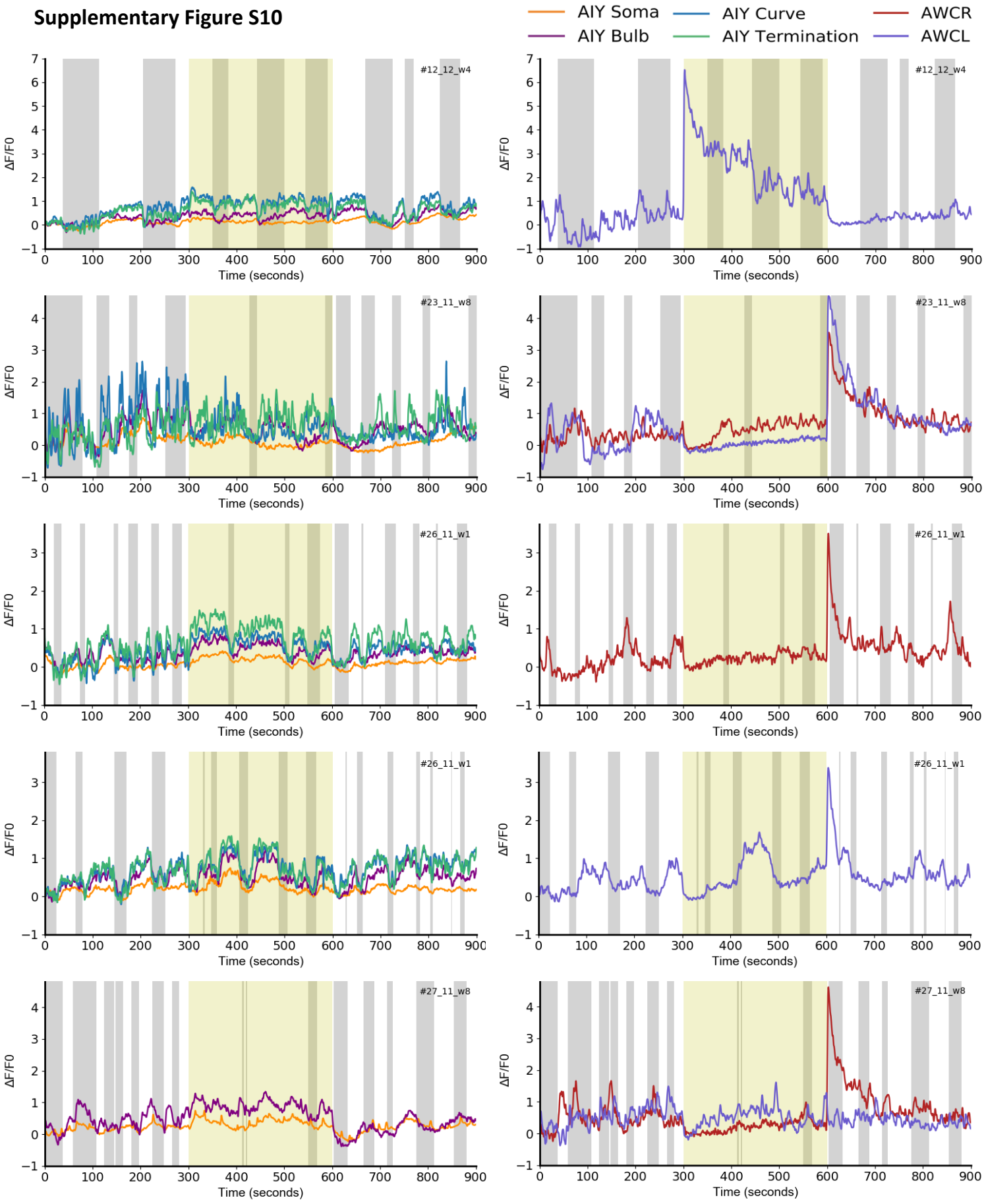

Supplementary Figure S10 (cont.)

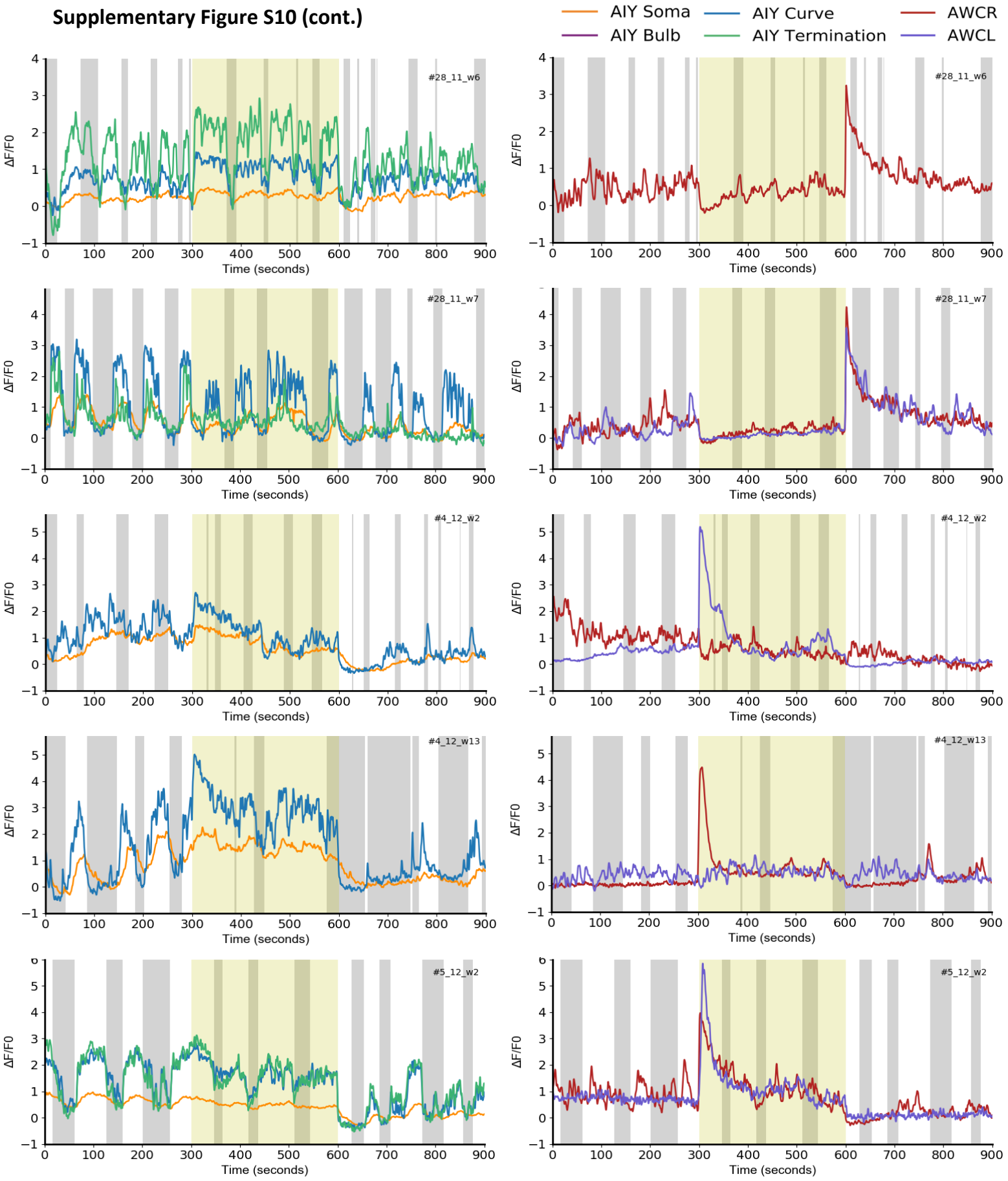

Supplementary Figure S10 (cont.)

Supplementary Figure S10: All $\Delta F/F_0$ traces of the condition NGM + LB vs. Bacterial Odour in the Olfactory Microfluidic Chamber, used for subsequent analysis. Traces for AIY soma and neurite regions are plotted on the left and AWC (Left and Right pairs), for the same worm, are plotted on the right. Worms were recorded for a total of 15 minutes. Grey shaded bars denoted reversing periods (inferred from RIM activity) and yellow shaded period denotes period of stimulation (5 minutes).

5.2. Supplementary Tables

Supplementary Table S1

Strain Name	Experiment	Genotype	Construct and injection concentration
ZIM2097	Chemotaxis Assays Freely Moving Imaging	lite-1 (ce314); mzmEx1260	Pttx-3::GCaMP7b - 25ng/ul Pttx-3::scarlet - 15ng/ul Podr-1::SV40NLS::GCaMP7s::egl-13 - 0.6ng/ul Podr-1::SV40NLS::scarlet::egl-13 - 0.2ng/ul Pflp-17::NLS mCherry - 0.5ng/ul
ZIM2123	Immobilised Ca^{2+} Imaging	lite-1 (ce314); mzmEx1260; mzmls37; mzmEx1269	Pttx-3::GCaMP7b - 25ng/ul Pttx-3::scarlet - 15ng/ul Podr-1::SV40NLS::GCaMP7s::egl-13 - 0.6ng/ul Podr-1::SV40NLS::scarlet::egl-13 - 0.2ng/ul Pflp-17::NLS mCherry - 0.5ng/ul Punc-122gfp (coelgfp) - 20ng/ul Pcex-1::NLSGCaMP5K - 25ng/uL myo-3::HisCl - 20ng/ul Pflp-17::mCherry - 1.5ng/ul

Supplementary Table S1: Details of strains used in this study.

Supplementary Table S2

Injection Number	Construct and injection concentration
353	(simple array) Pttx-3::GCaMP6f – 100ng/ul Pttx-3::Scarlet – 100ng/ul Podr-1::NLSGCaMP6f – 20ng/ul Podr-1::NLSScarlet – 20 ng/ul
355/356	(complex array) Pttx-3::GCaMP6f – 10ng/ul Pttx-3::Scarlet – 10ng/ul Podr-1::NLSGCaMP6f – 1ng/ul Podr-1::NLSScarlet – 0.5 ng/ul
359	(complex array) Pttx-3::GCaMP6f – 10ng/ul Pttx-3::Scarlet – 10ng/ul Podr-1::NLSGCaMP6f – 0.05ng/ul Podr-1::NLSScarlet – 0.05 ng/ul
371	(complex array) Pttx-3::GCaMP7b – 25ng/ul Pttx-3::Scarlet – 15ng/ul Podr-1::NLSGCaMP7s– 0.6ng/ul Podr-1::NLSScarlet – 0.08 ng/ul Pflp-17::NLS mCherry - 0.5ng/ul
375	(complex array) Pttx-3::GCaMP7b – 25ng/ul Pttx-3::Scarlet – 15ng/ul Podr-1::NLSGCaMP7s– 1.2ng/ul Podr-1::NLSScarlet – 0.3 ng/ul Pflp-17::NLS mCherry - 0.5ng/ul
376	(complex array) Pttx-3::GCaMP7b – 25ng/ul Pttx-3::Scarlet – 15ng/ul Podr-1::NLSGCaMP7s– 0.6ng/ul Podr-1::NLSScarlet – 0.2 ng/ul Pflp-17::NLS mCherry - 0.5ng/ul
377	(complex array) Pttx-3::GCaMP7b – 40ng/ul Pttx-3::Scarlet – 15ng/ul Podr-1::NLSGCaMP7s– 0.6ng/ul Podr-1::NLSScarlet – 0.2 ng/ul Pflp-17::NLS mCherry - 0.5ng/ul
383	(complex array) Pttx-3::GCaMP7b – 25ng/ul Pttx-3::Scarlet – 15ng/ul Podr-1::NLSGCaMP7s– 0.6ng/ul Podr-1::NLSScarlet – 0.2 ng/ul Pflp-17::NLS mCherry - 0.5ng/ul
386	(complex array) Pttx-3::GCaMP7b – 25ng/ul Pttx-3::Scarlet – 15ng/ul Podr-1::NLSGCaMP7s– 0.6ng/ul Podr-1::NLSScarlet – 0.2 ng/ul Pflp-17::NLS mCherry - 0.5ng/ul
387	(complex array) Pttx-3::GCaMP7b – 25ng/ul Pttx-3::Scarlet – 15ng/ul

	Podr-1::NLSGCaMP7s– 0.6ng/ul Podr-1::NLSScarlet – 0.3 ng/ul Pflp-17::NLSmCherry - 0.5ng/ul
389	(complex array) Pflp-18::DIO::GCaMP7b – 2.5ng/ul Pttx-3::CreVDH – 5 ng/ul Pttx-3::Scarlet – 15 ng/ul Podr-1::NLSGCaMP7s – 0.6ng/ul Podr-1::NLSScarlet – 0.2 ng/ul
391	(complex array) Pflp-18::DIO::GCaMP6f – 2.5ng/ul Pttx-3::CreVDH – 5 ng/ul
392	(complex array) Pflp-18::DIO::mCherry– 2.5ng/ul Pttx-3t::CreVDH – 5 ng/ul
393	(complex array) Pflp-18::DIO::mCherry::GCaMP7b – 5ng/ul Pttx-3t::CreVDH – 10 5ng/ul
394	(complex array) Pttx-3t::Scarlet (new prom.) – 5ng/ul
395	(complex array) Pflp-18::DIO::GCaMP7b::mCherry – 5ng/ul Pttx-3t::CreVDH – 5 ng/ul
396	(complex array) Pflp-18::DIO::GCaMP7b::mCherry – 10ng/ul Pttx-3t::CreVDH – 5 ng/ul
397	(complex array) Pttx-3t::scarlet (new prom.) – 5ng/ul
398	(complex array) Pttx-3t::Scarlet (new prom.) – 5ng/ul
406	(complex array) Pttx-3t::GCaMP7b (new prom.) – 2ng/ul (coel dsRed)
407	(complex array) Pttx-3t::GCaMP7b (new prom.) – 6ng/ul (coel dsRed)
411	(complex array) Psra-11::DIO::mCherry – 1.5ng/ul Ncs-1::CreVDH – 2ng/ul
415	(complex array) Psra-11::DIO::GCaMP7b – 3ng/ul Pncs-1::CreVDH – 1 ng/ul
416	(complex array) Psra-11::DIO::GCaMP7b – 5ng/ul Pncs-1::CreVDH – 1 ng/ul
417	(complex array) Psra-11::DIO::GCaMP7b – 10ng/ul Pncs-1::CreVDH – 1 ng/ul

Supplementary Table S2: Details of part of the strains generated as an attempt to overcome the weak pattern of GCaMP expression in AIY.

5.3. Supplementary Movies

Supplementary Movies are available in digital format only.

Supplementary Movie S1-S4: Maximum Intensity Projection movies of example recordings in the Oxygen Chip, in the absence of fluctuating sensory input. Video speed fastened so that changes in Ca^{2+} activity can be appreciated.

Supplementary Movie S5-S6: Maximum Intensity Projection movies of example recordings in the Olfactory Chip. Video speed fastened so that changes in Ca^{2+} activity can be appreciated.

Supplementary Movie S7-S8: Segments of example recording of freely moving worms, for green and red channels and behaviour. All movies speeds are fastened to twice their real frame rate.

6. REFERENCES

Aimon, S., Katsuki, T., Jia, T., Grosenick, L., Broxton, M., Deisseroth, K., Sejnowski, T. J., & Greenspan, R. J. (2019). Fast near-whole-brain imaging in adult Drosophila during responses to stimuli and behavior. *PLoS biology*, *17*(2), e2006732.

Albrecht, D., Bargmann (2011). C. High-content behavioral analysis of *Caenorhabditis elegans* in precise spatiotemporal chemical environments. *Nat Methods* 8, 599–605.

Artiushin, G., & Sehgal, A. (2017). The Drosophila circuitry of sleep-wake regulation. *Current Opinion in Neurobiology*, *44*.

Bargmann CI, Horvitz HR (1991). Chemosensory neurons with overlapping functions direct chemotaxis to multiple chemicals in C. elegans. Neuron 7:729–742.

Bargmann, C.I. Chemosensation in *C. elegans* (2006). *WormBook*, ed. The *C. elegans* Research Community, WormBook,

Ben Arous, J., Laffont, S., & Chatenay, D. (2009). Molecular and sensory basis of a food related two-state behavior in C. elegans. *PloS one*, *4*(10), e7584.

Bentley, B., Branicky, R., Barnes, C.L., Chew, Y.L., Yemini, E., Bullmore, E.T., Vértes, P.E., and Schafer, W.R. (2016). The Multilayer Connectome of Caenorhabditis elegans. PLoS Comput Biol *12*, e1005283–31.

Berry, J. A., Cervantes-Sandoval, I., Chakraborty, M., & Davis, R. L. (2015). Sleep Facilitates Memory by Blocking Dopamine Neuron-Mediated Forgetting. *Cell*, *161*(7), 1656–1667.

Bono, M. de & Villu Maricq (2005) A. Neuronal Substrates of Complex Behaviors in C. Elegans . *Annu. Rev. Neurosci.* 28, 451–501.

Brenner S. (1974). The genetics of Caenorhabditis elegans. *Genetics*, *77*(1), 71–94.

Chalasani, S.H., Chronis, N., Tsunozaki, M., Gray, J.M., Ramot, D., Goodman, M.B., and Bargmann, C.I. (2007). Dissecting a circuit for olfactory behaviour in Caenorhabditis elegans. Nature *450*, 63–70.

Chalasani, S.H., Kato, S., Albrecht, D.R., Nakagawa, T., Abbott, L.F., and Bargmann, C.I. (2010). Neuropeptide feedback modifies odor-evoked dynamics in Caenorhabditis elegans olfactory neurons. Nat Neurosci *13*, 615–621.

Chen, T.-W., Wardill, T.J., Sun, Y., Pulver, S.R., Renninger, S.L., Baohan, A., Schreiter, E.R., Kerr, R.A., Orger, M.B., Jayaraman, V., et al. (2013). Ultrasensitive fluorescent proteins for imaging neuronal activity. Nature *499*, 295–300.

Chronis, N., Zimmer, M., and Bargmann, C.I. (2007). Microfluidics for in vivo imaging of neuronal and behavioral activity in Caenorhabditis elegans. Nat Meth *4*, 727–731.

Clark, D.A., Biron, D., Sengupta, P., and Samuel, A.D.T. (2006). The AFD Sensory Neurons Encode Multiple Functions Underlying Thermotactic Behavior in Caenorhabditis elegans. J. Neurosci. *26*, 7444–7451.

Coen, P., & Murthy, M. (2016). Singing on the fly: sensorimotor integration and acoustic communication in Drosophila. Current Opinion in Neurobiology, 38, 38–45.

Cohn, R., Morantte, I., & Ruta, V. (2015). Coordinated and Compartmentalized Neuromodulation Shapes Sensory Processing in Drosophila. *Cell*, *163*(7), 1742–1755.

Dana, H., Mohar, B., Sun, Y., Narayan, S., Gordus, A., Hasseman, J.P., Tsegaye, G., Holt, G.T., Hu, A., Walpita, D., et al. (2016). Sensitive red protein calcium indicators for imaging neural activity. eLife *5*.

Dasgupta, S., Stevens, C. F. & Navlakha, S. (2017). A neural algorithm for a fundamental computing problem. *Science (80-.).* 358, 793–796.

Faumont, S., Rondeau, G., Thiele, T. R., Lawton, K. J., McCormick, K. E., Sottile, M., Griesbeck, O., Heckscher, E. S., Roberts, W. M., Doe, C. Q., & Lockery, S. R. (2011). An image-free opto-mechanical system for creating virtual environments and imaging neuronal activity in freely moving Caenorhabditis elegans. *PloS one*, *6*(9), e24666.

Flavell, S. W., Pokala, N., Macosko, E. Z., Albrecht, D. R., Larsch, J., & Bargmann, C. I. (2013). Serotonin and the Neuropeptide PDF Initiate and Extend Opposing Behavioral States in C. elegans. *Cell*, 1–13.

Fu, Y., Tucciarone, J. M., Espinosa, J. S., Sheng, N., Darcy, D. P., Nicoll, R. A., Huang, Z. J., & Stryker, M. P. (2014). A cortical circuit for gain control by behavioral state. *Cell*, *156*(6), 1139–1152.

Fujiwara, M., Sengupta, P. & McIntire, S. L. (2002). Regulation of Body Size and Behavioral State of C. elegans by Sensory Perception and the EGL-4 cGMP-Dependent Protein Kinase. *Neuron* 36, 1091–1102.

Georgopoulos, A. P., Kettner, R. E. & Schwartz, A. B. (1988). Primate motor cortex and free arm movements to visual targets in three- dimensional space. II. Coding of the direction of movement by a neuronal population. *J. Neurosci.* 8, 2928–2937.

Georgopoulos, A. P., Schwartz, A. B. & Kettner, R. E. (1986). Neuronal population coding of movement direction. *Science* 233, 1416–9.

Goodman, M. B., Hall, D. H., Avery, L., & Lockery, S. R. (1998). Active currents regulate sensitivity and dynamic range in C. elegans neurons. *Neuron*, *20*(4), 763–772.

Gordus, A., Pokala, N., Levy, S., Flavell, S. W., & Bargmann, C. I. (2015). Feedback from Network States Generates Variability in a Probabilistic Olfactory Circuit. *Cell*, *161*(2), 215–227.

Gray, J.M., Hill, J.J., and Bargmann, C.I. (2005). A circuit for navigation in Caenorhabditis elegans. Proc. Natl. Acad. Sci. U.S.a. *102*, 3184.

Guillermin, M.L., Carrillo, M.A., and Hallem, E.A. (2017). A Single Set of Interneurons Drives Opposite Behaviors in C.elegans. Current Biology 1–23.

Ha, H.-I., Hendricks, M., Shen, Y., Gabel, C. V., Fang-Yen, C., Qin, Y., et al. (2010). Functional Organization of a Neural Network for Aversive Olfactory Learning in Caenorhabditis elegans. *Neuron*, *68*(6), 1173–1186.

Hendricks, M., & Zhang, Y. (2013). Complex RIA calcium dynamics and its function in navigational behavior. *Worm*, *2*(3), e25546.

Hendricks, M., Ha, H., Maffey, N., & Zhang, Y. (2012). Compartmentalized calcium dynamics in a C. elegans interneuron encode head movement. Nature, 487, 99.

Hums, I., Riedl, J., Mende, F., Kato, S., Kaplan, H. S., Latham, R., Sonntag, M., Traunmüller, L., & Zimmer, M. (2016). Regulation of two motor patterns enables the gradual adjustment of locomotion strategy in Caenorhabditis elegans. *eLife*, *5*, e14116.

Huston, S. J., & Jayaraman, V. (2011). Studying sensorimotor integration in insects. Current Opinion in Neurobiology, 21(4), 527–534.

Iino, Y., and Yoshida, K. (2009). Parallel Use of Two Behavioral Mechanisms for Chemotaxis in Caenorhabditis elegans. J. Neurosci. *29*, 5370–5380.

Ince, R. A. A., Panzeri, S. & Kayser, C. (2013) Neural Codes Formed by Small and Temporally Precise Populations in Auditory Cortex. *J. Neurosci.* 33, 18277–18287.

Ji, N., Madan, G. K., Fabre, G. I., Dayan, A., Baker, C. M., Nwabudike, I., & Flavell, S. W. (2020). A neural circuit for flexible control of persistent behavioral states. *bioRxiv*, 2020.02.04.934547.

Ji, N., Venkatachalam, V., Rodgers, H., Hung, W., Kawano, T., Clark, C. M., et al. (2019). Corollary Discharge Promotes a Sustained Motor State in a Neural Circuit for Navigation. *bioRxiv*, 861559.

Kaplan, H. S., Nichols, A. L. A., & Zimmer, M. (2018). Sensorimotor integration in Caenorhabditis elegans: a reappraisal towards dynamic and distributed computations. *Philosophical Transactions of the Royal Society B: Biological Sciences*, *373*(1758), 20170371–12.

Kaplan, H. S., Thula, O. S., Khoss, N., & Zimmer, M. (2019). Nested Neuronal Dynamics Orchestrate a Behavioral Hierarchy across Timescales. *Neuron*, *105*(3), 562–576.e9.

Karadimas, S.K., Satkunendrarajah, K., Laliberte, A.M. *et al. (2019).* Sensory cortical control of movement. *Nat Neurosci* 23, 75–84.

Kato, S., Kaplan, H. S., Schrödel, T., Skora, S., Lindsay, T. H., Yemini, E., et al. (2015). Global Brain Dynamics Embed the Motor Command Sequence of Caenorhabditis elegans. Cell, 163(3), 656–669.

Kocabas, A., Shen, C.-H., Guo, Z. V., & Ramanathan, S. (2012). Controlling interneuron activity in Caenorhabditis elegans to evoke chemotactic behaviour.

Kunitomo, H., Sato, H., Iwata, R. *et al.* Concentration memory-dependent synaptic plasticity of a taste circuit regulates salt concentration chemotaxis in *Caenorhabditis elegans*. *Nat Commun* 4, 2210 (2013).

Larsch, J., Flavell, S. W., Liu, Q., Gordus, A., Albrecht, D. R., & Bargmann, C. I. (2015). A Circuit for Gradient Climbing in C. elegans Chemotaxis. *CellReports*, 1–14.

Larsch, J., Ventimiglia, D., Bargmann, C. I. & Albrecht, D. R. (2013). High-throughput imaging of neuronal activity in Caenorhabditis elegans. *Proc. Natl. Acad. Sci. U. S. A.* 110.

Laurent, P., Soltesz, Z., Nelson, G.M., Chen, C., Arellano-Carbajal, F., Levy, E., and de Bono, M. (2015). Decoding a neural circuit controlling global animal state in C. elegans. eLife *4*.

Li, Z., Liu, J., Zheng, M. & Xu, X. Z. S. (2014) Encoding of Both Analog- and Digital-like Behavioral Outputs by One *C. elegans* Interneuron. *Cell* 159, 751–765.

Lindsay, T. H., Thiele, T. R., & Lockery, S. R. (2011). Optogenetic analysis of synaptic transmission in the central nervous system of the nematode Caenorhabditis elegans. *Nature Communications*, *2*(1), 895–20.

Liu, H., Yang, W., Wu, T., Duan, F., Soucy, E., Jin, X., & Zhang, Y. (2018). Cholinergic Sensorimotor Integration Regulates Olfactory Steering. *Neuron*, *97*(2), 390–405.e3.

Luo, L., Wen, Q., Ren, J., Hendricks, M., Gershow, M., Qin, Y., et al. (2014). Dynamic Encoding of Perception, Memory, and Movement in a C. elegans Chemotaxis Circuit. *Neuron*, *82*(5), 1115–1128.

Matyas, F., Sreenivasan, V., Marbach, F., Wacongne, C., Barsy, B., Mateo, C., et al. (2010). Motor Control by Sensory Cortex. *Science*, *330*(6008), 1240.

Miall, R. C. & Wolpert, D. M. (1996). Forward Models for Physiological Motor Control. *Neural Networks* 9, 1265–1279.

Nakai, J., Ohkura, M., and Imoto, K. (2001). A high signal-to-noise Ca(2+) probe composed of a single green fluorescent protein. Nat Biotechnol *19*, 137–141.

Nguyen, J.P., Shipley, F.B., Linder, A.N., Plummer, G.S., Liu, M., Setru, S.U., Shaevitz, J.W., and Leifer, A.M. (2016). Whole-brain calcium imaging with cellular resolution in freely behaving Caenorhabditis elegans. Proc Natl Acad Sci USA *113*, E1074–E1081.

Nichols, A. L. A., Eichler, T., Latham, R., & Zimmer, M. (2017). A global brain state underlies C. elegansssleep behavior. Science, 356(6344), eaam6851–11.

Niell, C. M., & Stryker, M. P. (2010). Modulation of visual responses by behavioral state in mouse visual cortex. *Neuron*, *65*(4), 472–479.

Oda, S., Tomioka, M., and Iino, Y. (2011). Neuronal plasticity regulated by the insulin-like signaling pathway underlies salt chemotaxis learning in Caenorhabditis elegans. Journal of Neurophysiology *106*, 301–308.

Olberg, R. M., Seaman, R. C., Coats, M. I., & Henry, A. F. (2007). Eye movements and target fixation during dragonfly prey-interception flights. Journal of Comparative Physiology A, 193(7), 685–693.

Onken, A., Karunasekara, P., Kayser, C. & Panzeri, S. (2014). Understanding neural population coding: information-theoretic insights from the auditory system. *Adv. Neurosci.* 2014, 1–14.

Panzeri, S., Macke, J. H., Gross, J. & Kayser, C. (2015). Neural population coding: Combining insights from microscopic and mass signals. *Trends Cogn. Sci.* 19, 162–172.

Pietri, T., Romano, S. A., Pérez-Schuster, V., Boulanger-Weill, J., Candat, V., & Sumbre, G. (2017). The Emergence of the Spatial Structure of Tectal Spontaneous Activity Is Independent of Visual Inputs. *Cell reports*, *19*(5), 939–948.

Piggott, B.J., Liu, J., Feng, Z., Wescott, S.A., and Xu, X.Z.S. (2011). The Neural Circuits and Synaptic Mechanisms Underlying Motor Initiation in C. elegans. Cell *147*, 922–933.

Pokala, N., Liu, Q., Gordus, A., & Bargmann, C. I. (2014). Inducible and titratable silencing of Caenorhabditis elegans neurons in vivo with histamine-gated chloride channels. *Proceedings of the National Academy of Sciences*, *111*(7), 2770–2775.

Poulet, J. F., & Hedwig, B. (2003). Corollary discharge inhibition of ascending auditory neurons in the stridulating cricket. *The Journal of neuroscience : the official journal of the Society for Neuroscience*, *23*(11), 4717–4725.

Romano, S. A., Pietri, T., Pérez-Schuster, V., Jouary, A., Haudrechy, M., & Sumbre, G. (2015). Spontaneous neuronal network dynamics reveal circuit's functional adaptations for behavior.

Saleem, A. B., Diamanti, E. M., Fournier, J., Harris, K. D., & Carandini, M. (2018). Coherent encoding of subjective spatial position in visual cortex and hippocampus. *Nature*, *562*(7725), 124–127.

Salkoff, D. B., Zagha, E., McCarthy, E., & McCormick, D. A. (2019). Movement and Performance Explain Widespread Cortical Activity in a Visual Detection Task. *Cerebral Cortex*.

Schafer W. R. (2015). Mechanosensory molecules and circuits in C. elegans. *Pflugers Archiv : European journal of physiology*, *467*(1), 39–48.

Schneider, D. M., Nelson, A., & Mooney, R. (2014). A synaptic and circuit basis for corollary discharge in the auditory cortex. *Nature*, *513*(7517), 189–194.

Scholz, M., Linder, A.N., Randi, F., Sharma, A.K., Yu, X., Shaevitz, J.W., and Leifer, A.M. (2018). Predicting natural behavior from whole-brain neural dynamics. bioRxiv 445643.

Schrödel, T., Prevedel, R., Aumayr, K., Zimmer, M., and Vaziri, A. (2013). Brain-wide 3D imaging of neuronal activity in Caenorhabditis elegans with sculpted light. Nat Meth *10*, 1013–1020.

Straka, H., Simmers, J. & Chagnaud, B. P. (2018). A New Perspective on Predictive Motor Signaling. *Curr. Biol.* 28, R193–R194.

Stringer, C., Pachitariu, M., Steinmetz, N., Reddy, C. B., Carandini, M., & Harris, K. D. (2019). Spontaneous behaviors drive multidimensional, brainwide activity. *Science (New York, N.Y.)*, *364*(6437), 255.

Sulston, J.E., and Horvitz, H.R. (1977). Post-embryonic cell lineages of the nematode, Caenorhabditis elegans. Developmental Biology *56*, 110–156.

Tsalik, E.L., and Hobert, O. (2003). Functional mapping of neurons that control locomotory behavior inCaenorhabditis elegans. J. Neurobiol. *56*, 178–197.

Tsur, O., Khrapunsky, Y., & Azouz, R. (2019). Sensorimotor integration in the whisker somatosensory brain stem trigeminal loop. Journal of Neurophysiology, 122(5), 2061–2075.

Varshney, L.R., Chen, B.L., Paniagua, E., Hall, D.H., and Chklovskii, D.B. (2011). Structural Properties of the Caenorhabditis elegans Neuronal Network. PLoS Comput Biol *7*, e1001066–21.

Venkatachalam, V., Ji, N., Wang, X., Clark, C., Mitchell, J.K., Klein, M., Tabone, C.J., Florman, J., Ji, H., Greenwood, J., et al. (2016). Pan-neuronal imaging in roaming Caenorhabditis elegans. Proc Natl Acad Sci USA *113*, E1082–E1088.

Wakabayashi, T., Kitagawa, I., & Shingai, R. (2004). Neurons regulating the duration of forward locomotion in Caenorhabditis elegans. *Neuroscience Research*, *50*(1), 103–111.

Wehner, R. (2003). Desert ant navigation: how miniature brains solve complex tasks. Journal of Comparative Physiology A, 189(8), 579–588.

Wes, P., Bargmann, C. *C. elegans* odour discrimination requires asymmetric diversity in olfactory neurons (2001). *Nature* 410, 698–701.

White, J.G., Southgate, E., Thomson, J.N., and Brenner, S. (1986). The structure of the nervous system of the nematode Caenorhabditis elegans. Philosophical Transactions of the Royal Society B: Biological Sciences *314*, 1–340.

Wolpert, D. M., Ghahramani, Z. & Jordan, M. I. (1995). An internal model for sensorimotor integration. *Science* 269, 1880–2.

Zimmer, M., Gray, J.M., Pokala, N., Chang, A.J., Karow, D.S., Marletta, M.A., Hudson, M.L., Morton, D.B., Chronis, N., and Bargmann, C.I. (2009). Neurons Detect Increases and Decreases in Oxygen Levels Using Distinct Guanylate Cyclases. Neuron *61*, 865–879.